

https://dspace.org/

Dark matter constraints of galaxy clusters hosting diffuse radio emissions

Khanye, Nthabiseng F.

2022

https://hdl.handle.net/10539/34621

Downloaded from a DSpace repository. https://dspace.org/

UNIVERSITY OF THE WITWATERSRAND

DOCTORAL THESIS

Dark matter constraints of galaxy clusters hosting diffuse radio emissions

---

Author:
Nthabiseng F. KHANYE

Supervisor:
Dr. Paolo MARCHERGIANI
Dr. Geoff BECK

A thesis presented for the degree of
Doctor of Philosophy in the

School of Physics
Faculty of Science

September 10, 2021

Declaration of Authorship

I, Nthabiseng F. KHANYE, declare that this thesis titled, "Dark matter constraints of galaxy clusters hosting diffuse radio emissions" and the work presented in it are my own. I confirm that:

- This work was done wholly or mainly while in candidature for a research degree at this University.
- Where any part of this thesis has previously been submitted for a degree or any other qualification at this University or any other institution, this has been clearly stated.
- Where I have consulted the published work of others, this is always clearly attributed.
- Where I have quoted from the work of others, the source is always given. With the exception of such quotations, this thesis is entirely my own work.
- I have acknowledged all main sources of help.
- Where the thesis is based on work done by myself jointly with others, I have made clear exactly what was done by others and what I have contributed myself.

Signed:

Date:

"Thanks to my solid academic training, today I can write hundreds of words on virtually any topic without possessing a shred of information, which is how I got a good job in journalism."

Dave Barry

UNIVERSITY OF THE WITWATERSRAND

Abstract

Faculty Name
Faculty of Science

Doctor of Philosophy

Dark matter constraints of galaxy clusters hosting diffuse radio emissions

by Nthabiseng F. KHANYE

The existence of dark matter (DM) in the universe is extremely important as it explains the rotation of galaxies and hierarchical formation of astrophysical structures. However very little information is known about the formation, nature and interaction properties of DM. Attempts to directly observe DM have not yielded any conclusive results, making it impossible to directly study its physical composition and how it fundamentally interacts with itself and other matter in the universe. This elusive nature of DM has made us turn into indirect detection studies, so that we can be able to constrain some of its physical properties. One of the expected properties of DM particles such as WIMPs (i.e Weakly Interacting Massive Particles) is for them to annihilate inside DM halos found in galaxies and clusters. The annihilating WIMP particles are then expected to result in the production of standard model particles such as electrons and positrons which can lead to the occurrence of observable multi-frequency emissions (such as radio, X-ray etc...) when the produced electrons and positrons interact with magnetic fields and other particles found in galactic and (galaxy) cluster environments.
In this thesis we study the multi-frequency implications of DM annihilation in galaxy clusters that host diffuse radio emission by incorporating archival radio observations of said clusters. We focus on two massive and optically rich galaxy clusters, namely Abell 1689 and Abell 520. We assume that the diffuse radio emission found in these clusters is a by-product of the synchrotron radiation produced when electrons resulting from DM annihilation come into contact with cluster magnetic fields. We also present new multi-frequency radio analyses of the A1689 galaxy cluster using archival radio observations from six different radio surveys, to study the radio properties of the cluster and its diffuse radio emission

Acknowledgements

This work was supported by the South African Radio Radio Astronomy Observatory (SARAO) through the South African Research Chairs Initiative (SARchI) under the grant No. 77948.

I would first like to thank my supervisors, Dr. Paolo Marchegiani and Dr. Geoff Beck, whom without their assistance, after the passing of my first supervisor Prof Sergio Colafrancesco, this thesis would've not been possible. They have been of great resource and help throughout my graduate studies and continued to allow me to express my creativity and frustration in difficult times. Their passion and dedication to helping students cannot be over appreciated and I hope they will continue to do so for other upcoming students and aspiring scientists. I would also like to express my undying gratitude to my late supervisor Prof Sergio Colafrancesco who I started this project with, although his time in this world came to an end in an untimely manner, I will forever appreciate how he welcomed me into his group and taught me almost everything I know about astrophysics and cosmology in the short time he spent as my postgrad supervisor. I am grateful to Prof. Andrew Chen for keeping the astronomy group going and looking after us, after the passing of the Prof. Colafrancesco, his kindness and unconditional support helped us get through a very difficult period as a group and I wish he would continue to help more students in the future.

I would also like to extend my thanks to my group mates Charles Takalana, Siphiwe Thwala, Ashlynn Le Ray, Tanita Ramburuth-Hurt, Justine Beck, Ahmed Ayad, Charissa Button and Michael Sarkis as our fruitful conversations about astrophysics and cosmology have helped me get through my studies. I also appreciate them for safe keeping my office chair and space, when I regularly struggled to make it to the office. I am also very grateful to my family, especially my loving husband and my dear mother, for their unconditional support throughout my studies.

Contents

Declaration of Authorship iii

Abstract viii

Acknowledgements ix

1 Introduction 1
- 1.1 A brief history of dark matter . . . 1
- 1.2 Particle dark matter . . . 2
  - 1.2.1 WIMPs . . . 3
- 1.3 Detecting dark matter . . . 4
- 1.4 Diffuse radio emission in clusters . . . 5
- 1.5 Main objectives . . . 7
- 1.6 Outline . . . 7

2 The role of DM annihilation in the radio emission of A520 9
- 2.1 Introduction . . . 10
- 2.2 The integrated emission from the cluster . . . 12
- 2.3 Emission in the DM peak . . . 15
- 2.4 High-energy emission . . . 20
- 2.5 Discussion . . . 20
- 2.6 Conclusion . . . 23

3 Archival radio observations of the Abell 1689 cluster 25
- 3.1 Introduction . . . 26
- 3.2 Abell A1689 . . . 28
- 3.3 Observations and imaging . . . 29
  - 3.3.1 VLSSr . . . 30
  - 3.3.2 TGSS ADR1 . . . 30
  - 3.3.3 GLEAM . . . 30
  - 3.3.4 NVSS . . . 31
  - 3.3.5 FIRST . . . 31
  - 3.3.6 VLASS . . . 31

3.3.7 Imaging and Analysis 32
3.4 Results 33
3.4.1 Radio emission and cluster sources 33
3.4.2 Multi-ν counterparts 35
3.4.3 Diffuse emission in A1689 37
Flux density estimation 37
Morphology of diffuse emission 39
3.4.4 Spectral index imaging 42
3.5 Summary and conclusion 46

4 Effects of DM annihilation on the radio halo found in A1689. 49
4.1 Introduction 50
4.2 Radiation from DM annihilation 53
4.3 Radio analysis of the cluster 58
4.4 Annihilation cross-section 59
4.5 WIMP induced radio spectra 64
4.6 Conclusions 69

5 Concluding remarks 73
5.1 Concluding remarks 73

Bibliography 75

List of Figures

2.1 Spectrum of the radio halo flux in A520 for: (i) a neutralino model with mass M_χ = 9 GeV, annihilation final state $\tau^+\tau^-$, $\mathcal{B}\times < \sigma v >= 6 \times 10^{-25}$ cm^3 s^{-1} (solid line); (ii) a neutralino model with mass M_χ = 43 GeV, annihilation final state $b\bar{b}$, $\mathcal{B}\times < \sigma v > = 4 \times 10^{-24}$ cm^3 s^{-1} (dashed line); (iii) a hadronic model with proton spectral index s_p = 2.2 and a pressure ratio P_{CR}/P_{th} = 2.6 per cent (dot–dashed line). Data are from Vacca et al., 2014. 14

2.2 X-ray image from Chandra with NVSS contours overlapped (white); the black arrow indicates the peak of the NVSS map close to the P2 region; labels C and D are for radio galaxies as in Vacca et al., 2014 16

2.3 Optical image from ESO DSS with NVSS (white), TGSS (red), and from weak lensing (from Wang, Markevitch, and Giacintucci, 2016; black) overlapped. 17

2.4 Spectrum of the radio halo flux in the region P2 of A520 for a magnetic field of 3.8 μG (upper panel) and 5 μG (lower panel) and for: (i) a neutralino model with mass M_χ = 9 GeV, annihilation final state $\tau^+\tau^-$, $\mathcal{B}\times < \sigma v > = 6\times 10^{-25}$ cm^3 s^{-1} (solid line); (ii) a neutralino model with mass M_χ = 43 GeV, annihilation final state $b\bar{b}$, $\mathcal{B}\times < \sigma v > = 4\times 10^{-24}$ cm^3 s^{-1} (dashed line); (iii) a hadronic model with proton spectral index s_p = 2.2 and a pressure ratio P_{CR}/P_{th} =4 per cent (dot–dashed line). Data are from Table 2.1. 19

2.5 Spectral energy distribution of the high-energy emission from the whole cluster A520 (upper panel) and the P2 region (lower panel) for: (i) a neutralino model with mass M_χ = 9 GeV, annihilation final state $\tau^+\tau^-$,$\mathcal{B}\times < \sigma v >$ =6×10^{-25} cm^3 s^{-1} (solid line); (ii) a neutralino model with mass M_χ = 43 GeV, annihilation final state $b\bar{b}$, $\mathcal{B}\times < \sigma v >$ =4×10^{-24} cm^3 s^{-1} (dashed line); (iii) hadronic model with proton spectral index s_p = 2.2 and pressure ratios P_{CR}/P_{th}=2.6 per cent in the whole cluster and 4 per cent in the P2 region (dot–dashed line). We also show the sensitivity curves of Astro-H for 100 ks of time integration (from http://astro-h.isas.jaxa.jp/researchers/sim/sensitivity.html) and Fermi-LAT for 10 yr (from Funk, Hinton, and Consortium, 2013) 21

3.1 The NVSS 1400 MHz radio image of the cluster shown in colour with a resolution of $45'' \times 45''$ and rms noise of 0.5 mJy/b, overlaid with the GMRT 147.5 MHz radio contours. The contour lines are drawn at [1,2,4,8,16,...] $\times 2.5\sigma_{rms}$, where σ_{rms}=3.22 mJy/b. 34

3.2 Left to right: Radio continuum images of each titled survey (and observed frequency) with their respective contours levels drawn at $[1, 2, 4, 8, 16, 32, 64] \times 5\sigma_{\rm rms}$, where $\sigma_{\rm rms_{VLLSr}}, \sigma_{\rm rms_{TGSS}}, \sigma_{\rm rms_{NVSS}} = [109.75, 3.22, 0.53]$ mJy/beam. The beam sizes are shown on the lower left corner, with a resolution of $75'' \times 75''$, $27'' \times 25''$ and $45'' \times 45''$ for VLSSr, TGSS and NVSS, respectively. 35

3.3 Left: WISE infrared (W1, W2 and W3 bands) image of the cluster overlaid with the NVSS contour levels at [1,2,4,8,16,32,64]$\times 5\sigma_{\rm rms}$, where $\sigma_{\rm rms} = 0.53$ mJy/beam. Right: SDSS (r, g and i bands) images of the highlighted, silver infrared, regions with FIRST (teal;$\sigma_{\rm rms_{FIRST}} = 0.15$ mJy/beam) and VLASS (magenta;$\sigma_{\rm rms_{VLASS}} =$ 0.17 mJy/beam) contours at [1,2,4,8,...]$\times 3\sigma_{\rm rms_{FIRST}}$ and $5\sigma_{\rm rms_{VLASS}} + 3\sigma_{\rm rms_{VLASS}} \times [0, 1, 2, 4, 8, ...]$, respectively. 36

3.4 The spectrum of the diffuse emission found the A1689 cluster at frequencies ranging from 73.5 MHz to 1400 MHz with the errors obtained through equation 3.1, we have also included the flux density at 1200 MHz as calculated by Vacca et al. (2011). The blue line is the linear fit to the data. 40

3.5 The 147.5 MHz radio contours of the diffuse emission found in the cluster after the subtraction of point sources using PyBDSF. The resolution of the image is $\sim 27'' \times 25\,''$. The contour levels are [1,2,4,8,16,...]$\times 3\sigma_{rms}$ where σ_{rms}= 3.22 mJy/b. 41

3.6 The largest linear sizes of some well known radio halos compared to the redshift compared to the LLS for A1689 (in red) found in this study. Data points are taken from Feretti et al., 2012 43

3.7 **Top left panel:** Spectral index map between 147.5 and 1400 MHz at a resolution of $45'' \times 45\,''$, with a mask that covers the same region as the NVSS continuum image in Fig 3.2. **Top right panel:** Spectral index maps between 1400 and 3000 MHz at a resolution of $5'' \times 5\,''$, with a mask that covers the same region as the FIRST continuum image for values higher than $5\sigma_{\rm rms}$, highlighting identical regions found in Fig 3.3. **Bottom left and right panels:** The corresponding spectral index error maps of the detailed top panels. 45

4.1 The NVSS 1.4 GHz radio image of the A1689 cluster shown in colour with a resolution of $45'' \times 45''$ and an rms noise value of 0.5 mJy/b, the image has been overlaid with TGSS 147.5 MHz radio contours. The contour lines are drawn at [1,2,4,8,16,...]$\times 2.5\sigma$ 60

4.2 A1689 dark matter annihilation cross section upper limits $< \sigma v >$ as a function of WIMP mass for three annihilation final states. The solid graphs are for magnetic field B_0=10 μG and the dashed lines are for magnetic field B_0=4.7 μG. The blue lines represent the upper limit constraints from the $b\bar{b}$ annihilation state, the red lines represent the upper limit constraints from the $\mu^+\mu^-$ annihilation state and the green lines represent the upper limit constraints from the $\tau^+\tau^-$ annihilation state. The pink straight dash-dot line represents canonically thermally averaged cross section for a WIMP. 62

4.3 The predicted radio halo spectra from DM annihilation for a WIMP mass of m_χ=10 GeV for $b\bar{b}$, $\mu^-\mu^+$ and $\tau^-\tau^+$ annihilation final states at different B_0-field strength. The solid graphs are for magnetic parameters B_0=10 μG and the dashed lines are for magnetic field B_0=4.7 μG. The blue lines represent the expected radio spectra from the $b\bar{b}$ annihilation state, the red lines represent the expected radio spectra from the $\mu^+\mu^-$ annihilation state and the green lines represent the expected radio spectra from the $\tau^+\tau^-$ annihilation state. The predicted WIMP annihilation spectra are compared to observed radio fluxes of the radio halo (in scatter points) including a value of 8.7 mJy as reported by Vacca et al., 2011. 66

4.4 The predicated radio halo spectra from DM annihilation for a WIMP mass of m_χ=40 GeV for $b\bar{b}$, $\mu^-\mu^+$ and $\tau^-\tau^+$ annihilation final states at different B_0-field strength. The solid graphs are for magnetic field B_0=10 μG and the dashed lines are for magnetic field B_0=4.7 μG. The blue lines represent the expected radio spectra from the $b\bar{b}$ annihilation state, the red lines represent the expected radio spectra from the $\mu^+\mu^-$ annihilation state and the green lines represent the expected radio spectra from the $\tau^+\tau^-$ annihilation state. The predicted WIMP annihilation spectra are compared to observed radio fluxes of the radio halo (in scatter points) including a value of 8.7 mJy as reported by Vacca et al., 2011. 67

4.5 The predicated radio halo spectra from DM annihilation for a WIMP mass of m_χ=100 GeV for $b\bar{b}$, $\mu^-\mu^+$ and $\tau^-\tau^+$ annihilation final states at different B_0-field strength. The solid graphs are for magnetic field B_0=10 μG and the dashed lines are for magnetic field B_0=4.7 μG. The blue lines represent the expected radio spectra from the $b\bar{b}$ annihilation state, the red lines represent the expected radio spectra from the $\mu^+\mu^-$ annihilation state and the green lines represent the expected radio spectra from the $\tau^+\tau^-$ annihilation state. The predicted WIMP annihilation spectra are compared to observed radio fluxes of the radio halo (in scatter points) including a value of 8.7 mJy as reported by Vacca et al., 2011. 68

List of Tables

2.1 Radio fluxes estimated in a circular region centred in RA = 04 54 15.0, Dec. = + 02 56 31.4, and with a radius of 35 arcsec, as obtained from the surveys VLSSr (74 MHz), TGSS (150 MHz), and NVSS (1.4 GHz). 18

3.1 Global properties of the A1689 cluster and its radio halo (written as RH) at 1200 MHz. 29
3.2 Properties of the A1689 radio continuum images used in this study. Col. 1: survey name, col. 2: observation frequency, col. 3 synthesized beam size, col. 4: noise value of each image and col. 5 observation date. 32
3.3 Position, radio and general properties of the radio sources found in A1689 and along its field-of-view. Col. 1 shows the label of the cluster sources, Cols. 2 and 3 are the coordinates of the sources, Cols. 4 and 5 are their integrated flux densities at 147 MHz and 1400 MHz, Col. 6 is the redshift of the source and Col. 7 is the classification of the point source. (RG- radio-galaxy, BiC - Brightest galaxy in the cluster in Simbad). The associated source names (or identifier in Simbad) of each labelled sources are: *F* - TGN259Z069, *G* - SDSSJ131130.2-0120, *H* - 2MASX J13113265-0119590, *I* - A1308-0150D, *J*- TGN259Z044 , *K*- Slee ACO 1689 18 37
3.4 Flux densities of the diffuse emission found in the galaxy cluster at different radio frequencies, including the 1200 MHz flux density value from Vacca et al., 2011. The values at 147.5 MHz and 200 MHz are taken as upper limits, due to the poor resolution of the VLSSr and GLEAM observations. 38

4.1 Properties of the cluster used to study the cross section upper limits and radio signal from WIMP annihilation. 58

4.2 Properties of the A1689 radio continuum image which we used in our study. Col 1. represents the survey name, Col 2. is the central frequency, Col 3. is the surveys' synthesized beam size and Col 4. is the noise value of each image. 61
4.3 Flux densities of the radio halo found in the galaxy cluster at different frequencies. 61
4.4 Cross section upper limits for different WIMP masses at 3 different annihilation channels when B_0= 10 μG and when B_0= 4.7 μG. 63

List of Abbreviations

DM	**D**ark **M**atter
WIMP	**W**eakly **I**nteracting **M**assive **P**articles
ΛCDM	Λ **C**old **D**ark **M**atter
GMRT	**G**iant **M**etrewave **R**adio **T**elescope
TGSS	**TIFR GMRT S**ky **S**urvey
VLA	**V**ery **L**arge **A**rray
NVSS	**NRAO VLA S**ky **S**urvey
VLSS	**VLA L**ow-frequency **S**ky **S**urvey
MWA	**M**urchison **W**idefield **A**rray
GLEAM	**G**a**L**actic (and) **E**xtragalactic **A**ll-sky **MWA**
SKA	**S**quare **K**ilometre **A**rray
NFW	**N**avarro-**F**renk-**W**hite
ROSAT	**RO**entgen **SAT**ellite
ASCA	**A**dvanced **S**atellite (for) **C**osmology (and) **A**strophysics
CASA	**C**ommon **A**stronomy **S**oftware **A**pplication
PyBDSF	**Py**thon **B**lob **D**etector (and) **S**ource **F**inder

Physical Constants

Speed of Light	$c_0 = 2.9979 \times 10^8\,\mathrm{m\,s^{-1}}$
Solar Mass	$M_\odot = 1.989 \times 10^{30}\,\mathrm{kg}$
Electron Volt	$1\mathrm{eV} = 1.602 \times 10^{-19}\,\mathrm{J}$
Planck Constant	$\mathrm{h} = 6.626 \times 10^{-34}\,\mathrm{J\,s}$
Hubble constant	$\mathrm{H}_0 = 69.6\,\mathrm{km\,s^{-1}Mpc^{-1}}$
Gravitational constant	$\mathrm{G} = 6.674 \times 10^{-11}\,\mathrm{Nm^2\ kg^2}$
Charge of an electron	$\mathrm{e}^- = -1.602\,18 \times 10^{-19}\,\mathrm{C}$
Permittivity of space	$\epsilon\circ = 8.854 \times 10^{-12}\,\mathrm{F/\ m}$

Dedicated to my darling mother, Ivy…

Chapter 1

Introduction

1.1 A brief history of dark matter

The first evidence of DM in the universe was first discovered by Fritz Zwicky in 1933 when he was studying the velocity distributions of galaxies in the Coma cluster (Zwicky, 1933). Zwicky noticed a discrepancy between the luminous mass of the cluster and the radial velocity of the cluster galaxies. He noticed that the total luminous mass in the cluster was 400 times less than the mass required to produce and maintain the galactic radial velocity. He found the radial velocity to be 1000 km s^{-1}, this is in agreement with a more recent value of 1080 km s^{-1} found by Colless and Dunn, 1995. This value is very large if it was solely due to the luminous mass of the galaxies and their content. This led Zwicky to conclude that there must be huge amounts of "missing mass" in the Coma cluster, holding the cluster objects together. Zwicky referred to this "missing mass" as *"dunkle (kalte) materie"* or dark (cold) matter in his 1933 publication tittled "On the redshift of extragalactic nebulae". Three years after Zwicky made his publication a similar excess of non-luminous matter was discovered by Smith, 1936, in the Virgo cluster.

Babcock, 1939, was investigating the rotational velocity of the Andromeda galaxy (M31) when he discovered the anomalous behaviour of the rotational velocity of the galactic matter. He expected that the angular velocity of the galaxy will decrease moving away from the galactic centre in correlation with the galaxy's decreasing luminous matter, however the angular velocity remained constant throughout the galaxy. These findings led the author to conclude that there must either be a large concentration of mass situated at the galactic edges as opposed to the centre as expected, or there was an unexpected absorption of light by galactic dust towards the edges. Observations of the galaxy NGC3115 in 1940 by Oort, 1940, observed that "the distribution

of luminous mass of the system bared almost no relation to the distribution of the light", however this finding did not agree with Babcock's conclusion as NGC3115 is dust free (Van Dokkum and Franx, 1995). This indicated the first significant evidence for the existence of DM in galaxies.
Another significant study of DM was done by Rubin and Ford between the 1970's and 1980's when they studied the rotational curves of numerous galaxies including M31 and observed flat rotational curves for the galaxies. This indicated the presence of massive non-luminous halos of matter extending beyond the galactic radii (Rubin and Ford Jr, 1970; Rubin, Ford Jr, and D'Odorico, 1970).

Further evidence of the existence of DM is provided by the measurements of temperature fluctuations in the cosmic microwave background (CMB). These fluctuations represent small variations in the universe's density. The fluctuations are caused by the gravitational interaction between baryonic particles and CMB radiation, which is a relic of the epoch of recombination (EoR) (Archidiacono et al., 2019; Padmanabhan and Finkbeiner, 2005). The observed fluctuations strongly suggest the existence of a greater gravitational influence, exceeding the one expected from baryonic particles and CMB interactions. DM particles are expected to exert this gravitational influence without any additional interaction from CMB radiation (Archidiacono et al., 2019; Padmanabhan and Finkbeiner, 2005). Other evidence to support the existence of DM in the universe has also been found through gravitational lensing observations, the big bang nucleosynthesis (BBN, see Depta et al., 2019; Serpico and Raffelt, 2004 for review), X-ray observations of galaxy clusters and observations of merging galaxy clusters (see Bradač et al., 2008 for example studies).

1.2 Particle dark matter

The Standard Model of particles is the best theoretical work frame for the fundamental subatomic nature of the universe, however the ΛCDM (aka the "Lambda Cold Dark matter Matter") model forces us to assume a new particle outside the Standard Model to account for the missing mass and the expansion of the universe. In order to narrow down the search for DM particles, several constrains have been placed from observations (or lack thereof) for any potential candidate DM particles. These conditions are:

- DM particles must be non-relativistic, i.e "cold", to ensure the hierarchical formation of the universe. If DM particles were "hot", then larger structures in the universe, e.g., clusters of galaxies and bigger, would form first and smaller scale structures, e.g., stars and galaxies, would form later. However, observations indicate that structures in the universe form hierarchically from smaller to bigger. This condition rules out neutrinos as possible DM candidate as neutrinos are relativistic.

- DM particles must also be neutrally charged and interact weakly with themselves and the electromagnetic matter. If DM particles were charged then they would continuously interact with other charged particles, however, we know from the lack observations that this is not the case. This requirement rules out many Standard Model particles such potential candidates for DM particles.

- Finally, DM particles must be stable on cosmological timescales, because if DM particles are unstable on timescales shorter than the Hubble time, then the bulk of DM particles would have already decayed. This requirement also rules out most Standard Model particles.

Although there are numerous DM candidates which satisfy these constraints, WIMPs are the most well accepted and studied candidates. Features of WIMPs in some models such as supersymmetry (e.g., the neutralino) or Universal Extra Dimensions (e.g., the lightest Kaluza-Klein particle) allows their interaction cross section to be on a scale such that they can naturally produce the observed thermal relic abundance of DM in galaxies and clusters (Jungman, Kamionkowski, and Griest, 1996; Bertone, Hooper, and Silk, 2005; Hooper and Profumo, 2007).

1.2.1 WIMPs

WIMPs are the most viable non-baryonic DM candidates as they are stable, neutral and weakly interact with themselves and other Standard Model particles. WIMPs are expected to abundantly produced in thermal equilibrium in the universe when:

$$K_B T \gg m_\chi c^2, \tag{1.1}$$

where T is the temperature of the Universe and m_χ is the mass of the WIMP particle. WIMPs are also expected to be self-annihilating and their abundance has been preserved as the number of forward processes was equal to the number of backwards processes, i.e., the annihilating particle χ and their

anti-particle $\bar{\chi}$ would annihilate to form lighter particles l and anti-particle $\bar{l}$ which would also annihilate to form χ and $\bar{\chi}$ at the same time:

$$\chi\bar{\chi} \rightleftharpoons l\bar{l}. \tag{1.2}$$

As the temperature of the universe falls, the equilibrium abundance will also fall exponentially up until the forward process also falls below the Hubble expansion rate. At this point, the WIMPs will stop annihilating as they fall out of equilibrium (see Jungman, Kamionkowski, and Griest, 1996 for an extensive discussion).

The expansion of the universe, given by H, the Hubble constant, prevents the WIMPs from disappearing completely by reducing their concentration to a point where WIMP annihilation becomes improbable. This occurs when the WIMP population falls exponentially out of thermal equilibrium due to the rate of annihilation becoming smaller than the rate of the universe's spatial expansion, H, this is called the "freeze-out" and at this point, WIMPs cease to annihilate (Jungman, Kamionkowski, and Griest, 1996).

WIMPs have been popular DM candidates for a long time now, however their lack of detection through experimental searches have made many scientists sceptical about their existence. Recent reviews of the WIMP theoretical framework speculate that most of the formulations of WIMPs will be put to a final test by the proposed next-generation of detectors (Arcadi et al., 2018).

1.3 Detecting dark matter

The evidence for the existence of DM in the universe is convincing, however none of this evidence constitutes the actual detection of DM, which will be the best proof for its existence. This brings us to the question of *"which methods can we use to detect DM particles?"*. We know that the best detection of DM would be a direct detection of DM particles such as WIMPs, this has however proven to be very difficult since WIMPs weakly interact with themselves and with other particles. However, this method of detection requires WIMPs to elastically scatter with Standard Model particle nuclei as DM particles pass through Earth-based detectors. This type of interaction will also require energy within the keV range to detect which is difficult to achieve with current instrumentation. A number of direct detection experiments are

currently underway such as XENON1T (Collaboration-XENON et al., 2018) and the Large Underground Xenon experiment (the LUX, Akerib et al., 2017) noble gas detectors. No definitive DM signal has been detected so far, however direct detection efforts have led to constrains on the WIMP scattering cross section.

Another method of detection for DM is through collider searches. Collider searches rely on the production of DM particles occurring through the collision of Standard Model particles (i.e. proton-proton collisions at the large Hadron Collider, LHC). Since DM cannot be directly detected through the LHC, scientists are focusing on the signature of the "missing energy" which is believed to correspond to DM escaping the detector after the proton-proton collisions (Boveia and Doglioni, 2018). Collider searches have also not being successful on the detection of DM, however, they can be used to constrain the properties of some model-dependant interactions.

An alternative method of studying the nature of DM, is through indirect detection methods, where decay and annihilation of WIMPs produce Standard Model particles that are expected to be detected through multiple astronomy techniques. This method of detection encompasses multi-messenger astronomy, such as the detection of electromagnetic radiation (EM), neutrinos (Abazajian and Koushiappas, 2006; Boyarsky et al., 2019) and cosmic rays (Cholis, Linden, and Hooper, 2019; Barger et al., 2009). Indirect searches focus on detecting Standard Model particles created during DM annihilation or decays. The neutrinos can be detected directly while electrons and positrons are studied indirectly through the secondary EM radiation they produce, such as gamma-rays and X-rays, through various experiments, such as the FERMI-LAT. The FERMI-LAT collaboration focuses on detecting the gamma ray emissions produced through DM annihilation in galaxies and clusters (Abdo et al., 2010; Zhang et al., 2011; Ackermann et al., 2012; Huang, Vertongen, and Weniger, 2012; Abazajian and Keeley, 2016; Abazajian et al., 2020).

1.4 Diffuse radio emission in clusters

Galaxy clusters are the largest gravitationally bound entities in the universe, they typically contain between 100 to 1000's of galaxies. They are also rich in thermal X-ray hot plasma found in-between the galaxies. Stars, galaxies and all other baryonic matter make up only 12 to 15% of the mass in galaxy

clusters, most of the mass comes from DM, this makes galaxy clusters great laboratories to study the properties and composition of DM. The observations of galaxy clusters in different energy bands is essential as it can be used to probe different different astrophysical properties of the ICM to help us understand the formation, history and evolution of galaxy clusters, which will in turn help us understand the properties of the Universe. The ICM is heated to a high temperatures as it is filled with thermal plasma, magnetic fields and energetic particles. Their typical temperature ranges from 10^7 to 10^8 K and the energy density in between galaxies ranges from 10^{-3} to 10^{-1} cm^{-3}.

Some clusters have been found to harbour diffuse radio emission which cannot be associated with any galaxies in the cluster. The diffuse radio emission typically spreads over 500 kpc to $\sim$1 Mpc in size. The non-thermal emission can be classified as radio halos, radio relics or mini-halos depending on their size, polarity, morphology and position in the cluster:

- Radio halos are large areas of diffuse emission which are typically located in the central regions of the cluster, they tend to exhibit a regular spherical morphology, which traces the morphology of the cluster's X-ray gas. An example of a galaxy cluster which hosts a radio halo is the Coma cluster (Giovannini, Tordi, and Feretti, 1999).

- Radio relics are also extended areas of diffuse emission which are typically found in the peripheral regions of the cluster. Relics typically exhibit an elongated shape and are highly polarized unlike radio halos. An example of a galaxy cluster which hosts a radio relic is the Toothbrush cluster (Kang, Ryu, and Jones, 2017).

- Mini-halos are moderately-sized ($\sim$500 kpc) regions of diffuse radio emission which resemble radio halos. However they are typically found in clusters with a dominant central radio-galaxy, although their emission is not associated with the radio-galaxy. Mini-halos are a bit harder to detect as in most cases they are out-shined by the dominant radio-galaxy. An example of a galaxy cluster which hosts a mini-halo is the RXJ1347.5-1145 cluster (Gitti et al., 2007).

Diffuse radio emissions results from synchrotron radiation, which occurs when relativistic electrons spiral magnetic fields which permeate the galaxy cluster. Radio relics and mini-halos have very interesting features and models which explain their origin, however, in this study we are only interested

in the occurrence of radio halos.
Although the origin of radio is still unknown and a few models have been proposed to explain their origins, one of these models links the occurrence of diffuse radio emissions to annihilation of DM particles which will interact with intra-cluster (ICM) magnetic fields to form radio emission. This model assumes WIMPs as the best candidates for DM particles to explain the spherical shapes and spectral steepening of radio halos at higher frequencies. The model also predicts the position of the radio halo to be on the central regions of galaxy clusters, which will be coincident with the bulk of the X-ray emission (Colafrancesco and Mele, 2001; Hooper and Profumo, 2007).

1.5 Main objectives

In this thesis we aim to study the predicted WIMP annihilation (electromagnetic) emission in galaxy clusters that host diffuse radio emission, namely the Abell 1689 and Abell 520 clusters. We will incorporate radio observations, gravitational lensing measures and X-ray observations to constrain the properties of DM halos where DM particles self interact to form Standard Model particles. We will present observational limits on the predicted electromagnetic radiation to obtain the best window of detection for WIMP induced emissions.
We will also present a multi-frequency radio study of the Abell 1689 galaxy cluster using publicly available archival data from the VLA, GMRT, MWA, SDSS and WISE surveys. We use the radio observations to help us map out the radio morphology and spectral properties of the cluster and its radio halo.

1.6 Outline

This thesis is structured as follows:

In Chapter 2., we study the possibility that the radio halo found in Abell 520 results from the annihilation of DM particles using the radio observations and gravitational studies of the cluster. We determine the best fit values for the annihilation cross section and magnetic field of our DM model, which will fit the observed radio spectrum in a specific region of the cluster.
In Chapter 3., we present the radio, morphological and spectral analyses of the Abell 1689 cluster and its diffuse emission using publicly available

archival radio observations from the VLA, GMRT, MWA, SDSS and WISE surveys.
In Chapter 4., we present the DM annihilation study of the Abell 1689 galaxy cluster. We use observations of the cluster's radio halo to constrain the annihilation cross section of WIMPs in the cluster. We then place observational limits on the predicted WIMP induced radio signals, at two different magnetic fields and three different annihilation channels, by assuming that the diffuse emission in the cluster results from the annihilation of WIMPs.

In Chapter 5., we present our concluding remarks and discuss current issues with out results and future work.

Chapter 2

The role of DM annihilation in the radio emission of A520

This chapter of the thesis looks at the role of DM annihilation of the diffuse emission found in the Abell 520 cluster.

Note: This chapter is adapted from the published work:

Marchegiani P., Colafrancesco S. and Khanye N.F., "*The role of dark matter annihilation in the radio emission of the galaxy cluster A520*", 2019, MNRAS, 483, 2.

&

Marchegiani P., Colafrancesco S. and Khanye N.F., "*Possible Dark Matter annihilation in the galaxy cluster A520*", 2018, High Energy Astrophysics in Southern Africa (HEASA2018), 30.

The contribution of the candidate was significant, it included writing the algorithm which produced all the radio data, the radio and X-ray images. The selection of these figures and data reinforced the arguments made in this manuscript. The candidate contributed to the arguments expressed in the letter and was also involved in the writing, editing and submission of the manuscript and the proceeding paper to the publishers.

Abstract

A520 is a hot and luminous galaxy cluster, where gravitational lensing and X-ray measures reveal a different spatial distribution of baryonic and dark matter. This cluster hosts a radio halo, whose map shows a separation between the north-east and the south-west part of the cluster, similarly to what is observed in gravitational lensing maps. In this paper we study the possibility that the diffuse radio emission in this cluster is produced by dark matter annihilation. We find that in the whole cluster the radio emission should be dominated by baryonic phenomena; if a contribution from dark matter is present, it should be searched in a region in the NE part of the cluster, where a peak of the radio emission is located close to a dark matter subhalo, in a region where the X-ray emission is not very strong. By estimating the radio spectrum integrated in this region using data from publicly available surveys, we find that this spectrum can be reproduced by a dark matter model for a neutralino with mass 43 GeV and annihilation final state $b\bar{b}$ for a magnetic field of 5 μG.

2.1 Introduction

Galaxy clusters are supposed to be dominated by a component of dark matter (DM) of unknown nature. The annihilation of DM particles in a galaxy cluster can produce relativistic electrons and gamma-rays, whose possible detection can be used to test the properties of the DM particles and the cluster itself (Colafrancesco, Profumo, and Ullio, 2006). However, other processes in galaxy clusters can produce diffuse non-thermal emission in several spectral bands, like radio, X-rays, and gamma-rays (e.g. Feretti et al., 2012), making difficult to distinguish the emission of baryonic origin from the one originated by DM annihilation. Marchegiani and Colafrancesco, 2015 proposed to address this problem by considering clusters where the X-rays and gravitational lensing measures suggest that the baryonic and the DM haloes are located in different positions, like in the case of the Bullet cluster (Clowe et al., 2006), and studying the emission detected in the different regions of the cluster. This situation can usually be found in clusters during a merging event taking place approximately perpendicularly to the line of sight, when the DM haloes of the two clusters are expected to cross each other in a collisionless way, whereas the thermal gas haloes interact by ram pressure, producing a slowdown and an offset between DM and baryonic matter (e.g.

Roettiger, Loken, and Burns, 1997).

A520 is a hot and luminous galaxy cluster, where an ongoing merging event has been identified both with X-rays (Markevitch et al., 2005a) and optical observations (Proust et al., 2000). In A520 X-rays and gravitational lensing measures reveal a situation similar to the case of the Bullet cluster: the distribution of the DM density in fact results to be different from the baryonic one, with two main DM peaks located on the opposite sides of the cluster geometrical centre along the NE–SW direction, that is interpreted as the merging axis, whereas the X-ray emission shows a main peak close to the cluster geometrical centre, and an extension in the SW part of the cluster, where a second peak, associated with the Brightest Cluster Galaxy (BCG) of the secondary subcluster, is located close to the edge of the cluster, and presents a trail of cold gas, interpreted as the remnant of a cool core cluster that is going to be destroyed by ram pressure while crossing the main cluster (Clowe et al., 2012; Wang, Markevitch, and Giacintucci, 2016; Wang, Giacintucci, and Markevitch, 2018). The detection of a third peak in the DM distribution close to the X-ray peak is controversial: in some studies (e.g. Mahdavi et al., 2007) this peak results to be present, whereas in other studies (e.g. Clowe et al., 2012) this peak is not detected with sufficient statistical significance.

A520 hosts a giant bright radio halo (Govoni et al., 2001b; Govoni et al., 2004; Vacca et al., 2014; Wang, Giacintucci, and Markevitch, 2018), with a relatively flat spectral index (with integrated value between 325 and 1400 MHz of $\alpha \sim 1.12$; Vacca et al., 2014) that, although with fluctuations in its value across the cluster, does not present a systematic steepening towards the peripheral regions (Vacca et al., 2014), as instead observed in other clusters like Coma (Giovannini et al., 1993) and A665 (Feretti et al., 2004). The radio maps show that the halo is divided in two main subhaloes in the NE and SW regions of the cluster; this structure is interesting because it is analogue to the structure of the DM distribution in the cluster. We note that a similarity between radio halo and DM morphology is also observed, for example, in the Coma cluster (Brown and Rudnick, 2011; Marchegiani and Colafrancesco, 2016).

In this paper we check the possibility that the radio emission in A520 can be originated by DM annihilation. In Section 2.2 we study the emission expected from DM in the whole cluster, and compare it with the emission of baryonic origin. In Section 2.3 we focus on a region of the cluster where

a peak of the diffuse radio emission is located close to a DM peak, and in Section 2.4 we study the high-energy emission expected from the cluster. In Section 2.5 we discuss our results and make hypothesis on the origin of the electrons in the different regions of the cluster, and in Section 2.6 we summarize our conclusions.

Throughout the paper, we use a flat, vacuum-dominated cosmological model following the results of Planck, with $\Omega_m = 0.308$, $\Omega_\Lambda = 0.692$, and H_0=67.8 km s^{-1} Mpc^{-1} (Ade et al., 2016). With these values the luminosity distance of A520 at z =0.199 is D_L= 1005 Mpc and 1 arcmin corresponds to 203 kpc at this distance.

2.2 The integrated emission from the cluster

As a first step, we study the radio emission expected in the whole cluster for a baryonic model, where secondary electrons are produced by hadronic interactions between cosmic rays and thermal protons (e.g Blasi and Colafrancesco, 1999) and a DM model, where electrons are produced by DM annihilation (e.g Colafrancesco, Profumo, and Ullio, 2006).

In both the models, the equilibrium spectrum of electrons is obtained by solving the diffusion-loss equation (e.g (Sarazin, 1999))

$$\frac{\partial}{\partial t}\frac{dn_e}{dE} = \nabla\left(D(E,\mathbf{r})\nabla\frac{dn_e}{dE}\right) + \frac{\partial}{\partial E}\left(b(E,\mathbf{r})\frac{dn_e}{dE}\right) + Q_e(E,\mathbf{r}) \qquad (2.1)$$

where $(dn_e)/(dE)$ is the electron spectrum, $D(E,\mathbf{r})$ is the spatial diffusion coefficient, $b(E,\mathbf{r})$ is the energy-loss function, and $Q_e(E,\mathbf{r})$ is the electron source function, that can be calculated according to the physics of the hadronic interactions (e.g. Moskalenko and Strong, 1998) or the DM annihilation (e.g. Gondolo et al., 2004).

In the hadronic model, the source term is proportional to the product of the numerical density of thermal nuclei and the one of cosmic ray protons. For the density of the thermal gas we use the properties derived from X-rays observations: the radial profile can be described by a beta model

$$n_{th}(r) = n_{th,0}\left(1 + \left(\frac{r}{r_c}\right)^2\right)^{-q_{th}} \qquad (2.2)$$

(Cavaliere and Fusco-Femiano, 1976) with $n_{th,0}$= 3.8 $\times$ 10^{-3} cm^{-3}, r_c = 413 kpc, and q_{th} = 1.3 (see table 6 in Govoni et al., 2001b, after correcting for the different cosmological model). We assume that the cosmic ray protons have a spatial profile proportional to the thermal one, use power-law spectral distributions $N_p \propto \gamma^{-s_p}$ with several values of the spectral index, and let their central density as a free parameter, expressed through the ratio between the non-thermal and the thermal pressure (see e.g. Marchegiani, Perola, and Colafrancesco, 2007). This last value has been constrained to have upper limits of the order of 2-6 percent, depending on the spectral index, from stacked analysis of Fermi gamma-ray upper limits in galaxy clusters (Huber et al., 2013; Prokhorov and Churazov, 2014). At the moment there are no estimates of the magnetic field in A520 derived from Farady Rotation Measures available in literature; we therefore adopt a magnetic field similar to the one found in Coma, with a central value of 5 μG and a radial profile proportional to $n_{th}(\mathbf{r})^{1/2}$ (Bonafede et al., 2010).

For the DM models, we use two neutralino models with mass 9 GeV and annihilation final state $\tau^+\tau^-$, and mass 43 GeV and annihilation final state $b\bar{b}$, with the total normalizations, given by the product of the annihilation cross-section and the substructures boosting factor, $\mathcal{B}\times < \sigma v >$, as obtained from the fitting to the flux of the radio halo in the Coma cluster (Marchegiani and Colafrancesco, 2016). These normalizations can therefore be considered as upper limits on the DM emission, because they can be obtained for optimistic values of the annihilation cross-section as derived from the gamma-ray excess in the Galactic Centre (Abazajian and Keeley, 2016) and the substructures boosting factor (see discussion in (Marchegiani and Colafrancesco, 2016)), and because a higher value of this normalization would produce a radio emission in excess with respect to the flux observed in the Coma cluster. The density and the radial profile of the DM halo are assumed to have a Navarro, Frenk, and White, 1997 profile,

$$\rho(r) = \frac{\rho_s}{\left(\frac{r}{r_s}\right)\left(1+\frac{r}{r_s}\right)^2}, \tag{2.3}$$

with the parameters derived from the total mass, M_{200} = (9.1 $\pm$ 1.9) $\times$ 10^{14} M$\odot$ (Clowe et al., 2012), according to the procedure described in Bullock et al., 2001 and Colafrancesco, Marchegiani, and Beck, 2015: r_s = 472 kpc and ρ_s = 5.29 $\times$ $10^3\rho_c$, where ρ_c is the critical density of the Universe. We calculate the total flux by integrating in a volume with a radius of 0.5 Mpc, similar to

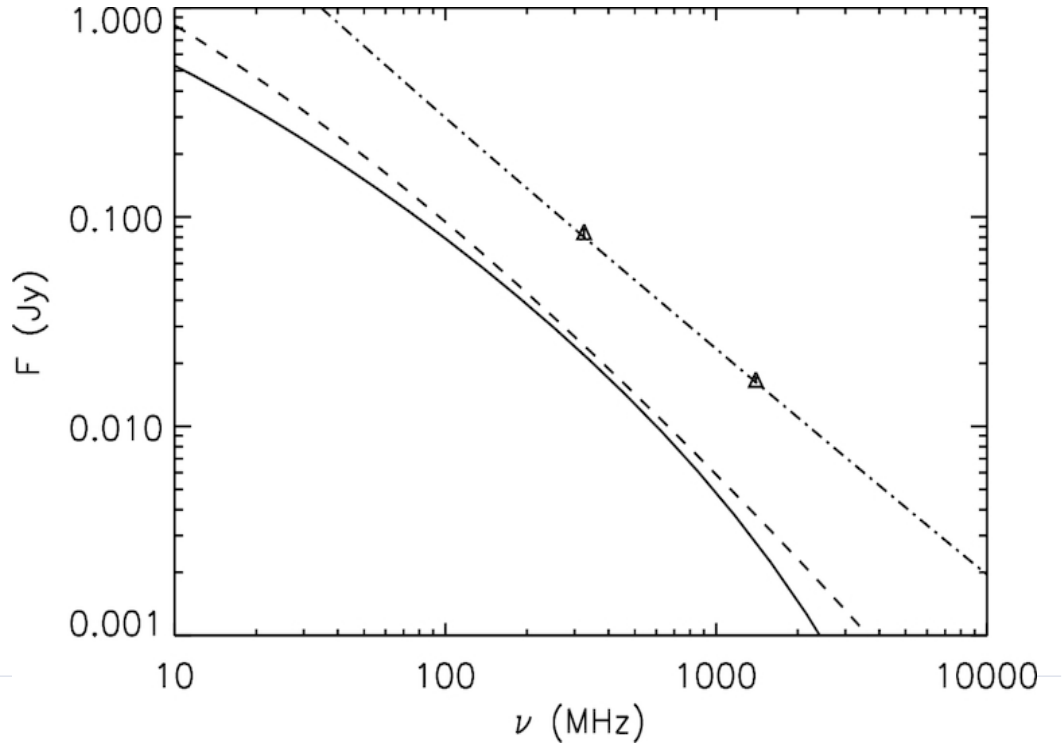


FIGURE 2.1: Spectrum of the radio halo flux in A520 for: (i) a neutralino model with mass M_χ = 9 GeV, annihilation final state $\tau^+\tau^-$, $\mathcal{B}\times < \sigma v >= 6 \times 10^{-25}$ cm^3 s^{-1} (solid line); (ii) a neutralino model with mass M_χ = 43 GeV, annihilation final state $b\bar{b}$, $\mathcal{B}\times < \sigma v > = 4 \times 10^{-24}$ cm^3 s^{-1} (dashed line); (iii) a hadronic model with proton spectral index s_p = 2.2 and a pressure ratio P_{CR}/P_{th} = 2.6 per cent (dot–dashed line). Data are from Vacca et al., 2014.

the radius of the whole radio halo.

The comparison between the prediction of these models and the observed total flux of the radio halo in A520 at 325 and 1400 MHz (Vacca et al., 2014) is given in Fig. 2.1. The hadronic model provides a good fit to the data for a spectral index s_p = 2.2 and a pressure ratio P_{CR}/P_{th} = 2.6 per cent that is of the order of the upper limits derived from stacked analysis of gamma-ray emission in clusters. The DM emission is instead lower than the observed flux by almost one order of magnitude, suggesting that the bulk of radio emission in A520 cannot be of DM origin. It is anyway possible that the DM can give a contribution in some regions of the cluster, as suggested in the case of the Bullet cluster (Marchegiani and Colafrancesco, 2015). In the next section we explore this possibility.

2.3 Emission in the DM peak

According to Clowe et al., 2012, the two most massive DM subhaloes inside the radio halo region in A520 are the ones labelled with P2 and P4, that are located respectively in the NE and SW parts of the halo. The subhalo P4 is located close to the BCG that is moving outwards producing the detected bow shock and leaving a cold gas trail; it is therefore reasonable to think that the radio emission in this region is dominated by the electrons (primary or secondary) originated by this galaxy or accelerated by the associated bow shock. The subhalo P2 is instead located in a region with a weak X-ray emission, but close to a peak of the radio emission, located between the radio galaxies labelled with C and D by Vacca et al., 2014 and visible also in the NVSS map (see Fig.2.2). This radio peak is better visible in the fig. 2a in Wang, Giacintucci, and Markevitch, 2018, where the diffuse radio emission is shown after the removal of point sources, at the approximated coordinates (J2000) RA = 04 54 15.0, Dec. = + 02 56 31.4. In Fig. 2.3 we show a zoom of this region, with the optical ESO-DSS map, where the contours from NVSS (Condon et al., 1998a) and TGSS (Intema et al., 2017) radio surveys, and from the gravitational lensing analysis (from fig. 1c in Wang, Markevitch, and Giacintucci, 2016) are overlapped. The radio peak located close to the centre of the image is visible in the TGSS contours, and is located between two lensing peaks; the distance between the centre of the TGSS peak and the lensing peaks is of the order of the TGSS resolution (25 arcsec), and therefore it is possible that in this peak there is a contribution from DM annihilation. At the centre of the TGSS peak there is a galaxy, presently not recognized as a radio source, that can also be the origin of the radio emission; this situation is similar to the one in the DM Eastern peak in the Bullet cluster, where the radio peak is located close to the DM peak but also to a possible radio galaxy (see Marchegiani and Colafrancesco, 2015).

In order to estimate the radio flux coming from this region, we analysed the data from a few radio surveys, i.e. VLSSr (Lane et al., 2014), TGSS, and NVSS, estimating the diffuse flux coming from a circle centred at the coordinates RA = 04 54 15.0, Dec. = + 02 56 31.4, and a radius of 35 arcsec (i.e. avoiding the emission from radio galaxies C and D), corresponding to 118 kpc. The data analysis has been done using the CASA package, and the results are reported in Table 2.1.

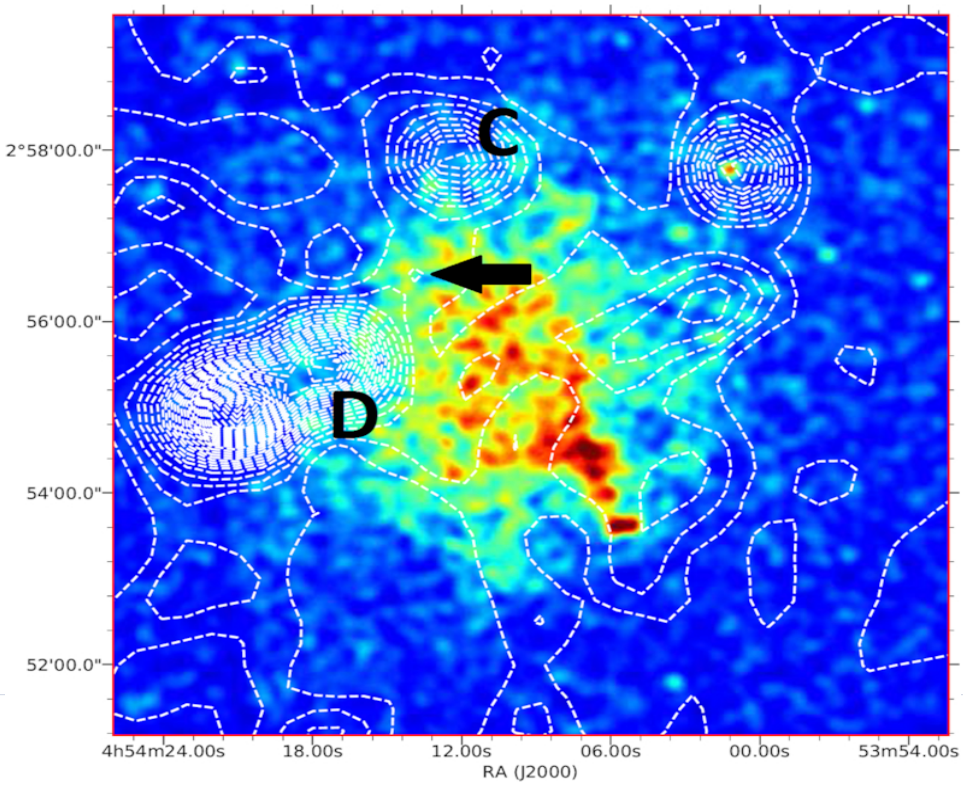


FIGURE 2.2: X-ray image from Chandra with NVSS contours overlapped (white); the black arrow indicates the peak of the NVSS map close to the P2 region; labels C and D are for radio galaxies as in Vacca et al., 2014

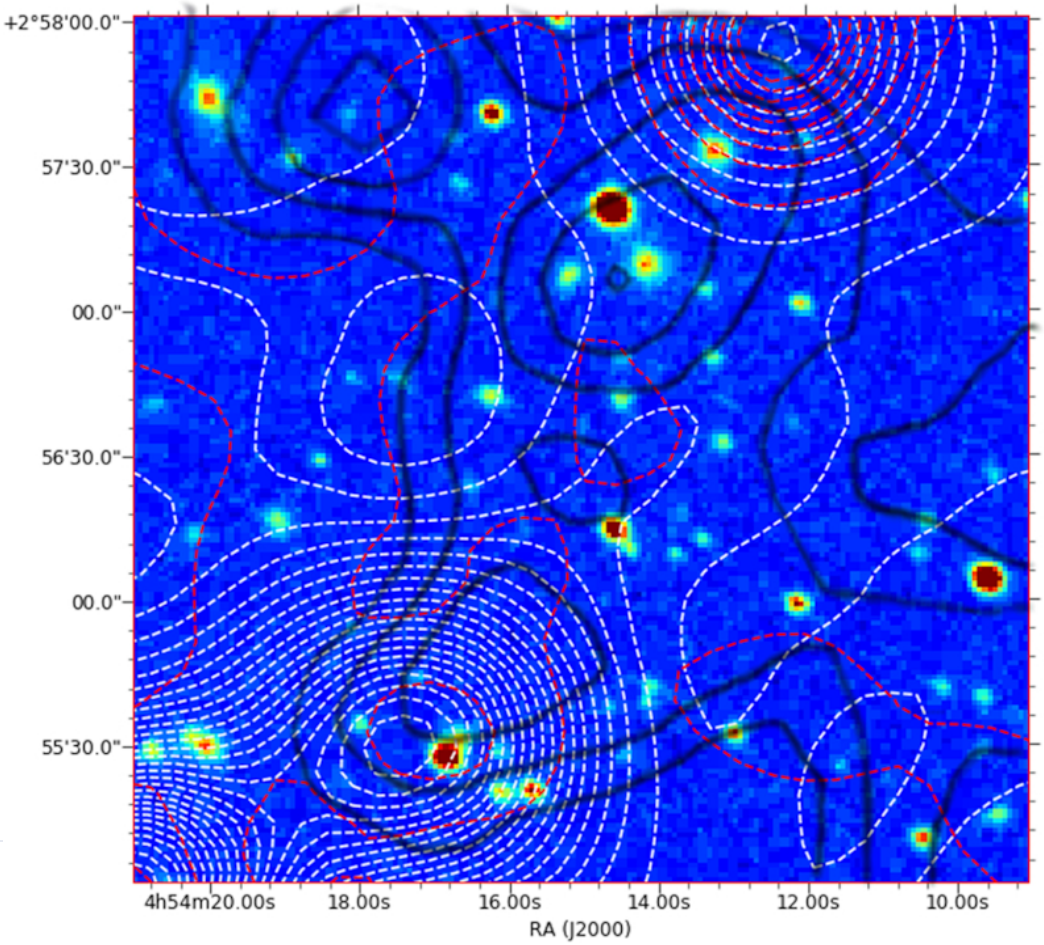


FIGURE 2.3: Optical image from ESO DSS with NVSS (white), TGSS (red), and from weak lensing (from Wang, Markevitch, and Giacintucci, 2016; black) overlapped.

$S_{74\,\mathrm{MHz}}$ (mJy)	$S_{150\,\mathrm{MHz}}$ (mJy)	$S_{1400\,\mathrm{MHz}}$ (mJy)
14.9 ± 5.2	7.01 ± 0.13	0.450 ± 0.047

TABLE 2.1: Radio fluxes estimated in a circular region centred in RA = 04 54 15.0, Dec. = + 02 56 31.4, and with a radius of 35 arcsec, as obtained from the surveys VLSSr (74 MHz), TGSS (150 MHz), and NVSS (1.4 GHz).

Then we calculated the hadronic and the DM emission in this region by using the models described in the previous section. According to the magnetic field model used in the previous calculations, we should expect at the distance of the P2 region from the cluster centre a magnetic field of the order of $\sim$3.8 μG and a thermal gas density of $\sim 1.6 \times 10^{-3}$ cm^{-3}. Since the size of this region is small compared to the core radius of the cluster, we use a constant magnetic field and constant densities of thermal electrons and non-thermal protons inside the region. According to Clowe et al., 2012, the mass of the P2 subhalo is $M = 4.08 \times 10^{13}$ M$_\odot$, from which the parameters for a NFW model $r_s = 112$ kpc (similar to the radius of the region we analysed) and $\rho_s = 1.37 \times 10^4 \rho_c$ can be derived.

In Fig. 2.4 we show the radio emission produced in this region for the hadronic and DM models, using for the hadronic model a reference pressure ratio $P_{CR}/P_{th} = 4$ per cent, higher than the one providing the best fitting to the whole radio halo. Even with this value, the DM emission appears to be dominant with respect to the hadronic one. This is because in a small region the contribution of the central peak of the DM emission is more important than the one provided from the flat profile of non-thermal protons. The expected DM radio emission is smaller than the flux estimated from the surveys in this region by a factor of 1.3–1.4.

We also found that, by using instead a magnetic field of the order of 5 μG, it is possible to obtain a radio flux produced by DM similar to the observed one (lower panel of Fig. 2.4). Since we do not have information on the magnetic field in this cluster, this possibility cannot be excluded. We note also that the model with neutralino mass 43 GeV reproduces the spectral shape of the radio emission better than the 9 GeV model. Therefore, the DM emission in the P2 region can be dominant on the hadronic one if the normalization of the DM emission is the same than the one that can reproduce the radio halo flux in Coma, and this suggests that the contribution of DM to the radio emission in the cluster, if present, can be found in this region.

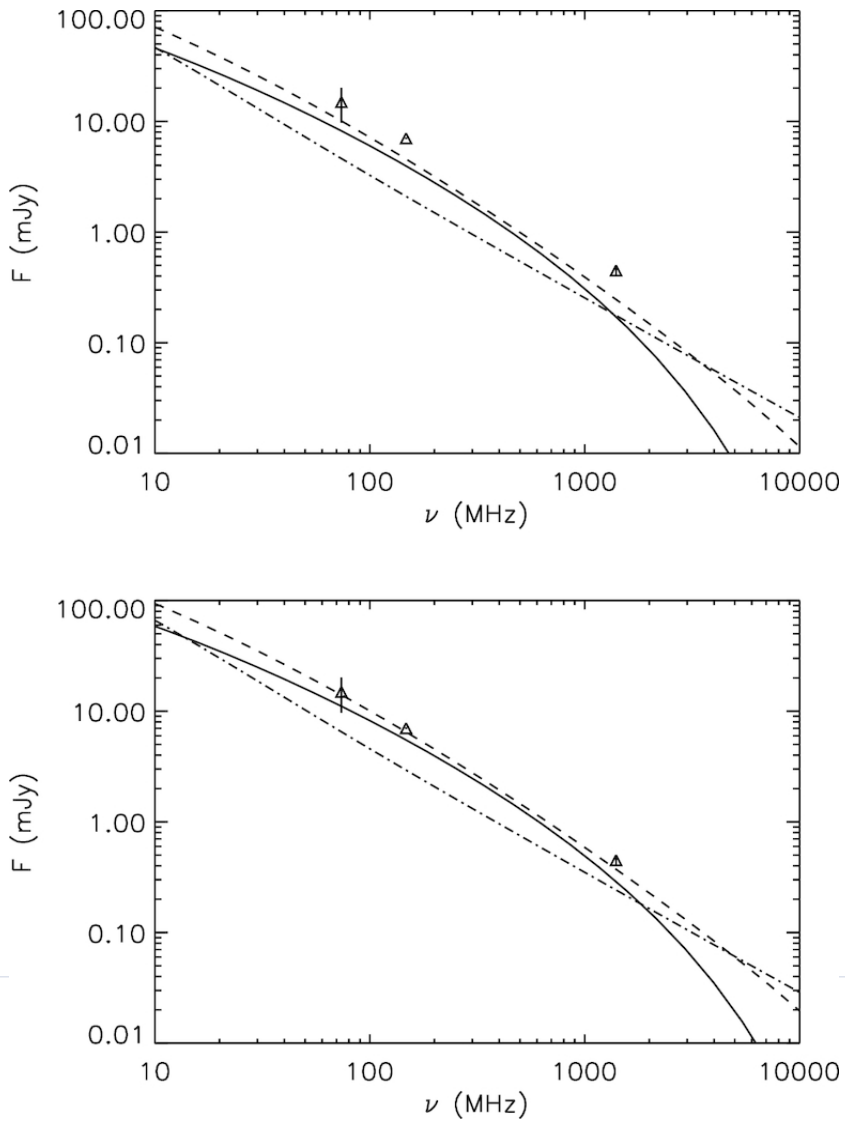


FIGURE 2.4: Spectrum of the radio halo flux in the region P2 of A520 for a magnetic field of 3.8 μG (upper panel) and 5 μG (lower panel) and for: (i) a neutralino model with mass M_χ = 9 GeV, annihilation final state $\tau^+\tau^-$, $\mathcal{B}\times < \sigma v > = 6\times10^{-25}$ cm^3 s^{-1} (solid line); (ii) a neutralino model with mass M_χ = 43 GeV, annihilation final state $b\bar{b}$, $\mathcal{B}\times < \sigma v > = 4\times10^{-24}$ cm^3 s^{-1} (dashed line); (iii) a hadronic model with proton spectral index s_p = 2.2 and a pressure ratio P_{CR}/P_{th} =4 per cent (dot–dashed line). Data are from Table 2.1.

2.4 High-energy emission

In this section we discuss if the emission produced in the high-energy bands (X-ray and gamma-ray) is suitable to be detected with present or forthcoming instruments, in order to understand if with this kind of observations it is possible to discriminate between the different models and derive more information on the properties and the origin of cosmic ray particles in A520 and in the P2 region.

In Fig. 2.5 we show the high-energy emission given by the sum of the Inverse Compton Scattering of the cosmic microwave background photons and non-thermal bremsstrahlung with the thermal ions from the secondary electrons, and the gamma-ray emission produced by neutral pions decay, for the three models we used in the past section, and for the two regions we considered: the whole cluster (upper panel), and the P2 region (lower panel).

We can see that in the whole cluster the hadronic emission dominates over the emission of DM origin along the whole spectrum, whereas in the P2 region the DM emission is stronger than the hadronic one in the X-ray band (between 0.3 and 400 keV for the 43 GeV model, and between 1 and 150 keV for the 9 GeV model), while in the gamma-rays the hadronic emission is generally stronger than the DM one, except for the spectral region between 1 and 10 GeV for the 43 GeV mass model, and between 2 and 4 GeV for the 9 GeV model. However, all these emissions are well below the sensitivity of present and forthcoming instruments (in the same Figure we show, for reference, the sensitivities of Astro-H for 100 ks of integration and Fermi-LAT for 10 yr) even for the whole cluster, so we do not expect that observations in these bands can help to discriminate the origin of the non-thermal emission in A520.

2.5 Discussion

Like in the Bullet cluster (Marchegiani and Colafrancesco, 2015)), in A520 the emission of DM origin probably is not producing the whole radio halo, but can be dominant in some regions of the cluster. In the whole cluster the baryonic emission is expected to be dominant on the DM one.

In the SW part of the cluster a possible source of acceleration of cosmic rays

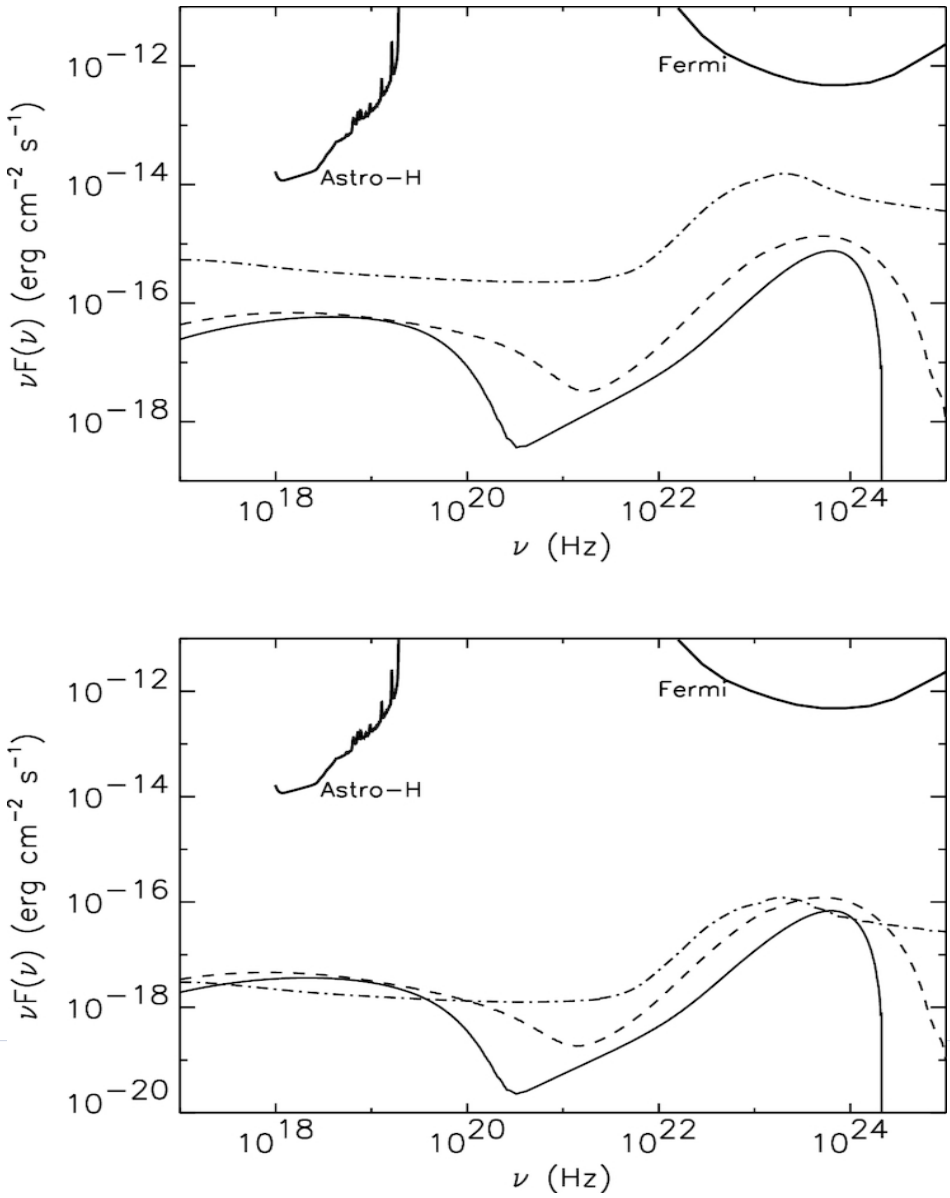


FIGURE 2.5: Spectral energy distribution of the high-energy emission from the whole cluster A520 (upper panel) and the P2 region (lower panel) for: (i) a neutralino model with mass M_χ = 9 GeV, annihilation final state $\tau^+\tau^-$,$\mathcal{B}\times < \sigma v >$ =6×10^{-25} cm^3 s^{-1} (solid line); (ii) a neutralino model with mass M_χ = 43 GeV, annihilation final state $b\bar{b}$, $\mathcal{B}\times < \sigma v >$ =4×10^{-24} cm^3 s^{-1} (dashed line); (iii) hadronic model with proton spectral index s_p = 2.2 and pressure ratios P_{CR}/P_{th}=2.6 per cent in the whole cluster and 4 per cent in the P2 region (dot–dashed line). We also show the sensitivity curves of Astro-H for 100 ks of time integration (from http://astro-h.isas.jaxa.jp/researchers/sim/sensitivity.html) and Fermi-LAT for 10 yr (from Funk, Hinton, and Consortium, 2013)

is the bow shock associated with the BCG at the edge of the radio halo that is moving outwards; however, Wang, Giacintucci, and Markevitch, 2018, using Chandra X-ray observations, found that the Mach number associated with this shock is $\mathcal{M} = 2.4^{+0.4}_{-0.2}$; according to the Diffusive Shock Acceleration theory (Drury, 1983), particles accelerated by a shock with this Mach number should produce a radio emission with a spectral index equal to or steeper than 1.3, that is steeper than the values of 1.1–1.2 found in this region Vacca et al., 2014. Another possible source of cosmic rays is the BCG itself, that can have injected the particles during its passage through the Intra Cluster Medium (ICM). Since the particles are diffused up a distance of the order of 500 kpc (much higher than the typical diffusion length of electrons in magnetized plasma in galaxy clusters, that is of the order of 50 kpc, see e.g. Blasi and Colafrancesco, 1999), this emission probably is of hadronic origin.

In the NE part of the cluster we have identified a peak of the radio halo that is located very close to one of the peaks of the DM distribution (the P2 peak in (Clowe et al., 2012)). We have found that in this region the emission of DM origin is expected to dominate on the emission of baryonic origin, if the DM has properties similar to the ones providing the best fitting to the spectrum of the radio halo in Coma Marchegiani and Colafrancesco, 2016, when optimistic, but possible, values for the annihilation cross-section and the substructure boosting factor are assumed. Therefore, if a contribution from DM to the radio halo is present in this cluster, it needs to be searched in this region. We note that, while in the Coma cluster the DM model providing the best fitting to the radio halo spectrum is the one with mass 9 GeV and annihilation final state $\tau^+\tau^-$, in the P2 region of A520 the model providing the best fitting to the radio spectrum is the one with mass 43 GeV and annihilation final state $b\bar{b}$. Therefore other studies, even considering similar situations in other clusters, need to be performed in order to clarify the strength of this result.

The whole NE part of the radio halo is more extended than the P2 region alone, that has a radius similar to the core radius expected for a DM halo having the corresponding mass ($\approx$115 kpc); therefore other mechanisms that can accelerate the electrons on larger scales need to be present. The apparent separation of the NE part of the radio halo from the SW part suggests that other mechanisms different from the injection from the BCG can take place. As suggested by Wang, Giacintucci, and Markevitch, 2018, a possible

mechanism is the reacceleration caused by merger-induced turbulences, as suggested also by the high values of the temperature found in this region (Govoni et al., 2004; Wang, Markevitch, and Giacintucci, 2016). Another possibility is that an important role is played by the radio galaxy labelled with D in Vacca et al., 2014: in the temperature map of Govoni et al., 2004 it is possible to see that a region of hot gas is present on the west of the galaxy (i.e. in the probable direction of its motion), and is bending north and south of the galaxy. It is therefore possible that the bow shock produced by the galaxy motion is providing energy to the cosmic ray electrons by diffusive shock acceleration or adiabatic compression. A shock is not visible in this region of the X-ray maps (Wang, Markevitch, and Giacintucci, 2016), but this fact can be explained because this radio galaxy is probably part of a subcluster that is falling on the main cluster along a direction close to the line of sightProust et al., 2000. It is also possible that the radio galaxy, by crossing a merger shock front, is giving origin to a relic-like structure (like in the case of Perseus cluster, see Pfrommer and Jones, 2011) that would appear roundish because associated with a shock front produced in a merger happening close to the line of sight, as suggested by Vacca et al., 2014.

2.6 Conclusion

In this paper we have found that in the cluster A520 the radio emission produced by DM is expected to be lower than the emission of baryonic origin. However, DM can have an important role in the region around the subhalo P2, where a peak of the radio emission is detected.

We have estimated the radio flux in the P2 region, and found that DM models with the same properties as the ones providing a good fitting to the radio halo in the Coma cluster (Marchegiani and Colafrancesco, 2016) predict a radio emission similar to the observed one, for a magnetic field of the order of 5 μG. The best-fitting model suggested by the spectral shape of the radio emission in the P2 region is for a neutralino with mass 43 GeV and annihilation final state $b\bar{b}$; this situation is different from the Coma case, where the favourite model was for mass 9 GeV and final state $\tau^+\tau^-$.

In the SW part of the cluster, a possible origin of the radio halo is given by hadronic interactions, where the cosmic rays are injected by the BCG moving

through the ICM. In the NE part, other than the DM in the P2 region, an important role can be played by the radio galaxy D that is probably interacting with the ICM, emitting cosmic rays and/or producing a bow shock.

Finally, the expected high-energy emission from the whole cluster and the P2 region is well below the sensitivities of present and forthcoming instruments, and therefore measures in high-energy spectral bands do not appear to be suitable to obtain better information on the non-thermal emission in A520.

Acknowledgements

SC passed away during the final stages of the preparation of this paper; he gave a valuable contribution to its realization and we strongly thank him. We also thank Prof. J. Carter for his support in a difficult moment. This work is based on the research supported by the South African Research Chairs Initiative of the Department of Science and Technology and National Research Foundation of South Africa (Grant No 77948). PM and NK acknowledge support from the Department of Science and Technology/National Research Foundation (DST/NRF) Square Kilometre Array (SKA) post-graduate bursary initiative under the same Grant

Chapter 3

Archival radio observations of the Abell 1689 cluster

This chapter of the thesis focuses on the multi-frequency radio analyses of the Abell 1689 cluster and its diffuse radio emission.

Note: This chapter is adapted from the ongoing work by: Khanye N.F., Thwala S.A. and Marchegiani P., tittled "*Archival radio observations of the Abell 1689 cluster* ". The work is currently being prepared for submission to the Monthly Notices of Royal Astronomy journal.

The candidate is the primary author of this work and has been responsible for retrieving, mapping and analysis of the data. The candidate is also co-writing the manuscript with Thwala S.A., under the supervision of Dr. Marchegiani and Dr. Beck.

Abstract

Over the course of recent years, our knowledge on the evolution and dynamics of galaxy clusters has improved.This is due to the progress in radio and X-ray surveys and in the development of theoretical models which try to explain the intra-cluster medium (ICM). These advances in understanding have raised more questions about the origin of cluster magnetic fields and the origin of large areas of diffuse synchrotron emission, such as radio halos. In this paper, we present new radio analyses of the Abell 1689 galaxy cluster, using publicly available archival data from the VLA; GMRT; MWA; SDSS and WISE surveys. We use the radio observations to help us understand and map out the morphology and spectral properties of the radio emission in the cluster. The optical and infrared observations are then used to cross match the observed features with their possible optical and infrared counterparts. We calculated the integrated flux density of the radio halo to be 8.7 mJy at 1400 MHz and 202.9 mJy at 147.5 MHz from the NVSS and TGSS observations respectively. We also, for the first time, present the spectral index image of the cluster using observations from the NVSS and TGSS observations and find a power-law correlation in the radio spectrum of the diffuse emission, with a spectral index of α= -1.34 (where S$\propto \nu^{\alpha}$).

3.1 Introduction

The radio emission observed in galaxy clusters is usually attributed to the effects of shocks and turbulence that produce (re-)acceleration of relativistic particles in magnetic fields which permeate the cluster atmospheres (Feretti et al., 2012). Clusters contain different sources of radio emissions ranging from active galactic nuclei (AGN) to enormous regions of diffuse radio emission which lack optical counterparts. The large regions of diffuse radio emission are thought to result from the re-acceleration of relativistic particles and can be classified into three classes: (i) radio halos, (ii) radio mini-halos and (iii) radio relics. Radio halos are large low-surface brightness diffuse radio sources which are generally located at the cluster centre with a very steep spectrum ($\alpha \leq$ -1, where S$\propto \nu^{\alpha}$). They have a regular spherical morphology and are mostly found to be unpolarized. Examples of galaxy clusters which host radio halos are Abell 2163 in (Feretti et al., 2001) and Abell 1351 (Giovannini et al., 2009). Radio mini-halos are similar to radio halos, with the differentiating factors being that, they are usually found in relaxed, cool-core

clusters, coupled with the extent of the radio emission (around the central radio galaxy) being confined to smaller scales (∼500 kpc, see e.g., Ignesti et al., 2020 and references therein). Examples of galaxy clusters that host mini-halos are Abell 2029 and the Ophiuchus cluster (Govoni et al., 2009). Radio relics are also large low surface brightness regions, however, unlike radio halos they are mostly located in the peripheral regions of the cluster and have an elongated, irregular morphology. Radio relics are usually strongly polarized e.g the Toothbrush cluster (Ogrean et al., 2013) and the double radio relic found in CIZA J2242.8+5301 (Van Weeren et al., 2010; Van Weeren et al., 2011).

The origin of diffuse radio emissions in galaxy clusters is still up for debate. This is due to the difficulty in explaining their large sizes and the short life span of radiating electrons, which are vital for their occurrence. A number of models have been introduced to try and explain their puzzling origin. This includes: (i) the widely accepted primary acceleration model, which attributes the occurrence of radio halos to the diffusion of relativistic electrons into the intra-cluster medium (ICM) by different events occurring in the cluster, such as shocks and turbulence from cluster merger events (Rephaeli, 1979; Brunetti et al., 2004) and AGN activities (Jaffe, 1977; Ferrari et al., 2008); (ii) the secondary electron model, which predicts that relativistic electrons may result from the inelastic hadronic collisions between non-thermal and thermal protons from the hot gas in the ICM (Blasi and Colafrancesco, 1999); and (iii) the secondary electron production from dark matter (DM) annihilation model, which predicts the generation of gamma-rays, electrons and positrons during the annihilation of DM particles such as weakly interacting massive particles (WIMPs) (Colafrancesco and Mele, 2001; Bertone, Hooper, and Silk, 2005; Colafrancesco, Profumo, and Ullio, 2006).

The occurrence of radio relics in galaxy clusters is also highly associated with the presence of merger shocks within the cluster's X-ray gas, which are caused by highly energetic merger events that are capable of re-accelerating cosmic rays. The merger shocks are expected to lead to the amplification of magnetic fields in the cluster and enable the occurrence of large areas of diffuse emission on the outskirts of the clusters, when they come in contact with relativistic electrons. This phenomena can also lead to the formation of shock fronts, which are sharp contact discontinuities between regions of the ICM gas with different entropies. Shock fronts exhibit a sharp gas density

edge and a temperature jump (prerequisites for determining the gas velocity and density jumps in the ICM). Shock fronts have been observed in a few galaxy clusters that host diffuse radio emission (Markevitch et al., 2005a; Markevitch, 2005b).

In this work, we present the radio observations of Abell 1689 (A1689 from here-on) at four different radio frequencies, while also paying attention to the properties of the diffuse radio emission found in the cluster, whose presence was first reported by Vacca et al., 2011. We also provide the spectral analyses of the cluster using an integrated radio spectrum and spectral index images of the cluster, to develop a better understanding of the energy spectrum of the relativistic electrons.

Throughout the paper we have employed a flat, vacuum dominated cosmological model with H_0= 69.6 km $s^{-1}Mpc^{-1}$, Ω_m = 0.286, Ω_Λ = 0.714 . With these parameters the luminosity distance of A1689 at z = 0.183 is D_L = 894.6 Mpc and 1 arcmin corresponds to 185.94 kpc

3.2 Abell A1689

A1689 is a massive optically rich galaxy cluster at redshift $z = 0.183$ (Struble and Rood, 1999). The cluster is well used for strong and weak gravitational lensing studies due to its display of gravitational arcs, arclets and multiple image systems as seen in the optical regime (Broadhurst et al., 2005a). The cluster also hosts the largest Einstein radius known so far (Tyson, Valdes, and Wenk, 1990; Taylor et al., 1998; Oguri and Blandford, 2009) and further strong lensing studies have also revealed several substructures with different concentrations in the central and north eastern regions of the cluster. These optical properties and the discrepancies in mass, $\sim$ 10, between the X-ray and gravitational lensing observations (Tyson and Fischer, 1995; Shan et al., 2010; Sereno et al., 2013) are what makes A1689 an interesting laboratory for indirect studies of dark matter (Sereno and Umetsu, 2011). XMM-Newton observations compared with ASCA, ROSAT and Chandra data suggest that the cluster is in a post merger scenario, with the core of the cluster not being fully relaxed (Andersson and Madejski, 2004; see Vacca et al., 2011 for a comprehensive review of the clusters, X-ray, dynamics and history).
Vacca et al., 2011 reported on the detection of diffuse radio emission in the cluster, at 1200 and 1400 MHz, using the Very Large Array (VLA) in different

Parameter	value	ref
RA (J2000)	13 11 30.2	-
DEC (J2000)	-01 20 10.6	-
z	0.183	Struble and Rood, 1999
$L_x^{0.1-2.4}$	1.2×10^{45}	Vacca et al., 2011
$M_{\rm cool}$ ($M_\odot {\rm yr}^{-1}$)	$683\ ^{239}_{128}$	Chen et al., 2007
$t_{\rm cool}$ (Gyr)	4.7 ± 0.4	Chen et al., 2007
M_{200} ($M_\odot h^{-1}$)	$1.25 \pm 0.3 \times 10^{14}$	Leonard, King, and Goldberg, 2011
$S^{\rm RH}_{1200\ {\rm MHz}}$ (mJy)	11.7 ± 3.4	Vacca et al., 2011
LLS (kpc)	730	Vacca et al., 2011
$P^{\rm RH}_{1200\ {\rm MHz}}$ ($\times 10^{24}$ WHz^{-1})	1.08	Vacca et al., 2011

TABLE 3.1: Global properties of the A1689 cluster and its radio halo (written as RH) at 1200 MHz.

configurations. The diffuse emission spreads over the central regions of the cluster and is mostly outshined by several radio galaxies found throughout the cluster. The authors estimated the largest linear size (LLS) of the diffuse emission to be $\sim$ 730 kpc and classified the emission as a small radio halo with a central radio brightness of $\simeq 1.7\ \mu$Jy/arcsec^2 at 1200 MHz and estimated a flux density of 9.9 mJy at 1400 MHz, for the radio halo. They also investigated the radio halo–X-ray correlation of the cluster, using Chandra X-ray observations, and found that there is a non-linear relation due to the radio radial profile being much flatter than the X-ray profile. The global properties of the cluster are listed in Table 3.1.

3.3 Observations and imaging

To perform the study, on the extended radio emission in the galaxy cluster, we used archival radio continuum observations from six radio surveys (full survey descriptions are detailed below): VLSSr, TGSS, GLEAM, NVSS, FIRST, and VLASS at their respective central frequencies of 74; 150; 200; 1400; 1400 and 3000 MHz, by retrieving images of the galaxy cluster from their image cutout services. The cutout images were already cleaned and calibrated by the relevant survey teams before being publicly released, and thus, no calibration (step) was necessary for this study.

We discuss the specifications of each of the surveys used, their data reduction methods and how we carried out the image analyses in the following sections. A summary of all the radio continuum images used in this study is provided in Table 3.2.

3.3.1 VLSSr

The VLA Low frequency Sky Survey imaged the sky north of declination -30°, at 74 MHz (bandwidth of $\Delta\nu \sim 1.56$ MHz) and a resolution of $80^{''} \times 80^{''}$. The observations were made between 2001 to 2007 in the VLA B (for a declination in the range: $-10^{\circ} < \delta < 80^{\circ}$) and BnA (for $\delta < -10^{\circ}$ and $\delta > 80^{\circ}$) configurations. The survey has an intergrated time of ≈ 75 minutes per pointing achieving an rms noise level of 100 mJy/beam (Cohen et al., 2007). For our study we used the re-reduced VLSS data, the VLSS Redux (VLSSr) which re-processed the VLSS data using an older version of the AIPS software (Lane et al., 2014). The final VLSSr catalogue contains over 92 000 radio sources with a resolution of $75^{''} \times 75^{''}$ (see Lane et al., 2014 for more details). The observation of A1689 with VLSS was carried out on the 20th of September 2003, the image retrieved had an rms value of 110 mJy/beam and was observed at the 73.5 MHz.

3.3.2 TGSS ADR1

The TIFR GMRT Sky Survey alternative data release 1 (TGSS ADR1) is a publicly accessible catalogue based on the GMRT observations of the radio sky at 150 MHz ($\Delta\nu \sim 16.7$ MHz) and an angular resolution of $25^{''} \times 25^{''}$. The survey achieved over 2000 hours of observations with each pointing being carried for about 15 minutes between the declination of -20° and +60°(Intema et al., 2017). The data was processed using the GMRT's automated radio data pipeline, SPAM (Source Peeling and Atmospheric Modeling) which is a python based program that uses AIPS (the Astronomical Image Processing Pipeline) to reduce low frequency, high resolution interferometric radio data (see Intema et al., 2009; Intema et al., 2017 for more information). The observation of the A1689 cluster were carried out on the 16 of March 2016 at a frequency of 147.5 MHz and a resolution of $27^{''} \times 25^{''}$, with an rms value of 3 mJy/beam.

3.3.3 GLEAM

The GaLactic and Extragalactic All-Sky MWA (GLEAM) survey is one of the Square Kilometre Array (SKA) pathfinder telescopes. The survey maps the entire sky, south of the declination δ = +25°, at radio frequencies ranging from 72 to 231 MHz ($\Delta\nu \sim 7.68$ MHz), grouped into four central frequencies: 88; 118; 155 and 200 MHz. The observations were made from August 2013

and lasted for 2 years (see Wayth et al., 2015 for more details). In this study we use the data released from the first year of observation, the data reduction process was carried out by the GLEAM team and has been described in Hurley-Walker et al., 2017. We selected an image observed at 200 MHz on the 9th of August 2013 with an rms value of 6.4 mJy/beam.

3.3.4 NVSS

The NRAO VLA Sky survey (NVSS) is a publicly accessible archive containing more than 1.8 million radio sources with flux densities stronger than $S_{1.4\,\mathrm{GHz}} > 2.5$ mJy. The NVSS mapped the sky at 1400 MHz ($\Delta\nu \sim 50$ MHz) north of declination $\delta = -40^{\circ}$, using the VLA D and DnC configurations between September 1993 and October 1996 for a total of 2700 hrs. The NVSS catalogue completely overlaps with the TGSS ADR1 catalogue (see Condon et al., 1998b for more details). The observations of the A1689 cluster was carried out on the 27th of February 1996 with an rms value of 0.53 mJy/beam.

3.3.5 FIRST

The Faint Images of the Radio Sky at Twenty centimeters survey (FIRST in short (Becker, White, and Helfand, 1995)) was carried out using the NRAO VLA at 1400 MHz in the B-array between 1993 and 2002. The survey is the radio equivalent of the Sloan Digital Sky Survey (SDSS) covering $\sim 10,000$ square degrees of the North and South Galactic Cap. The archive consists of 3-minute snapshots which cover a hexagonal grid using fourteen 3 MHz frequency channels. The survey's 5σ flux density limit is 1 mJy, with a restoring beam FWHM of 5.4 arcsec and an rms of 0.15 mJy/beam. The final catalog is expected to contain $\sim 9 \times 10^5$ radio sources, roughly 40% of which are resolved on scales from 2-30 arcsec[1]. The observation of the A1689 cluster was carried out in August of 1998 with an rms value of 0.15 mJy/beam.

3.3.6 VLASS

The Very Large Array Sky Survey (VLASS) is a synoptic, all-sky radio survey being carried out with the Karl G. Jansky VLA in B-configuration and S-band, between the period of September 2014 and October 2024. The survey has a central frequency of 3000 MHz ($\Delta\nu \sim$ 2-4 GHz) with an angular

[1] http://sundog.stsci.edu/

Survey	ν(MHz)	Resolution	$\sigma_{\rm rms}$(mJy/b)	Obs. date
VLSSr	73.5	$75'' \times 75''$	109.75	2003/09/20
TGSS DR1	147.5	$27'' \times 25''$	3.22	2016/03/15
GLEAM-4	200	$142'' \times 132''$	18.97	2014/03/10
NVSS	1400	$45'' \times 45''$	0.53	1995/02/27
FIRST	1400	$5'' \times 5''$	0.15	1998/08/-
VLASS	3000	$3'' \times 2''$	0.17	2019/04/21

TABLE 3.2: Properties of the A1689 radio continuum images used in this study. Col. 1: survey name, col. 2: observation frequency, col. 3 synthesized beam size, col. 4: noise value of each image and col. 5 observation date.

resolution of $\sim 3''$ and a sensitivity goal of 70 μJy at 1σ. VLASS will use approximately 5500 hours and observe the whole sky north of of declination $\delta = -40^{\circ}$ covering a total of 33,885 square degrees (see Lacy et al., 2020 for a detailed description of the survey). The A1689 cluster was observed on the 21st of April 2019 with an rms value of 0.17 mJy/beam.

3.3.7 Imaging and Analysis

The differences in survey configurations, resolution and sensitivity across the publicly available archival image products requires a detailed systematic approach to matching complementary surveys for extended emission analyses. We made informed decisions about which surveys to match, from the considered data products, by considering the nature of the extended radio and diffuse emission found in proximity of the galaxy cluster.
In light of the fact that diffuse emission has a low-surface brightness, which is typically resolved out in high angular resolution images, we opt for the usage of lower angular resolution surveys (with survey configurations) that are optimised for extended emission, namely TGSS and NVSS in this study, to map out the spectral properties of the relativistic electrons characterising this emission. We note that there are still issues with the differences in integration times, affecting the observed depth and extent of the sources (see Thwala et al., 2019) which cannot be trivially addressed.

The high angular resolution images (with increased sensitivity, namely FIRST and VLASS in this study) map and probe the radio emission at deeper depths, allowing us to better distinguish candidate sources of the observed extended emission. We used products from these two surveys to perform multi-wavelength

cross matching, with infrared and optical counterparts and produce a spectral index map of the cluster sources at mid-high frequencies. Thus, given the two survey combinations of TGSS with NVSS, and FIRST with VLASS; we can provide spectra analyses of the cluster's diffuse emission and candidate radio sources, respectively, using the computed spectral index maps between 150-1400 MHz and 1400-3000 MHz (see Figure 3.7). We now detail the image packages used to produce these results and the integrated flux values.

The imaging in this paper was done using the Common Astronomy Sofware Application (or CASA in short, Jaeger, 2008) and python, using Astropy (and its affiliated packages; Price-Whelan et al., 2018). We used PyBDSF (Python Blob Detector and Source Finder, Mohan and Rafferty, 2015) to perform source finding, subtraction (see Section 3.4.3.) and calculate the integrated flux density, as well as the rms values of the radio continuum images used. To match the image area and resolution, in preparation for the computation of the spectral index and error maps, we utilised Miriad (Sault, Teuben, and Wright, 2006) for re-gridding and smoothing the previously mentioned survey combinations (where we smoothed the higher angular resolution image, to match the resolution of the lower angular resolution image, see Section 3.4.4 for a full description of how the specific surveys were matched). The spectral index maps and their error maps were then computed using Astropy.

3.4 Results

3.4.1 Radio emission and cluster sources

Figure 3.1 and 3.2 show the radio maps of the cluster as observed by VLSSr, TGSS, and NVSS at 74, 150, and 1400 MHz. At these frequencies, the central region of the cluster is dominated by a very bright emission, resulting from multiple radio galaxies (RGs, labelled A; B; BiC and C in Figure 3.3). The FIRST and VLASS radio contours resolve one of these sources, labelled A in Figure 3.3, to be a double jet extended radio galaxy, coincident with an optical and infrared counterpart (see Figure 3.3, and discussion in 3.4.2). Sources B, BiC, and C appear to be point sources in both surveys.

Mid-high frequency observations also confirm the appearance of additional

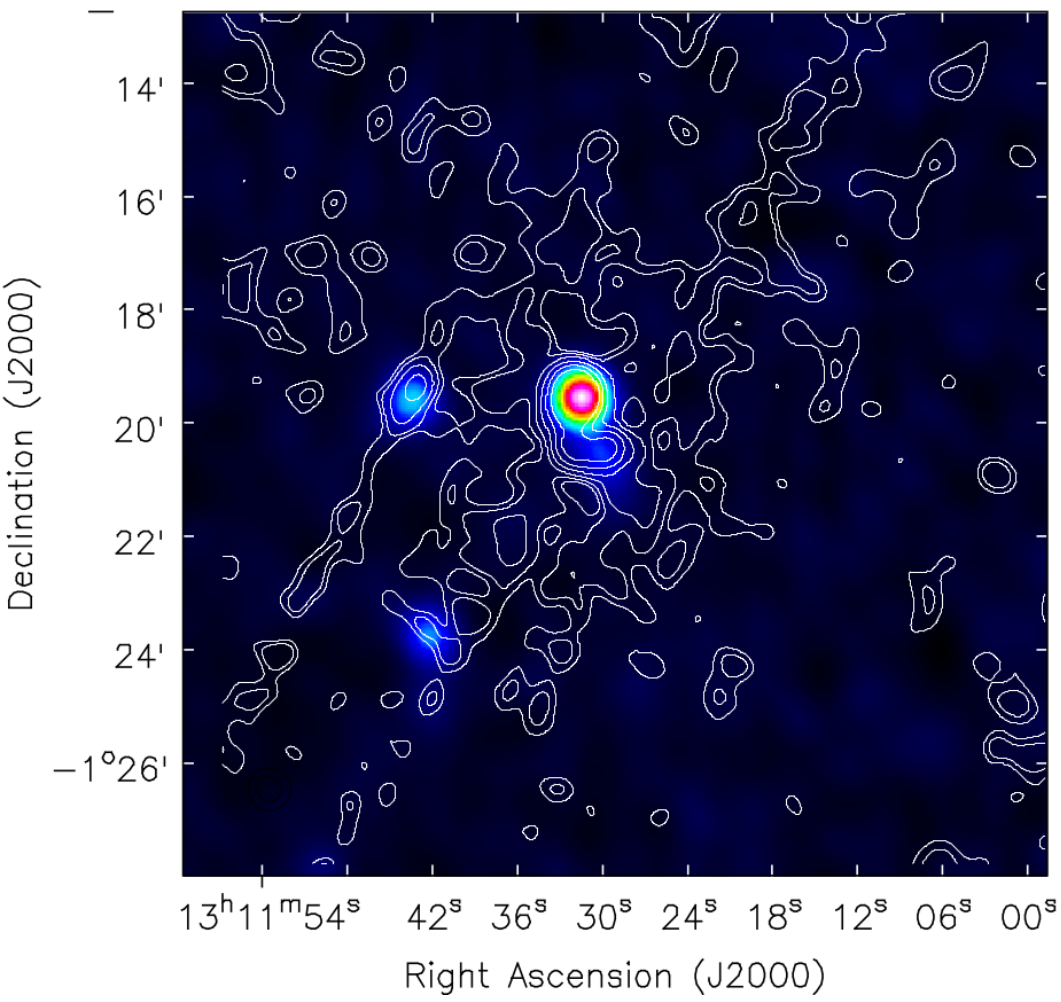


FIGURE 3.1: The NVSS 1400 MHz radio image of the cluster shown in colour with a resolution of $45'' \times 45''$ and rms noise of 0.5 mJy/b, overlaid with the GMRT 147.5 MHz radio contours. The contour lines are drawn at [1,2,4,8,16,...] $\times$ 2.5σ_{rms}, where σ_{rms}=3.22 mJy/b.

RGs (D and E in Fig. 3.3)) towards east of the cluster as observed by Vacca et al., 2011. These seem to dim with a decrease in observing frequency, with a detection of the northern source in TGSS and no detection for both sources, in the VLSSr image. This is likely to be caused by the sensitivity of the low frequency surveys as well as the low-surface brightness of the sources.

The lower resolution images, in Figure 3.1, reveal the presence of diffuse radio emission that permeates the cluster, surrounding the central RGs, and extends beyond the centre of the cluster.

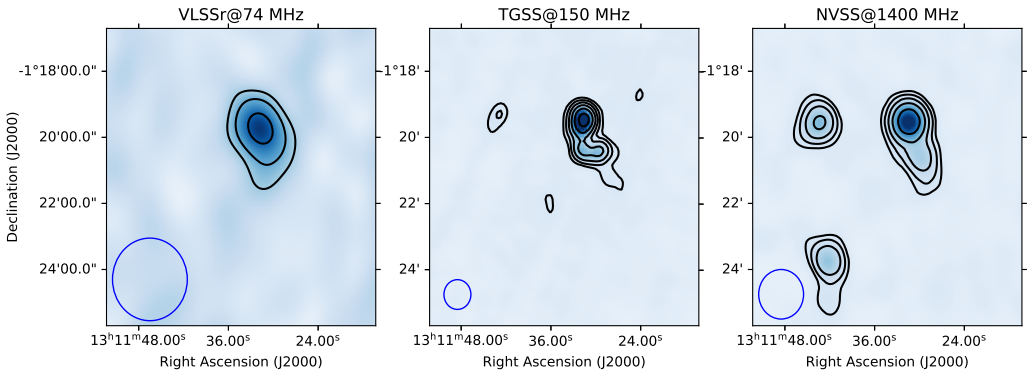


FIGURE 3.2: Left to right: Radio continuum images of each titled survey (and observed frequency) with their respective contours levels drawn at $[1, 2, 4, 8, 16, 32, 64] \times 5\sigma_{\mathrm{rms}}$, where $\sigma_{\mathrm{rms}_{\mathrm{VLLSr}}}, \sigma_{\mathrm{rms}_{\mathrm{TGSS}}}, \sigma_{\mathrm{rms}_{\mathrm{NVSS}}} = [109.75, 3.22, 0.53]$ mJy/beam. The beam sizes are shown on the lower left corner, with a resolution of $75'' \times 75''$, $27'' \times 25''$ and $45'' \times 45''$ for VLSSr, TGSS and NVSS, respectively.

3.4.2 Multi-ν counterparts

In order to learn more about the bright emission that dominates the cluster's centre, we turned to observations from the FIRST and VLASS surveys at 1400 MHz and 3000 MHz, with a resolution of $5'' \times 5''$ and $3'' \times 2''$, respectively. We overlapped the FIRST and VLASS observations with infrared (IR) observations from the Wide-field Infrared Survey Explorer (WISE, Wright et al., 2010) telescope. We do this in order to understand the positions of the RGs in relations to each other and confirm the number of existing point sources in the cluster centre and along the cluster's field-of-view in the radio frequencies. The resulting image is show in Figure 3.3.

The IR-Radio observations reveal that the centre of the cluster has four radio emitting galaxies, three of which were reported in detail by Vacca et al., 2011, these galaxies are labelled as galaxies A, B and C in Figure 3.3. Galaxy A is the cluster's dominant radio-galaxy, located 64.25 arcsec away from the cluster centre and associated with the optical source, TGN259Z069, which has a redshift of $z = 0.187$. Galaxy B is a radio-galaxy associated with the optical source SDSSJ131130.2-0120, which has a redshift of $z = 0.181$. Vacca et al., 2011 revealed that this point source is located at the cluster's X-ray peak. Galaxy C appears to be the dimmest RG, compared to all the other central RGs, and is associated with an optical source, Slee ACO 1689 12, located at $z = 0.195$.

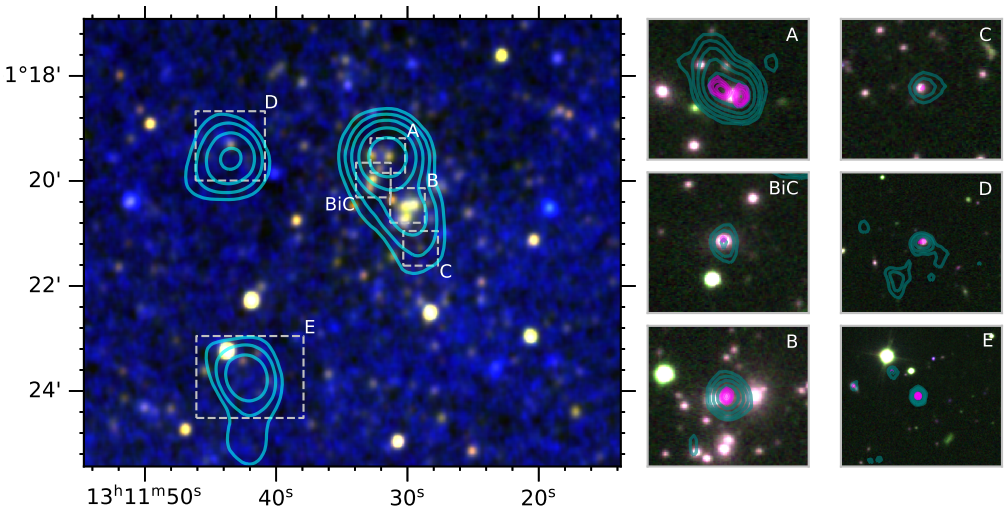


FIGURE 3.3: Left: WISE infrared (W1, W2 and W3 bands) image of the cluster overlaid with the NVSS contour levels at [1,2,4,8,16,32,64]$\times 5\sigma_{\text{rms}}$, where $\sigma_{\text{rms}} = 0.53$ mJy/beam. Right: SDSS (r, g and i bands) images of the highlighted, silver infrared, regions with FIRST (teal;$\sigma_{\text{rms}_{\text{FIRST}}} = 0.15$ mJy/beam) and VLASS (magenta;$\sigma_{\text{rms}_{\text{VLASS}}} = 0.17$ mJy/beam) contours at [1,2,4,8,...]$\times 3\sigma_{\text{rms}_{\text{FIRST}}}$ and $5\sigma_{\text{rms}_{\text{VLASS}}} + 3\sigma_{\text{rms}_{\text{VLASS}}} \times [0, 1, 2, 4, 8, ...]$, respectively.

The fourth central radio source (associated with the optical source 2MASX J13113265-0119590), which we labelled as BiC in Figure 3.3., is outshined by the dominant radio-galaxy, making it very easy to miss at low frequencies and poor resolutions due to its proximity to the dominant radio-galaxy. This radio-galaxy is located 55.45 arcsec away from the cluster centre and is associated with the brightest galaxy in the cluster (BiC) in the X-ray band, which is located at $z = 0.202$. This difference in redshifts amongst the central galaxies can also indicate the possibility of sub-cluster mergers occurring in the cluster.

We have listed the properties of the four central radio sources and the two peripheral sources (D and E) foubd in the cluster and along its field of view in Table 3.3, where we used Simbad[2] and the Space Science Data Centre (SSDC) Sky Explorer[3] tool to study the redshift, source name and the classification of the cluster's point sources. We used PyBDSF to calculate the flux densities of the galaxies at 147.5 MHz with TGSS and 1400 MHz with FIRST. We calculated the flux density values of the point sources, we modelled the

[2]http://simbad.u-strasbg.fr/simbad/
[3]https://tools.ssdc.asi.it/

Sources	RA (J2000)	DEC (J2000)	$S_{147.5\,\mathrm{MHz}}$ (mJy)	$S_{1400\,\mathrm{MHz}}$ (mJy)	z	Object type
A^F	13:11:31.5	-01:19:31	443.53 ±29.01	41.95±1.92	0.187	RG
B^G	13:11:30.0	-01:20:28	119.32 ± 12.05	8.44 ±0.73	0.181	RG
C^I	13:11:29.0	-01:21:17	111.5 ± 10.56	2.14 ±0.22	0.195	RG
BiC^H	13:11:32.6	-01:19:59	-	2.04 ±0.19	0.202	BiC
D^J	13:11:43.5	-01:19:20	51.29 ± 4.81	6.22±0.61	0.183	RG
E^K	13:11:42.0	-01:23:44	-	10.09 ±0.92	-	RG

TABLE 3.3: Position, radio and general properties of the radio sources found in A1689 and along its field-of-view. Col. 1 shows the label of the cluster sources, Cols. 2 and 3 are the coordinates of the sources, Cols. 4 and 5 are their integrated flux densities at 147 MHz and 1400 MHz, Col. 6 is the redshift of the source and Col. 7 is the classification of the point source. (RG- radio-galaxy, BiC - Brightest galaxy in the cluster in Simbad). The associated source names (or identifier in Simbad) of each labelled sources are: *F* - TGN259Z069, *G* - SDSSJ131130.2-0120, *H* - 2MASX J13113265-0119590, *I* - A1308-0150D, *J*- TGN259Z044 , *K*- Slee ACO 1689 18 .

point sources as described in Section 3.4.3. We are unable to obtain an integrated flux density value for the point source associated with the optical source 2MASX J13113265-0119590 at 147.5 MHz as the source cannot be distinctly resolved from Galaxy A by the TGSS.
In Figure 3.1, the diffuse emission permeating the cluster seems to extend beyond the cluster central region at 147.5 MHz, while at 1400 MHz the diffuse emission is almost completely outshined by the the prominent point sources. However, to better understand the extend of the diffuse emission in all the frequencies we have to separate the point sources from the diffuse emission.

3.4.3 Diffuse emission in A1689

Flux density estimation

To estimate the flux density of the diffuse radio emission in the cluster, we have to start by subtracting the flux densities of all the compact radio sources (and their extended emission) from the total emission in the cluster. We used PyBDSF to model the point sources, with a Gaussian fitting function and estimated their corresponding integrated flux densities (such as the ones presented in Table 3.3) at the different observed frequencies. The FIRST survey was used to resolve positions of potential point sources within the studied fov and 13 point sources were identified.

To get the integrated flux density of the diffuse radio emission, the total

ν (MHz)	73.5	147.5	200	1200	1400
S_ν (mJy)	497.3 $\pm$ 61.3	202.9 $\pm$ 19.8	153.3 $\pm$ 16.8	11.7 $\pm$ 3.4	8.7$\pm$ 0.86

TABLE 3.4: Flux densities of the diffuse emission found in the galaxy cluster at different radio frequencies, including the 1200 MHz flux density value from Vacca et al., 2011. The values at 147.5 MHz and 200 MHz are taken as upper limits, due to the poor resolution of the VLSSr and GLEAM observations.

flux density contributions of the embedded point sources (and their extended emission) at that particular frequency are modelled and then subtracted from the total emission in the observed radio image in PyBDSF . The resulting images then produces a low-surface brightness residual map that contain emission which could not be modelled as point sources by the source finder. We then use this emission to calculate the diffuse emission contained within the fov of the continuum radio images.

The errors in the flux density measurements of the diffuse emission are estimated by taking into account the errors that are caused by the flux densities used to calibrate the radio images and the errors resulting from the noise of the image. These two errors are then added together for the flux density error estimation, using the formula:

$$\Delta S_\nu = \sqrt{(\sigma_{\rm cal} S_\nu)^2 + \left(\sigma_{\rm rms}\sqrt{N_{\rm beam}}\right)^2}, \tag{3.1}$$

where $\sigma_{\rm cal}$ is the uncertainty in the calibration, $\sigma_{\rm rms}$ is the noise of the radio image as obtained from from the FITS files and $N_{\rm beam}$ is the number of beams present in the extended source. We assumed $\sigma_{\rm cal}$ to be 10 % for the TGSS, NVSS and GLEAM images (Intema et al., 2017; Condon et al., 1998b; Hurley-Walker et al., 2017) and assumed it to be 15% for the VLSSr images (Lane et al., 2014).

Table 3.4 shows the flux densities of the diffuse emission at the different radio frequencies, after the subtraction of all the point sources. We found the flux density of the diffuse emission at 147.5 MHz to be $S_{147.5\,\rm MHz}$ = 202.9$\pm$19.8 mJy and to be $S_{1400\,\rm MHz}$ = 8.7$\pm$0.86 mJy at 1400 MHz, for the NVSS survey. We have also included the value from Vacca et al., 2011 at 1200 MHz on our table. The VLSSr and GLEAM images had the highest noise levels due to their surveys' low resolutions and poor sensitivities, making them less ideal for detecting low-surface brightness features such as radio halos. Thus, their

resulting integrated flux densities of the diffuse emission at 73.5 MHz and 200 MHz are taken only as upper limits. The flux density at 1400 MHz is comparable to the the value estimated by Vacca et al., 2011 at 1400 MHz, which was 9.9 mJy. We didn't find any diffuse emission in the VLASS and FIRST radio images above 3σ.

We use the flux density values stated in Table 3.4. to plot a radio spectrum for the diffuse emission in the cluster. The radio spectrum is shown in Figure 3.4 and it includes the flux density value of the Radio halo at 1200 MHz as calculated by Vacca et al., 2011. The flux density values at 73.5 MHz and 200 MHz are also expressed as upper limits in the radio spectrum. Using the radio spectrum plot, we see that the diffuse emission in the cluster follows a power law relation with a steepness of α_{diffuse}= -1.34$\pm$0.14 using a linear fit. We estimate this value as the spectral index of the diffuse emission. This spectral index value and the flux density value $S_{1400\,\text{MHz}}$ = 8.7 $\pm$0.86 corresponds to a radio power $P_{1400\,\text{MHz}}$= 9.81 $\pm$ 0.77 $\times$ 10^{23} WHz^{-1} at 1400 MHz.

Morphology of diffuse emission

Figure 3.5 shows the diffuse emission map in the cluster at 147.5 MHz after the subtraction of the point sources as described in the previous subsection. At 147.5 MHz the diffuse emission extends beyond the central regions of the cluster, this is in agreement with what has been observed at 1200 MHz by Vacca et al., 2011, where the radio halo was mainly concentrated at the cluster centre. The diffuse radio map at 147.5 MHz reveals that the cluster hosts numerous diffuse radio filaments and peaks, with the major peak being found in the cluster centre. The major peak, labelled L, displays an irregular morphology and has sharp edges and occupies the cluster centre. this is the same structure detected at 1200 MHz by Vacca et al., 2011. We found that the longest linear size (LLS) of the radio halo peak located at the centre, peak A, to be LLS $\sim$720 kpc at 147.5 MHz. This value is not too far from the one reported in Vacca et al., 2011, where they found LLS=730 kpc for the radio halo. However, we expected this value to be greater than 730 kpc at 147.5 MHz as radio halos tend to appear bigger in size at lower frequencies, due to lower frequencies being optimal for the detection of low surface brightness radio emission. We may be obtaining a lower LLS value due to the sensitivity limitations and calibration & cleaning techniques of publicly available TGSS data. The short LLS may also hint at the diffuse emission being in a

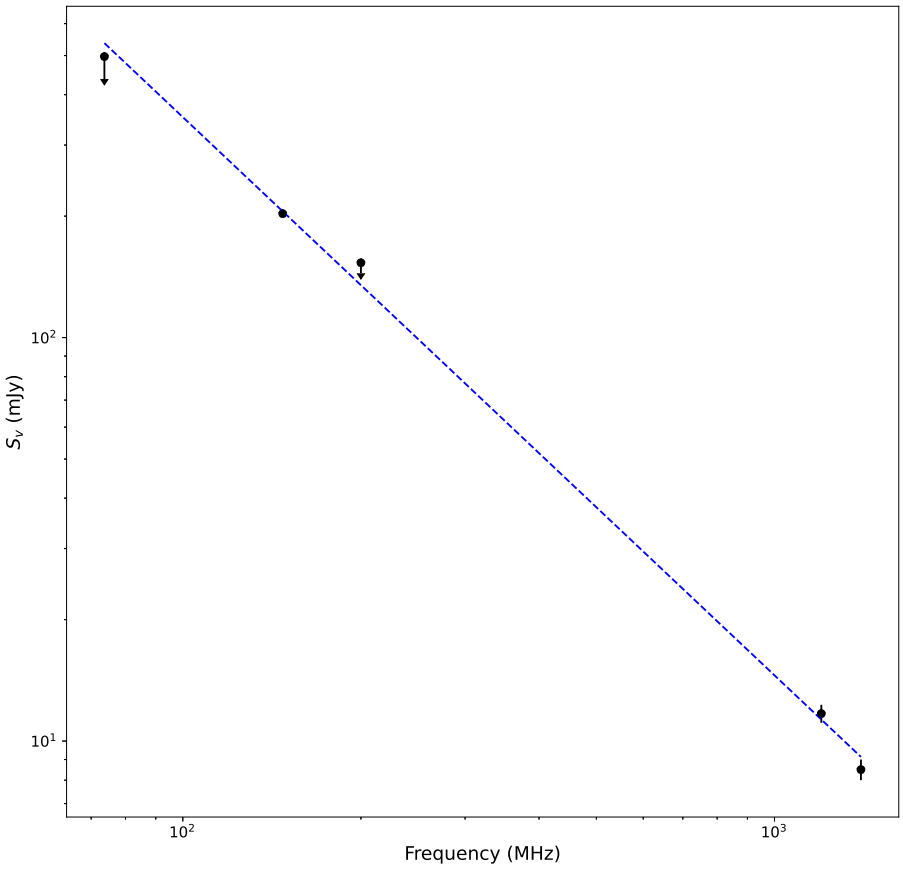


FIGURE 3.4: The spectrum of the diffuse emission found the A1689 cluster at frequencies ranging from 73.5 MHz to 1400 MHz with the errors obtained through equation 3.1, we have also included the flux density at 1200 MHz as calculated by Vacca et al. (2011). The blue line is the linear fit to the data.

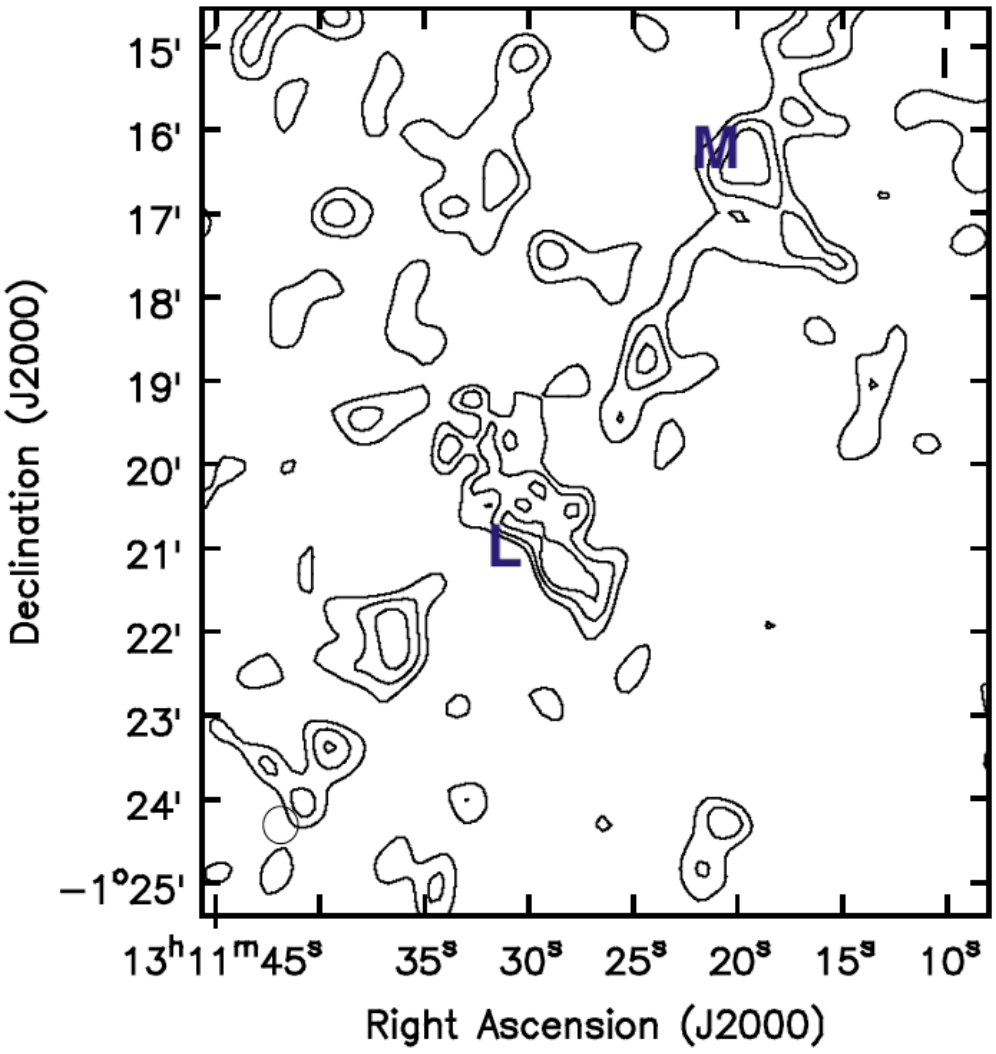


FIGURE 3.5: The 147.5 MHz radio contours of the diffuse emission found in the cluster after the subtraction of point sources using PyBDSF. The resolution of the image is $\sim 27'' \times 25''$. The contour levels are [1,2,4,8,16,...]$\times 3\sigma_{rms}$ where σ_{rms}= 3.22 mJy/b.

transitional phase from being a mini-halo to a radio halo, with the gas sloshing of the central galaxies and sub-cluster mergers as possible sources of the turbulence producing diffuse radio emission. The central diffuse emission is expected to be incident with the X-ray peak of the cluster as shown in Vacca et al., 2011. In figure 3.6 we compare the LLS of the cluster's radio halo to other well known radio halos at different cluster redshift. From figure 3.6 we observe that the LLS, for the radio halo in A1689, obtained from this study is small to medium sized when compared to radio halos of the same redshift range..

We also observe the presence of another irregular diffuse structure in the north-western region of the cluster, labelled M, this is the second largest diffuse structure after the main one found in the cluster. There is a possibility that the irregular diffuse structure is a radio relic, however, this possibility has to be investigated independently with low frequency radio observations paired with polarization and X-ray studies. The rest of the radio filaments, spread unevenly throughout the cluster, although most of them are found in the northern to south eastern regions of the cluster. Most of the filaments also form part of the diffuse radio emission as they mostly lack optical counterparts. The diffuse filaments can also result from possible smaller scale sub-cluster merger events, which have not been able to destroy the central cool-core of the cluster.
The main diffuse structure is still quite small in size even at 147.5 MHz compared to most radio halos, raising the possibility of a mini-halo instead, although this will be hard to argue at this sensitivity.

3.4.4 Spectral index imaging

Spectral index images can be used to constrain the energy spectrum of relativistic electrons and for studies of magnetic field distribution in clusters hosting diffuse radio emission.Thus, providing useful information to understand the formation and evolution of cluster merger processes.
In order to further examine the cluster dynamics of A1689 at radio frequencies, we computed spectral index distribution maps of the cluster using a combination of images from TGSS & NVSS, at low-mid frequencies and images from FIRST & VLASS, at mid-high frequencies, with overlapping coverages.

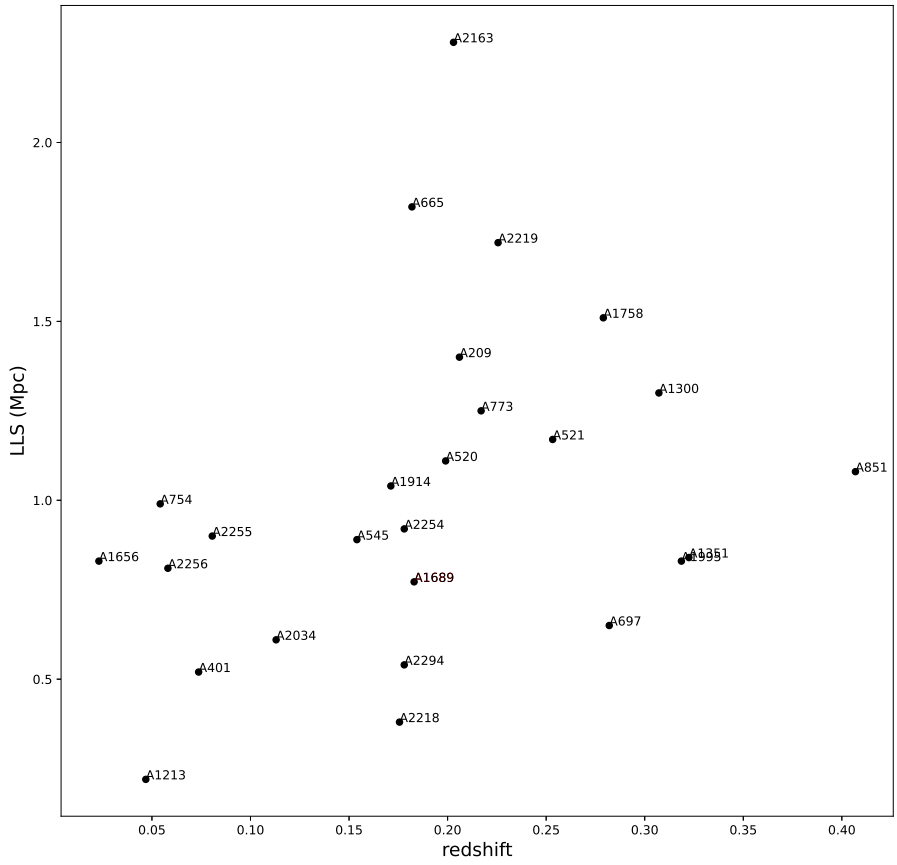


FIGURE 3.6: The largest linear sizes of some well known radio halos compared to the redshift compared to the LLS for A1689 (in red) found in this study. Data points are taken from Feretti et al., 2012

.

For the preparation step, the TGSS radio continuum image was re-gridded to match the size of the NVSS image. We then smoothed the TGSS image (using the SMOOTH task in MIRIAD) in order to match it to the resolution of the NVSS image(i.e., $45'' \times 45''$) with a 2-D elliptical Gaussian function. The same process was followed to match the high resolution VLASS image with the FIRST image. The spectral index image was created using ASTROPY and its affiliated packages, where regions with surface brightness values that are less than desired noise level of each image were blanked out. The formula used for the spectral index map was of the form: $S_\nu \propto \nu^\alpha$, where S_ν is the surface brightness at a frequency ν and α is the spectral index value. The uncertainty in the spectral index value was calculated using the formula:

$$\Delta\alpha = \frac{1}{\ln\left(\frac{\nu_1}{\nu_2}\right)} \sqrt{\left(\frac{\sigma_{1,\mathrm{rms}}}{I_1}\right)^2 + \left(\frac{\sigma_{2,\mathrm{rms}}}{I_2}\right)^2} \tag{3.2}$$

where $\sigma_{1,2,\mathrm{rms}}$ are the rms values of the TGSS & NVSS and FIRST & VLASS images. $I_{1,2}$ are the surface brightness values of the respective frequencies at each pixel and $\nu_1 > \nu_2$.

Figure 3.7. shows the resulting spectral index and error map between 147.5 MHz & 1400 MHz, alongside the spectral index images (computed between 1400 & 3000 MHz) of the previously highlighted regions in Figure 3.3. From the computed spectral index maps, we notice that the central region of the cluster does not show enhanced spectral index features, with the spectral index of the extended radio source varying from $\alpha^{1400\mathrm{MHz}}_{147.5\mathrm{MHz}} = -1.8$ to $\alpha^{1400\mathrm{MHz}}_{147.5\mathrm{MHz}} = -0.8$. The central flatter regions have an average value of $\alpha^{1400\mathrm{MHz}}_{147.5\mathrm{MHz}} = -1.0$, surrounded by regions which steepen towards the edges of the source.
The two peripheral regions have flatter spectral index values, with region E exhibiting average inverted spectral index values closer to $\alpha^{1400\mathrm{MHz}}_{147.5\mathrm{MHz}} = 0.2$, and average flatter $\alpha^{1400\mathrm{MHz}}_{147.5\mathrm{MHz}} = -0.35$ for region D. We note that this is likely to be caused by the sensitivity of the TGSS survey, since both region D and E are sites of low-surface brightness emission that might not be properly picked up by the legacy survey. If these features are not from systematics, a possible interpretation of the physical phenomenon could be that; since A1689 is a cool-core cluster, most of the energy radiated by the source is radiated at higher frequencies. This would potentially explain why the extension of the

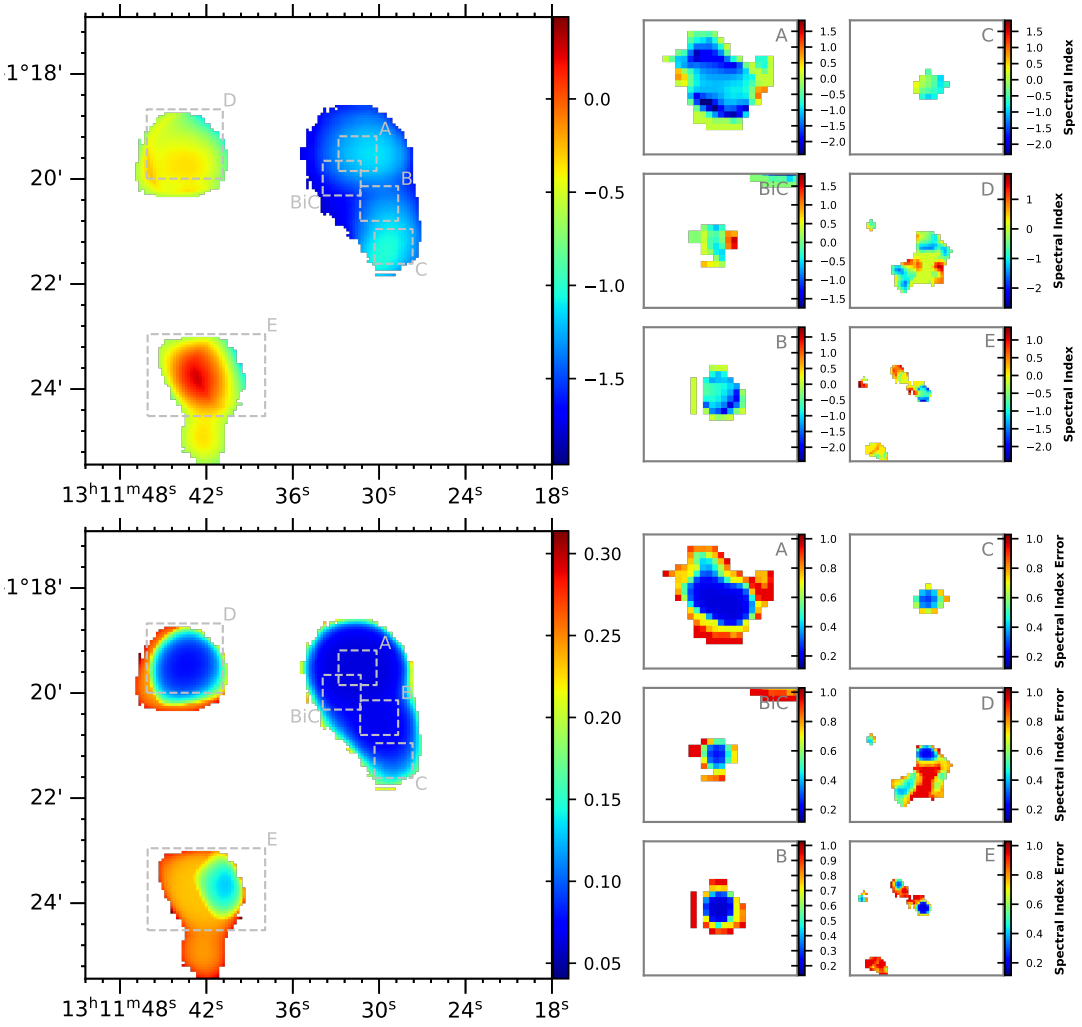


FIGURE 3.7: **Top left panel:** Spectral index map between 147.5 and 1400 MHz at a resolution of $45'' \times 45''$, with a mask that covers the same region as the NVSS continuum image in Fig 3.2. **Top right panel:** Spectral index maps between 1400 and 3000 MHz at a resolution of $5'' \times 5''$, with a mask that covers the same region as the FIRST continuum image for values higher than $5\sigma_{\mathrm{rms}}$, highlighting identical regions found in Fig 3.3. **Bottom left and right panels:** The corresponding spectral index error maps of the detailed top panels.

source is decreasing with frequency and why we are not observing a consistent power-law relation that is expected with synchrotron emission.

We also notice that the centre of the cluster is the steepest region, with α <-2**.** This steepness is due to the combination of all the unresolved point sources at the central regions of the cluster and along its field of view. This poor resolution of unrelated sources creates an unevenly steep central region compared to other regions with resolved radio maps in the cluster.

We currently refrain from using these spectral index images to estimate the spectral index of the cluster's diffuse radio emission, since the diffuse emission in the NVSS, 1400 MHz image does not extend as much as the diffuse emission on the 147.5 MHz image. Also the mask used to blank out values in the spectral index image was derived from the FIRST radio map and so it leaves out most of the diffuse radio emission observed at 147.5 MHz.

3.5 Summary and conclusion

In this paper we studied the radio properties of A1689 using archival radio observations from numerous radio telescopes. The study confirmed the presence of an irregular shaped radio halo in the central regions of the cluster, as previously reported by Vacca et al., 2011 at 1200 MHz. We found that the diffuse emission in the cluster is outshined by four radio-galaxies found in the cluster's centre, one of which is the central radio-galaxy, located at redshift z= 0.187 and with flux density of $S_{147.5\,\mathrm{MHz}}$= 443.53 mJy.

At 147.5 MHz we also found the existence of more diffuse radio structures and filaments which spread over the cluster. These diffuse filaments could result from the re-acceleration of cosmic electrons by small scale sub-cluster mergers. We also found the LLS of the main radio halo at 147.5 MHz to be LLS$\sim$ 720 kpc which is within range to the value of LLS = 730 kpc reported by Vacca et al., 2011 at 1200 MHz. We expected the LLS value to be more than 730 kpc at 147.5 MHz, however due to the spatial resolution, calibration and imaging techniques of the TGSS, we obtained a smaller value for the LLS.
Due to the NVSS's short baseline, it is insensitive to extended, low surface brightness emissions larger than $15^{'}$ and so using PyBDSF we tried our best to estimate the integrated flux density of the diffuse emission at 1400 MHz. We

found the flux density of the diffuse emission in the cluster to be $S_{1400\,\mathrm{MHz}}$= 8.7 $\pm$ 0.86 mJy which is not that far from the value of $S_{1400\mathrm{MHz}}$ =9.9 mJy, estimated by Vacca et al., 2011. A spectral analysis of the cluster from the integrated flux densities of the diffuse emission at 5 frequencies shows that the diffuse emission in the cluster follows a power law relation. We estimated the spectral index value of the diffuse emission to be $\alpha_{\mathrm{diffuse}}$ = -1.34. $\pm$ 0.14. This spectral index value and the flux density value at 1400 MHz corresponds to the radio power of the diffuse emission to be $P_{1400\,\mathrm{MHz}}$= 9.81 $\pm$ 0.77 $\times$ 10^{23} W Hz^{-1} In this study we have also presented the first spectral index image of the cluster, computed between 147.5 MHz & 1400 MHz and 1400 MHz & 3000 MHz. The spectral index image reveals that the central region of the cluster is the steepest, most likely due to the combination of different radio-galaxies.

The revelation of the radio halo and more diffuse radio filaments at 147.5 MHz compared to higher observational frequencies shows the importance of combining low radio frequencies and sharp sensitivity in telescopes for the optimal detection of diffuse radio emission. An improvement in the sensitivity and spatial resolution of the observations at lower frequencies would allow us to study the relationship between the diffuse emission and the central radio-galaxies in the cluster better. This study can be possible for the cluster with the launch of the SKA, which will assist in the study of the cluster dynamics which lead to the occurrence of diffuse emission.

Data availability

All the data used in this work is available on the archives of the NVSS[4], TGSS[5], VLSS[6], MWA[7], VLASS[8] and FIRST [9] websites.

[4]https://www.cv.nrao.edu/nvss/
[5]http://tgssadr.strw.leidenuniv.nl/doku.php
[6]https://heasarc.gsfc.nasa.gov/W3Browse/all/vlss.html
[7]https://www.mwatelescope.org/gleam
[8]https://science.nrao.edu/science/surveys/vlass
[9]https://science.nrao.edu/science/surveys/first

Acknowledgements

NFK and ST acknowledges support from the Department of Science and Technology/National Research Foundation(DST/NRF) Square Kilometre Array (SKA) post-graduate bursary initiative under the same Grant.

Chapter 4

Effects of DM annihilation on the radio halo found in A1689.

On this chapter we look at the multi-frequency effects of dark matter annihilation in the Abell 1689 galaxy cluster using radio observations.

Note: This chapter is adapted from the work: Khanye N.F. and Marchegiani P. "*Effects of dark matter annihilation on the radio halo found in A1689*" which is being reviewed with the Monthly Notices of Royal Astronomy Society (MNRAS). Submission no: **MN-21-1393-MJ**.

The contribution of the candidate was very significant and it included: producing all the images, graphs and writing all the text in the manuscript, under the supervision of Dr Marchegiani.

Abstract

Aim: As part of an ongoing effort to study the influence of dark matter in emission found in galaxy clusters, we study the multi-frequency predictions of various dark matter annihilation scenarios in the Abell 1689 galaxy cluster in order to explore the possibility that the diffuse emission found in the cluster originates from the annihilation of dark matter particles.
Methods: We study the multi-frequency radio spectrum expected to result from three dark matter annihilation models with light (m_χ=10 GeV), intermediate (m_χ=40 GeV) and high (m_χ=100 GeV) dark matter particle masses at three different annihilation channels i.e the $b\bar{b}$, $\mu^+\mu^-$ and $\tau^+\tau^-$ channels. The spectra are obtained by constraining the DM particle cross section upper limits using known radio properties of the diffuse emission found in Abell 1689.
Results: We find that the best fit for the WIMP annihilation cross section to be higher than canonically thermally average annihilation cross section of $< \sigma v >= 3\times10^{-26}\mathrm{cm}^3\mathrm{s}^{-1}$ by an order of 2 to 3 times using an NFW profile . We also find that the best dark matter scenario to reproduce the observed radio properties of the radio halo to be when m_χ=10 GeV through the $b\bar{b}$ final states with the magnetic field strength of B_0=10 μG and the cross section value of $< \sigma v >= 6.60\times10^{-25}\mathrm{cm}^3\mathrm{s}^{-1}$.

4.1 Introduction

The origin of dark matter (DM), which makes up to $\sim$ 80% of the matter in the universe is still unknown. Although numerous attempts to directly detect and study DM have been made over the past several decades, all the studies have came back empty handed. This is why scientist have also focused on indirect studies of DM to try and constrain properties of DM particles (Carr et al., 2015; Conrad and Reimer, 2017; Stref, Lacroix, and Lavalle, 2019). Albeit the particle nature of DM is still unknown, there are several constrains from observations (or lack thereof) that any potential DM candidate is expected satisfy and these are (Profumo, 2017; Buckley and Peter, 2018):
(*i*) DM particles are expected to be non-relativistic i.e "cold", because if DM particles were relativistic then large astrophysical systems such as galaxy clusters would form first while smaller systems such as galaxies would form later, which is not the case;
(*ii*) DM particles are expected to be "dissipation-less" and therefore very weakly

interact with electromagnetic radiation and among themselves;
(*iii*) DM particles must also be stable, if they were unstable most of the DM in the universe would've already decayed with very little trace of it left and so its lifetime is expected to be approximately the same as the universe.

Several DM particle candidates, such as axions; primordial black holes and weakly interacting massive particles (WIMPs), which may be able to explain the nature of particle DM have been proposed (see Bertone, Hooper, and Silk, 2005; Colafrancesco, Profumo, and Ullio, 2006; Bergström, 2009 for a further discussion on candidates and properties of DM particles). WIMPs are the best motivated candidates for DM as they are assumed to be weakly interacting, cold and massive ranging in the scales of GeV to TeV. WIMPs are considered to be a group of Majorana self-annihilating particles, which can yield Standard Model particles as products of its annihilation.The resulting Standard Model products from WIMP annihilation are expected to generally yield a wide range of observable electromagnetic emissions such, as γ-rays, X-rays and radio emission (Regis and Ullio, 2008; Bœhm et al., 2014). The resultant electromagnetic emission will be a result of the Standard model products (such as electrons) interacting with magnetic fields that permeate galaxy cluster through the following processes:
(*i*) γ-ray emission can be formed from the prompt decay of neutral pions or from the radiative process of bremsstrahlung radiation which is produced by the deceleration of a charged particle when it is deflected by another charged particle.
(*ii*) X-ray emission can also result from bremsstrahlung radiation or from Inverse Compton (IC) scattering which occurs when a photon is scattered by a charged particle, which is usually an electron.
(*iii*) Radio emission may result from synchrotron radiation which is produced when relativistic electrons are accelerated through a magnetic field.

Observations of γ-ray in galaxy clusters can be used to confirm the existence of electromagnetic radiation resulting from the annihilations of DM particles inside DM halos. However, attempts to detect γ-ray observation in galaxy clusters have not been entirely successful so far (Bringmann and Weniger, 2012; Macías-Ramírez et al., 2012; Acciari et al., 2018). Although Adam et al., 2021 recently reported a possible detection of γ-rays in the Coma cluster with the FERMI-LAT, this is yet to be confirmed (see Ackermann et al., 2010; Ackermann et al., 2012; Ackermann et al., 2015 for detailed information). An

observation of non-thermal X-ray emission resulting from the annihilation products is difficult to detect as the emission cannot be differentiated from X-ray emission resulting from other baryonic activities in the intra-cluster medium (Jeltema and Profumo, 2008; Zandanel, Weniger, and Ando, 2015). This leaves us with the option of studying large scale non-thermal emission found in clusters, which are also expected to be one of the by-products of WIMP annihilation, the best way to study this emission is to study the diffuse radio emission such as radio halos that are found in some galaxy clusters. This indirect method of studying DM has been used to constrain the rate and annihilation cross section of DM annihilation of galaxies and galaxy clusters inside DM halos such as the Coma, the Ophiuchus and the Bullet clusters (Storm et al., 2013; Marchegiani and Colafrancesco, 2015; Marchegiani and Colafrancesco, 2016; Kiew, Hwang, and Zainal Abibin, 2017) and galaxies such as the M31, M49 and NGC4636 (Colafrancesco, Profumo, and Ullio, 2007; Regis et al., 2014; McDaniel, Jeltema, and Profumo, 2018; Kar et al., 2019) .

In this chapter we focus on the massive cool-core galaxy cluster Abell 1689 (referred to as A1689 from here-on) which is located at $z = 0.183$. A1689 is an optically rich cluster which is widely used in gravitational lensing studies due its rich presence of lensed arcs and arclets of strong and weakly lensing background galaxies (Miralda-Escude and Babul, 1994; Tyson, Valdes, and Wenk, 1990; Limousin et al., 2007; Sereno and Umetsu, 2011). The cluster's lensing properties have also been widely used to indirectly map and study its dark matter composition (Nieuwenhuizen, 2009; Halkola, Seitz, and Pannella, 2007). The cluster also has the largest known Einstein radius so far. A1689 hosts a small radio halo which is located in its central region, the radio halo was first discovered by Vacca et al., 2011 when they used VLA 1200 MHz observations to study the cluster's radio features. They estimated the longest linear size of the cluster to be $\approx$ 730 kpc with a central radio brightness of $\approx 1.7\ \mu\text{Jy/arcsec}^2$ at 1200 MHz. They also estimated the flux density of the radio halo at 1400 MHz to be 9.9 mJy by assuming that the flux density at 1400 MHz to be 85% of the value the flux densities at 1200 MHz which they found to be 11.7 mJy. This estimation was motivated by an estimation of the spectral index between the two frequencies to be α=1. In Khanye, Thwala, and Marchegiani, 2021 we also conduct an extensive study of the radio emission found in the cluster including the diffuse radio emission using the VLA, GMRT and MWA radio archival data at 73.5 MHz, 147.5 MHz and 200 MHz.

The occurrence of a radio halo in A1689 supports the argument made by Leonard, King, and Goldberg, 2011 that the cluster may have recently undergone a merger, showing that the cluster is not in a relaxed state.

By assuming the that the diffuse emission in the cluster results from the annihilations of WIMPs, in this chapter we aim to use the cluster's radio observations to constrain the DM annihilation cross section of A1689. We also study the radio spectrum that is expected to result from the annihilation of WIMPs in the cluster and compare it with the observational data of the radio halo.

The rest of this chapter is structured as follows, in Section 4.2. we describe the models and parameters we have used to calculate the WIMP annihilation cross section and the resultant multi-frequency radio spectra. In Section 4.3. we take a brief look at the radio properties of the cluster using archival radio observations. In Section 4.4. we present the constraints of the WIMP annihilation cross section for the $b\bar{b}$, $\tau^+\tau^-$ and $\mu^+\mu^-$ annihilation channels. In Section 4.5. we study the expected radio spectrum due to synchrotron emission from electrons produced by DM annihilation at WIMP masses of m_χ= 10 GeV, m_χ= 40 GeV and m_χ= 100 GeV. We also compare our results to the radio spectrum of the cluster's radio halo obtained from observations and in Section 4.6. we conclude our study and take a look at some of the major uncertainties which affect our study.

Throughout the chapter we have employed a flat, vacuum dominated cosmological model with H_0= 69.6 km s^{-1}Mpc^{-1}, Ω_m = 0.286, Ω_Λ = 0.714 . With these parameters the luminosity distance of A1689 at z = 0.183 is D_L = 894.6 Mpc and 1 arcmin corresponds to 185.94 kpc.

4.2 Radiation from DM annihilation

Dark matter halo profile

In this study we model our DM halo density distribution following the results of the N-body cosmological collisionless simulation from Navarro, Frenk, and White, 1997. Using the Navarro-Frenk-White (NFW) profile which is given by:

$$\rho(r) = \frac{\rho_s}{\left(\frac{r}{r_s}\right)\left(1+\frac{r}{r_s}\right)^2}, \tag{4.1}$$

where ρ_s is the central density of the DM halo with a scale radius, r_s. Following Ackermann et al., 2010, we can derive ρ_s and r_s from observations using the virial mass M_{vir} and radius R_{vir} of the cluster, which are determined by X-ray observations and gravitational lensing studies. r_s is obtained from the concentration parameters c_{vir}, which is is given by (Bullock et al., 2001):

$$c_{vir} = \frac{9}{1+z}\left(\frac{M_{vir}}{1.3\times10^{13}h^{-1}M_\odot}\right)^{-0.172}, \tag{4.2}$$

where $c_{vir} = R_{vir}/r_s$ for the NFW profile. We determined M_{vir} and R_{vir} from M_{500}, where the overdensity is 500 times the critical density of the universe. We obtained M_{500} for A1689 from the X-ray scaling relations presented in Chen et al., 2007, we corrected M_{500} by the gas fraction, f_{gas}, which is also given in Chen et al., 2007 so that we are left with the mass of cluster's dark matter. We then determined R_{vir} from the corrected M_{vir} using the relation:

$$M_{vir} = \frac{4\pi}{3}\Delta_c\rho_c R_{vir}^3, \tag{4.3}$$

where $\Delta_c \approx 100$ is the collapse overdensity, which is cosmology dependent and ρ_c is the critical density of the universe given as a function of the Hubble constant, H and the gravitational constant, G:

$$\rho_c(z) = \frac{3H^2(z)}{8\pi G}. \tag{4.4}$$

We can then use the M_{vir}, R_{vir} and r_s to solve for the central density, ρ_s following Colafrancesco, Marchegiani, and Beck, 2015.

$$\frac{\rho_s}{\rho_c} = \frac{\Delta_c}{3}\frac{c_{vir}^3}{\ln(1+c_{vir}) - \frac{c_{vir}}{1+c_{vir}}}. \tag{4.5}$$

In the hierarchical assembly of DM halos, early varialized halos often merge with each other to form larger halos, this results to a population of sub-halos

existing inside other larger DM halo structures. The presence of sub-halos in galaxies and clusters has astrophysical consequences we can't ignore when studying DM profiles and distribution. Sub-halos can serve as hosts for satellite galaxies and also boost the DM annihilation signal from larger DM structures. In the latter phenomena we expect the effects of smaller sub-halos to boost the secondary electrons and γ-rays resulting from DM annihilation by a multiplicative boosting factor, $\mathcal{B}$ (see Pieri et al., 2011 and Kaplinghat, Tulin, and Yu, 2016 for an extensive study and discussion on the implication of subhalos on the secondary DM annihilation emission). Although the sizes of the sub-halos are difficult to determine due to their lack of optical counterparts and undetectability, however their masses have been estimated to range from $10^{-6}M_{\odot} - 10^{-2}M_{\odot}$ and are expected to boost the secondary DM annihilation signals by factors ranging from 10 to 30 times in galaxy clusters. However, to simplify our study, in this chapter we will be ignoring the effects of substructures on the resulting WIMP products and focus mainly on the effects of the main DM structures of the cluster.

Electron source function

To calculate the resulting IC and synchrotron emission from the annihilation of DM we first have to calculate the electron-positron equilibrium spectrum, which is obtained by solving the diffusion equation:

$$\frac{\partial}{\partial t}\frac{dn_e}{dE} = \nabla\left(D(E,\mathbf{r})\nabla\frac{dn_e}{dE}\right) + \frac{\partial}{\partial E}\left(b(E,\mathbf{r})\frac{dn_e}{dE}\right) + Q_e(E,\mathbf{r}), \tag{4.6}$$

where $Q_r(E,\mathbf{r})$ is the electron source function, $D(E,\mathbf{r})$ is the diffusion electron term, $b(E,\mathbf{r})$ is the energy loss function and $\frac{dn_e}{dE}$ is the equilibrium electron density. In galaxy clusters, the timescales in which electrons spatially diffuse occurs is much larger than the timescales in which electrons radiate, so we ignore the diffusion terms on the rhs of equation 4.6. The source function which describes the production of particles e at equilibrium, produced by WIMP annihilation is given by:

$$Q_e(E,\mathbf{r}) = \langle\sigma v\rangle \sum_f \frac{dN_i^f}{dE} B_f \mathcal{N}_\chi(\mathbf{r}), \tag{4.7}$$

where $\langle\sigma v\rangle$ is the non-relativistic, thermally-averaged annihilation cross section at 0 K, the index f labels the final annihilation states for branching ratio

B_f and sprectrum $\frac{dN_i^f}{dE}$ and WIMP pair density $\mathcal{N}_\chi(\mathbf{r})$ for a given DM halo radius, **r**.
The generic solution for $\frac{dn_e}{dE}$ for galaxy clusters, where the effects of the diffusion of electrons are negligible is of the form:

$$\frac{dn_e}{dE} = \frac{1}{b_{loss}(E)} \int_E^{M_\chi} Q_e(E', r) dE', \tag{4.8}$$

see Appendix A in Colafrancesco, Profumo, and Ullio, 2006 for the detailed derivation of the equilibrium number density. We use the Fortran based package DarkSuSy (Gondolo et al., 2001) to calculate the electron/ positron per DM annihilation event $\frac{dN_i^f}{dE}$, which is dependent on the WIMP mass m_χ, the DM annihilation channel f and the source energy, E, or our study we will assume a brancing ratio of 1 for the annihilation channels: $b\bar{b}$, $\tau^+\tau^-$ and $\mu^+\mu^-$ at three WIMP masses m_χ= 10, 40 and 100 GeV.

The energy loss function includes the contributions from the synchrotron, Coulomb, Bremsstrahlung and inverse Compton energy losses given by:

$$b_{loss}(E) = b_{sync}(E, r) + b_{IC}(E) + b_{Coul}(E) + b_{Brem}(E) \tag{4.9}$$

$$= b_{IC}^0 E^2 + b_{sync}^0 B^2(r) E^2 + b_{Coul}^0 \left(1 + log\left(\frac{E/m_e}{n_e}\right)/75\right) \tag{4.10}$$

$$+ b_{Brem}^0 \left(log\left(\frac{E/m_e}{n_e}\right) + 0.36\right). \tag{4.11}$$

where b_{sync}, b_{IC}, b_{Coul} and b_{Brem} are the synchrotron, inverse Compton, Coulomb and Bremsstrahlung energy loss factors respectively with units of 1×10^{-16} GeV, n_e is the average electron density which is $\approx 1 \times 10^{-3}\text{cm}^{-3}$ for the cluster, $B(r)$ is the magnetic field in μG and E is the energy in GeV.

Synchrotron emission

In galaxy clusters, synchrotron radiation is created when relativistic electrons spiral in the presence of a magnetic field, B, the average power of the synchrotron radiation emitted by an electron with energy E at frequency ν is given by: (Longair, 2011)

$$P_v(\nu, E, r, z) = 2\pi\sqrt{3}r_0 m_e c\nu_0 \int_0^{\pi} d\theta \frac{\sin\theta}{2} \sin\theta F\left(\frac{x}{\sin\theta}\right), \tag{4.12}$$

where m_e= is the mass of the electron, $\nu_0 = \frac{eB}{2\pi m_e}$ represents the electron's non-relativistic gyrofrequency, θ is the pitch angle and r_0 is the classical electron's radius, the quantities x an F are defined as:

$$x \equiv \frac{2\nu}{3\nu_0\gamma^2}\left[1 + \left(\frac{\gamma\nu_p}{\nu}\right)^2\right]^{3/2} \tag{4.13}$$

and

$$F(s) \equiv s\int_s^{\infty} d\xi K_{5/3}(\xi) \simeq 1.25 s^{1/3} e^{-s}[648 + s^2]^{1/12}, \tag{4.14}$$

where $K_{5/3}$ is the Bessel function modified to the order of $5/3$.
The local emissivity at frequency ν of the synchrotron emission as a function of the equilibrium electrons or positrons, $\frac{dne^{\pm}}{dE}$, and synchrotron power P_{synch} is given by:

$$j_{synch}(v, r) = 2\int_{me}^{M\chi} dE \left(\frac{dne^-}{dE} + \frac{dne^+}{dE}\right) P_{synch}(\nu, E, r, z). \tag{4.15}$$

After obtaining $j_{synch}(v, r)$, we can use it to calculate the expected flux density spectrum of the synchrotron emission at frequency ν using the form:

$$S_{synch}(\nu) = \int d^3r \frac{j_{synch}(v, r)}{4\pi D_L^2}, \tag{4.16}$$

where D_L is the luminosity distance of the cluster.

Magnetic field modelling

The charged annihilation bi-products are accelerated through a magnetic field leading to the presence of radio and X-ray emission through synchrotron and IC radiation. Faraday rotation measures studies have shown that the magnetic field strength in galaxy clusters range from 1-10 μG and are strongest in the centre and tend to get weaker towards the edges of the cluster (see Carilli and Taylor, 2002; Govoni and Feretti, 2004 for studies and detection

Parameter	Value	Ref
z	0.183	
M_{vir} (10^{14} $M_\odot$)	14.36	Chen et al., 2007
β	0.690	Chen et al., 2007
B_0 (μG)	4.7; 10	
r_c (kpc)	128	Chen et al., 2007
ν (MHz)	1400	
S_v (mJy)	9.9	Vacca et al., 2011

TABLE 4.1: Properties of the cluster used to study the cross section upper limits and radio signal from WIMP annihilation.

on cluster magnetic fields). This is why we adopted the β-model to describe the magnetic field profile of the cluster:

$$B(r) = B_0 \left(1 + \left(\frac{r}{r_c}\right)^2\right)^{-q_b}, \tag{4.17}$$

where B_0 is the central magnetic field strength, r and r_c represent the radial distance from the cluster center and the radius of the DM density profile respectively and q_b is the scaling parameter, which we have chosen to be 0.5. We assumed that magnetic field profile scales proportionally to the thermal gas density within the DM halo, which is:

$$n_e(r) = n_0 \left(1 + \left(\frac{r}{r_c}\right)^2\right)^{-q_e}. \tag{4.18}$$

Currently, there are no published Faraday rotation measures for A1689 and thus we do not have any published values of the cluster's magnetic field. Cool-core clusters tend to have a higher magnetic field strength compared to non-cool-core clusters and since A1689 is a cool-core cluster, we followed Storm et al., 2013; Kiew, Hwang, and Zainal Abibin, 2017 and set B_0= 10 μG and also tested for a scenario where the magnetic intensity is lowered to B_0= 4.7 μG.

4.3 Radio analysis of the cluster

We retrieved archival radio observations of the A1689 cluster from the TIFR GMRT Sky Survey alternate data release (TGSS ADR1 in short, Intema et al.,

2017), the VLA Low-Frequency Sky Survey Redux (VLSSr, Cohen et al., 2007), the Galactic and Extragalactic All-sky (GLEAM, Wayth et al., 2015) and the NRAO VLA Sky Survey (NVSS, Condon et al., 1998a) data archives, in order to help us expand on the radio properties of the radio halo beyond the ones listed in Vacca et al., 2011. We particularly concentrate on obtaining the flux density values of the radio halo at frequencies less than 1200 MHz, in order to be able to compare the observed radio signal to the signal expected from WIMP annihilations. We have listed the properties of the radio continuum images in Table 4.2.

Figure 4.1. shows the radio map of the A1689 cluster at at 1400 MHz and 147.5 MHz. The radio map and contours were imaged using the Common Astronomy Software Application (CASA)[1].
In order to estimate the flux densities of the radio halo found in the cluster, we perform a source extraction to remove all the contribution from point sources and their extended emissions. To do this we use the Python source finding software PyBDSF, which is capable of processing and analysing FITS file obtained from the radio surveys. We modelled the point sources using a Gaussian function to estimate the flux densities of all the point sources we found. The total flux density of all these embedded point sources is then subtracted from the total emission in the cluster, this process will be explained in detail Khanye, Thwala, and Marchegiani, 2021 where we conduct an extensive study on the radio emission found in the cluster.
We list the flux densities of the emission at different frequencies in Table 4.3. The values for at 73.5 MHz and at 200 MHz are taken as upper limits due to the high noise levels of the VLSSr and the GLEAM images, a consequence of the respective surveys' poor resolution. The flux density values at 1200 MHz and 1400 MHz are taken from Vacca et al., 2011. These flux density values will help us determine the best fit model and conditions for the feasible detection of WIMP induced radio emission in the cluster.

4.4 Annihilation cross-section

We first calculate the $< \sigma v >$-m_χ constraints of the galaxy cluster by using the radio observations of the diffuse emission at 1.4 GHz as stated in Table 4.1. We consider the primary annihilation channels $b\bar{b}$, $\mu^+\mu^-$ and $\tau^+\tau^-$ within

[1]https://casa.nrao.edu/

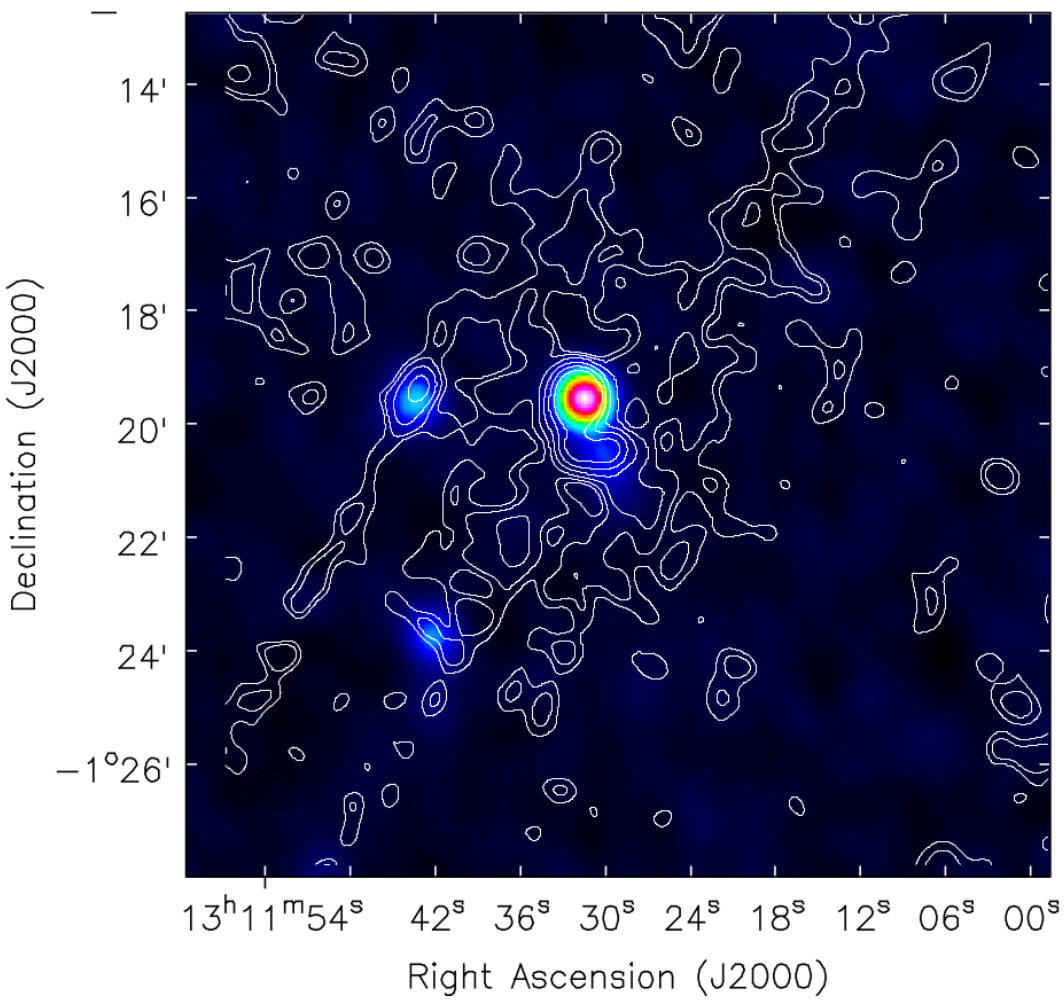


FIGURE 4.1: The NVSS 1.4 GHz radio image of the A1689 cluster shown in colour with a resolution of $45'' \times 45''$ and an rms noise value of 0.5 mJy/b, the image has been overlaid with TGSS 147.5 MHz radio contours. The contour lines are drawn at [1,2,4,8,16,...]$\times 2.5\sigma$

.

Survey	ν (MHz)	resolution	σ (mJy/beam)
VLSSr	73.5	$75'' \times 75''$	110
TGSS	147.5	$27'' \times 27''$	3
GLEAM-1	200	$100'' \times 100''$	6.4
NVSS	1400	$45'' \times 45''$	0.53

TABLE 4.2: Properties of the A1689 radio continuum image which we used in our study. Col 1. represents the survey name, Col 2. is the central frequency, Col 3. is the surveys' synthesized beam size and Col 4. is the noise value of each image.

ν (MHz)	73.5	147.5	200	1200	1400
S_ν (mJy)	497.3 ± 61.3	202.9 ± 19.8	153.3 ± 16.8	11.7 ± 3.4	$9.9\pm$ 2,9

TABLE 4.3: Flux densities of the radio halo found in the galaxy cluster at different frequencies.

the WIMP mass range $[10\ \text{GeV}, m_\chi, 1000\ \text{GeV}]$ and within the $< \sigma\nu >$ range of $\left[10^{-27}\ \text{cm}^3\text{s}^{-1}, < \sigma\nu >, 10^{-21}\ \text{cm}^3\text{s}^{-1}\right]$. No solid magnetic field studies of the cluster have been done before, this is mainly due to a lack of Faraday rotational measures for southern galaxy clusters. This is however expected to change with the launch of the Square Kilometer Array (SKA) all-sky survey of Faraday Rotation measures (Beck, Gaensler, and Feretti, 2007; Stepanov et al., 2008; Bonafede et al., 2015). In this study, to account for the presence of the magnetic fields in the cluster's ICM, which is essential for the occurrence of the radio halo found in the central region of the cluster, we have decided to estimate the magnetic field strength and profile of the cluster in two ways. Since the cluster is a cool-core cluster, we can expect it to have a higher inferred magnetic field strengths compared to clusters that are non-cool-core clusters. Magnetic fields for cool-core clusters are expected to range from 10 to 40 μG while non-cool-core clusters are expected to range from 0.1 to 10 μG (Taylor, Fabian, and Allen, 2002; Kuchar and Ensslin, 2011; Vacca et al., 2012). We then assume the central magnetic field intensity, B_0 to be 10 μG for our first magnetic field scenario. We are also interested in seeing how the annihilation cross section and resulting radio spectra is affected by the magnetic field, and so we also test for a scenario where B_0 is lower as it can be expected for clusters hosting radio halos. In the second scenario we adopt the central magnetic field strength of the Coma cluster B_0= 4.7 μG (Bonafede et al., 2010).

In Figure 4.2. we present the upper limit constraint on the WIMP annihilation cross section when assuming that the diffuse radio emission in the A1689

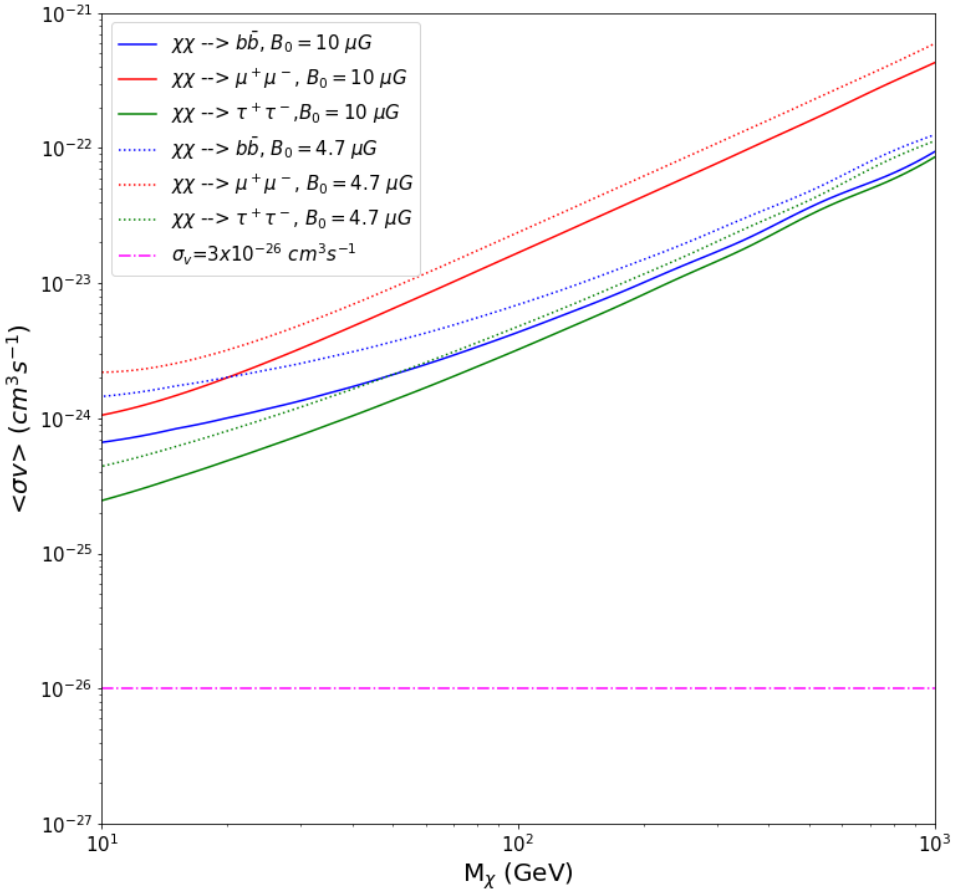


FIGURE 4.2: A1689 dark matter annihilation cross section upper limits $< \sigma v >$ as a function of WIMP mass for three annihilation final states. The solid graphs are for magnetic field B_0=10 μG and the dashed lines are for magnetic field B_0=4.7 μG. The blue lines represent the upper limit constraints from the $b\bar{b}$ annihilation state, the red lines represent the upper limit constraints from the $\mu^+\mu^-$ annihilation state and the green lines represent the upper limit constraints from the $\tau^+\tau^-$ annihilation state. The pink straight dash-dot line represents canonically thermally averaged cross section for a WIMP.

m_χ (GeV)	f	$<\sigma v>_{10\,\mu G}$ $(cm^3 s^{-1})$	$<\sigma v>_{4.7\,\mu G}$ $(cm^3 s^{-1})$
10	$b\bar{b}$	6.60×10^{-25}	1.45×10^{-24}
	$\mu^+\mu^-$	1.06×10^{-24}	2.19×10^{-24}
	$\tau^+\tau^-$	2.49×10^{-25}	4.45×10^{-25}
40	$b\bar{b}$	1.70×10^{-24}	3.12×10^{-24}
	$\mu^+\mu^-$	4.8×10^{-24}	7.10×10^{-24}
	$\tau^+\tau^-$	1.05×10^{-24}	1.65×10^{-24}
100	$b\bar{b}$	4.21×10^{-24}	6.90×10^{-24}
	$\mu^+\mu^-$	1.69×10^{-23}	2.32×10^{-23}
	$\tau^+\tau^-$	3.20×10^{-24}	4.70×10^{-24}

TABLE 4.4: Cross section upper limits for different WIMP masses at 3 different annihilation channels when B_0= 10 μG and when B_0= 4.7 μG.

cluster resulted from electrons and positrons produced by the annihilation of WIMPs inside spherical DM halos. The cross section upper limits are normalised with the 1.4 GHz flux density value as shown in Table 4.1. We note that the derived cross section limits are sensitive to the strength of the cluster's central magnetic field for all three annihilation channels. The best cross section constraint for all the annihilation channels are observed when B_0=10 μG, while the constraints for when B_0=4.7 μG give constraints which are 2-5 times weaker than when B_0=10 μG. This relationship between the magnetic field intensity and the cross section upper limit is similar to the one recently reported in the A2199 and Ophiuchus clusters for the similar studies (Storm et al., 2013; Beck, 2020).

The summary of our results for the annihilation cross section for masses of 10, 40 and 100 GeV for the both magnetic field models are presented in Table 4.4. From figure 4.2. we observe that the $\tau^+\tau^-$ channel yields the best cross sectional limit at lower WIMP masses, while the $b\bar{b}$ and $\tau^+\tau^-$ channels yield the best cross sectional upper limits at higher WIMP masses. The $\mu^+\mu^-$ annihilation channel yields poor cross sectional constrain at both lower and higher WIMP masses. In most clusters which have been studied so far the $\tau^+\tau^-$ and $\mu^+\mu^-$ channels have yielded the best annihilation limit at lower masses while the $b\bar{b}$ channel yields the best limit at higher masses (Kar et al., 2019; Vollmann et al., 2020). This is due to the fact that the $\tau^+\tau^-$ and $\mu^+\mu^-$ channels tend to produce more positrons and electrons at lower masses compared to the $b\bar{b}$ channel which tends to produce more positrons and electrons at WIMP higher masses. This relationship has also been recently shown for the A2199 cool core cluster in Kiew, Hwang, and Zainal Abibin, 2017, where the

author also showed that a higher magnetic field does not necessarily translate to high DM induced radio flux densities.

The main sources of uncertainty on our cross section upper limit analysis are the cluster's mass, the inferred magnetic field and our neglect of the additive effect of the DM sub-halos inside the cluster's main DM halos. The cluster's mass has been obtained from Chen et al., 2007 where the authors X-ray observations were based on the ROSAT and ASCA observations. An uncertainty in the cluster's mass determination translate to inaccuracies in the determination of the DM density profile and distribution, as they are dependant on M_{500}.

4.5 WIMP induced radio spectra

In Figure 4.3, 4.4 and 4.5. we present the WIMP induced radio spectra expected to result from the secondary electrons produced at different masses of 10 GeV, 40 GeV and 100 GeV respectively. The WIMP induced radio spectra are compared at the two different magnetic fields of B_0 = 4.7 μG and B_0 = 10 μG using the β-model to describe the magnetic profiles of the cluster. All the radio spectra are normalized by the cross section values corresponding to each annihilation channel, magnetic field and WIMP mass as stated in Table 4.4. We also compare the fluxes from WIMP annihilation to flux densities of the radio halo as obtained from the radio analysis of the cluster through observations in this thesis and by Vacca et al., 2011. This comparison will enable us to understand which WIMP model better fits the real radio observations of the diffuse emission.

According to the results obtained in Figure 4.3., at WIMP masses of m_χ=10 GeV the $b\bar{b}$ annihilation channel at B_0 = 10 GeV fits most of the observational data of the radio halo except for the 8.7 mJy at the 1.2 GHz data point. The radio spectra obtained from the $\tau^+\tau^-$ annihilation channel at B_0 = 4.7 GeV also marginally retrieves the observed flux densities of the radio halo, although the WIMP induced flux densities are generally lower than the observed flux densities. The $\mu^-\mu^+$ annihilation channel gives us poor radio fluxes as compared to the observational fluxes at both magnetic filed intensities.

At m_χ=40 GeV, in Figure 4.4. only the $b\bar{b}$ spectra marginally retrieves the observational data points at both magnetic field intensities, while the $\tau^+\tau^-$

and $\mu^-\mu^+$ WIMP induced spectra fail to closely trace the observational data due to poor WIMP induced radio fluxes.
At m_χ=100 GeV, in Figure 4.5. none of the WIMP induced spectra closely trace the observational data except for the 1.4 GHz value which happens to be the normalization value and the 1.2 GHz value which neighbours the 1.4 GHz value. The m_χ=100 GeV spectra yields the weakest radio constraint compared to the m_χ=10 GeV and m_χ=40 GeV WIMP induced spectra.

The WIMP induced radio fluxes are influenced by a change in the magnetic field intensity B_0. A point by point of comparison when B_0 = 10 μG and when B_0 = 4.7 μG at m_χ=10 GeV shows that the flux values at B_0 = 4.7 μG varies by up to 3 times than that of flux values at B_0 = 10 μG up until the cross section normalizing observational flux at 1.4 GHz. After ν=1.4 GHz the signal at B_0 = 10 μG then varies by up to 3 times from the signal at B_0 = 4.7 μG. When m_χ= 40 GeV we notice a decrease in the variation factor of the signals, with the signal from B_0 = 4.7 varying by to 3x for the $\tau^-\tau^+$ annihilation channel, and only varying by a factor of up to $\sim$ 2 for for the $b\bar{b}$ and $\mu^-\mu^+$ channels. When m_χ=100 GeV the effects of the magnetic field on the synchrotron signal become almost negligible for the $b\bar{b}$ and $\mu^-\mu^+$ up until ν=1.4 GHz. A change in the cluster's magnetic field strength influences a change in the WIMP induced fluxes due to the fact that a change in the strength of the magnetic field will affect the energies of the electrons which will emit by synchrotron in that specific wavelength range. However, for m_χ=100 GeV, the power law shape of the electrons spectrum is maintained in a wider energy range, so even shifting the energies of the electrons emitting in a given frequency range the shape of radio spectrum does not change as much as it would for the lower masses, at least until some frequency.

A comparison of the DM induced synchrotron signals when m_χ=10 GeV,m_χ=40 GeV and m_χ=100 GeV shows that as the WIMP mass increases, the synchrotron signal gets flatter, and also deviates further from the observed flux densities of the radio halo. This implies that, at higher WIMP masses, the synchrotron signal produced through WIMP annihilation may be undetectable at low frequencies compared to the synchrotron signal from lower to intermediate WIMP masses. If this is the case, then it places a limit on the window of detectability for the synchrotron emission produced through WIMP annihilation in the ICM to be in-between lower and intermediate WIMP masses.

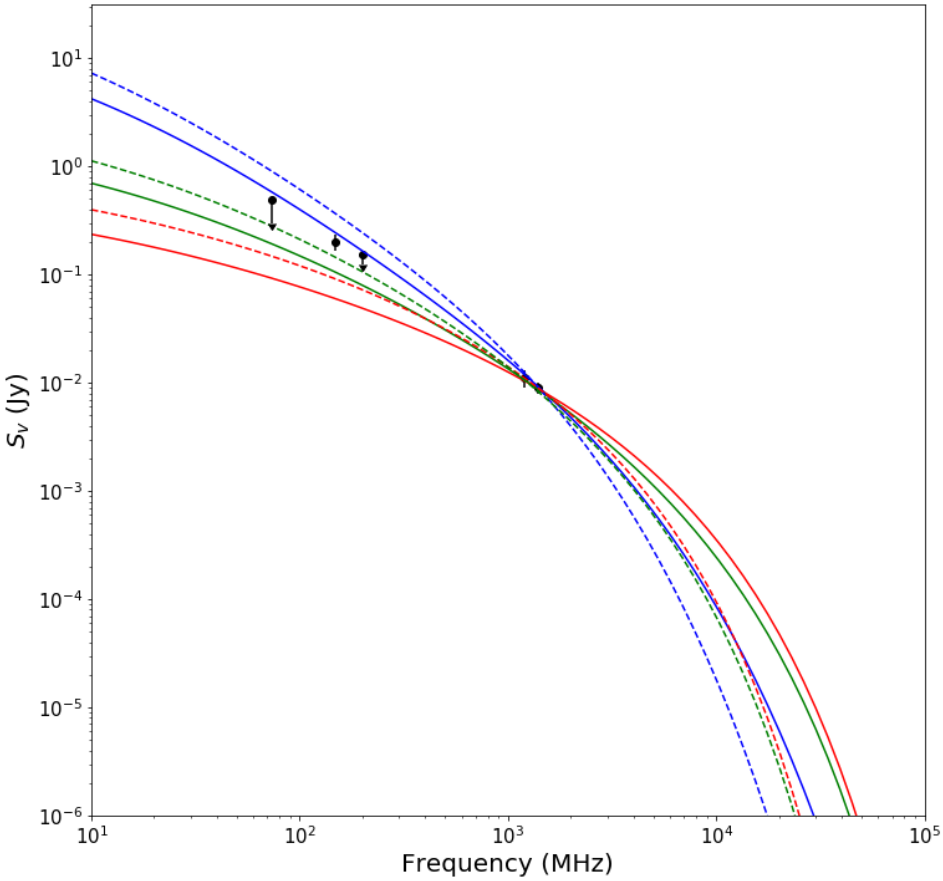


FIGURE 4.3: The predicted radio halo spectra from DM annihilation for a WIMP mass of m_χ=10 GeV for $b\bar{b}$, $\mu^-\mu^+$ and $\tau^-\tau^+$ annihilation final states at different B_0-field strength. The solid graphs are for magnetic parameters B_0=10 μG and the dashed lines are for magnetic field B_0=4.7 μG. The blue lines represent the expected radio spectra from the $b\bar{b}$ annihilation state, the red lines represent the expected radio spectra from the $\mu^+\mu^-$ annihilation state and the green lines represent the expected radio spectra from the $\tau^+\tau^-$ annihilation state. The predicted WIMP annihilation spectra are compared to observed radio fluxes of the radio halo (in scatter points) including a value of 8.7 mJy as reported by Vacca et al., 2011.

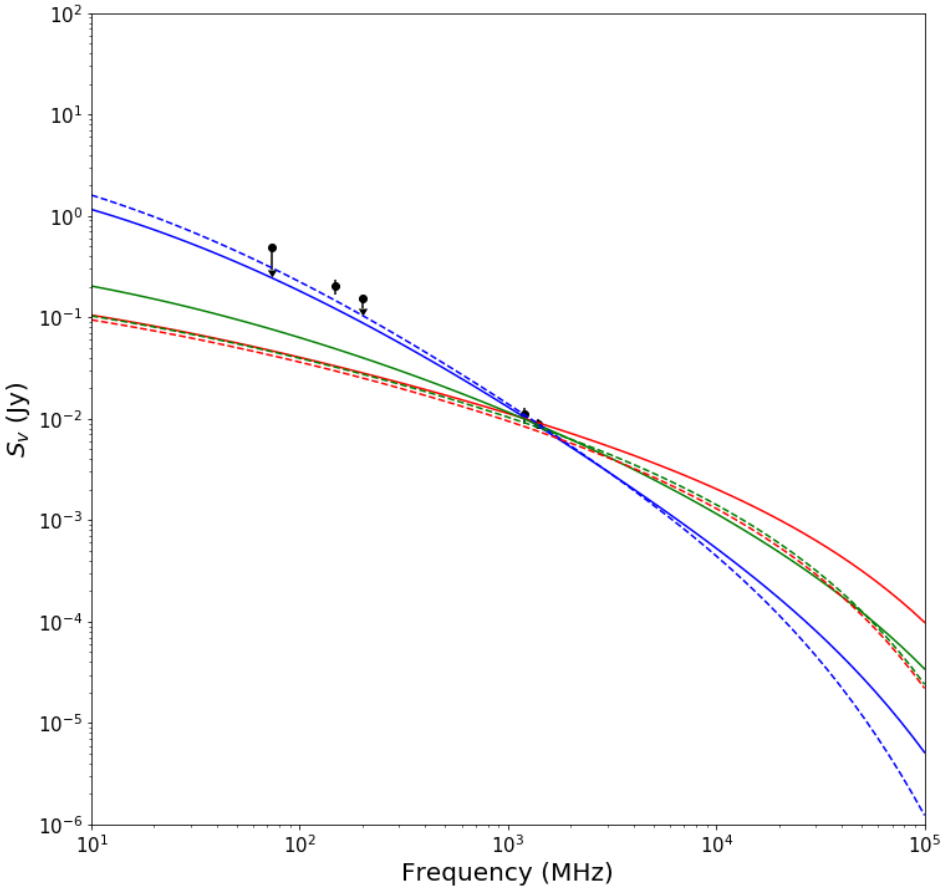


FIGURE 4.4: The predicated radio halo spectra from DM annihilation for a WIMP mass of m_χ=40 GeV for $b\bar{b}$, $\mu^-\mu^+$ and $\tau^-\tau^+$ annihilation final states at different B_0-field strength. The solid graphs are for magnetic field B_0=10 μG and the dashed lines are for magnetic field B_0=4.7 μG. The blue lines represent the expected radio spectra from the $b\bar{b}$ annihilation state, the red lines represent the expected radio spectra from the $\mu^+\mu^-$ annihilation state and the green lines represent the expected radio spectra from the $\tau^+\tau^-$ annihilation state. The predicted WIMP annihilation spectra are compared to observed radio fluxes of the radio halo (in scatter points) including a value of 8.7 mJy as reported by Vacca et al., 2011.

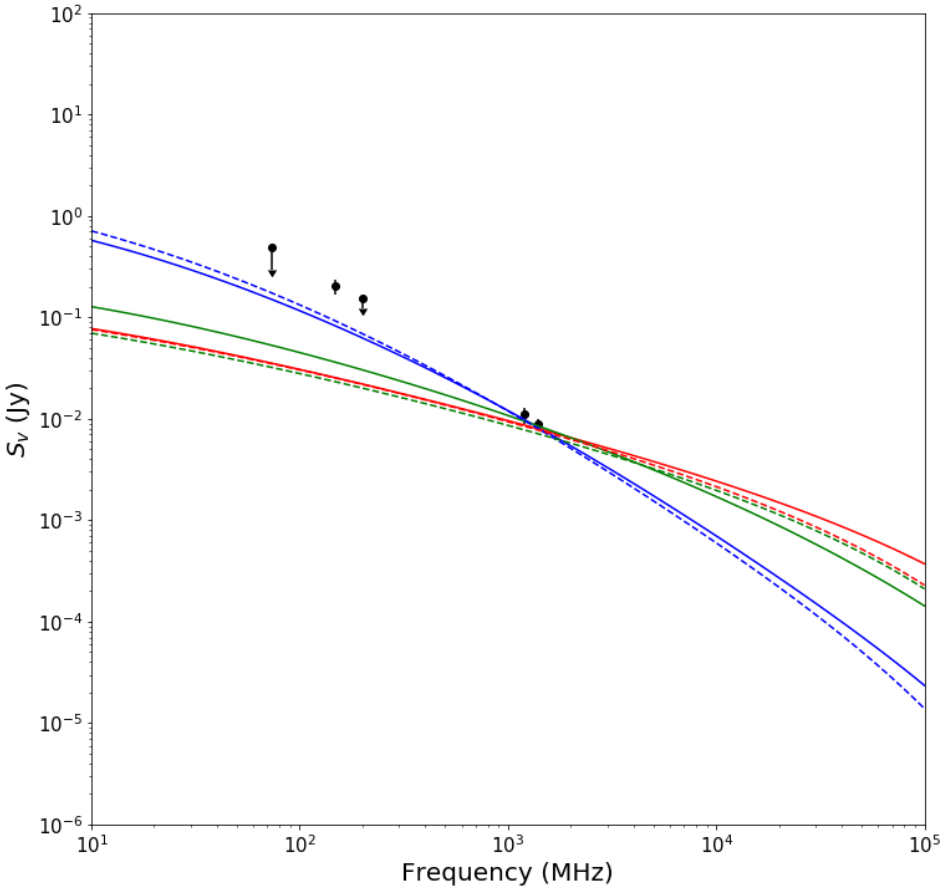


FIGURE 4.5: The predicated radio halo spectra from DM annihilation for a WIMP mass of m_χ=100 GeV for $b\bar{b}$, $\mu^-\mu^+$ and $\tau^-\tau^+$ annihilation final states at different B_0-field strength. The solid graphs are for magnetic field B_0=10 μG and the dashed lines are for magnetic field B_0=4.7 μG. The blue lines represent the expected radio spectra from the $b\bar{b}$ annihilation state, the red lines represent the expected radio spectra from the $\mu^+\mu^-$ annihilation state and the green lines represent the expected radio spectra from the $\tau^+\tau^-$ annihilation state. The predicted WIMP annihilation spectra are compared to observed radio fluxes of the radio halo (in scatter points) including a value of 8.7 mJy as reported by Vacca et al., 2011.

It is important to note that the radio spectra from the secondary electrons produced through WIMP annihilation may not perfectly trace out the radio data from the observations. This is due to the fact that the data points are calculated from different radio surveys which have different sensitivities, systematics and data reduction techniques, especially considering the fact that the calibration and cleaning of the radio images used were performed by their respective surveys (with the exception of the 1.2 and 1.4 GHz data point, which are taken from Vacca et al., 2011). These differences in reduction techniques and sensitivities makes it difficult for the expected DM spectral curves to match the radio data with high accuracy, this problem has also been frequently observed when studying the effects of DM annihilation Coma cluster due to a larger data set of radio fluxes from different surveys (e.g, Brunetti et al., 2013) . However, since we obtained a regular integrated spectrum from radio observations we are able to find a great fit for the DM induced spectra without having to worry about too many outliers. The lack of radio observations for the radio halo beyond 1.4 GHz also limits the accuracy of our prediction on which WIMP model will best describes the radio halo.
Another uncertainty in the expected radio spectra from WIMP annihilation comes from the lack of magnetic field studies for the A1689 cluster leading us to use make bold assumption about the magnetic field properties of the cluster, which has been discussed in section 4.4, however we estimate that the uncertainties in the cluster's magnetic field leads to uncertainties in the WIMP spectra by factors ranging between 3 to 6 times at the lowest WIMP masses and by a factor of 2 times or less for higher WIMP masses.
The results show that the $b\bar{b}$ annihilation channel at a WIMP mass of m_χ=10 GeV and a magnetic field B_0 = 10 GeV fits the observational data slightly better than all the other models at the same mass and so we can then expect to find the signal from WIMP annihilation at low to intermediate masses in this cluster. However, the results from the model still perform poorly compared to similar studies performed on merging and cool core clusters. The constraints are also ruled out by the Fermi dwarf limits

4.6 Conclusions

In this chapter we studied the possibility that the diffuse emission found in the the A1689 cluster results from the annihilation of secondary electrons produced through the annihilation of DM particles known as WIMPs and derived new cross section limits on the WIMP. We explored different factors

i.e WIMP mass, annihilation channels and magnetic field to determine the a model which will best fit radio observations of the galaxy cluster.
We found our best fit WIMP annihilation cross section to be higher than the current thermally averaged annihilation cross section value of $3 \times 10^{-26} \mathrm{cm}^3\mathrm{s}^{-1}$ by $\sim$ 2-3 orders of magnitude, with the $\tau^-\tau^+$ annihilation channel yielding the closest value to the cross sectional limit when B_0= 10 μG.

Our best fit model turned out to be in the final state $b\bar{b}$ with a WIMP mass of m_χ=10 GeV and 6.60 $\times 10^{-25}$ $\mathrm{cm}^3\mathrm{s}^{-1}$ at a magnetic field intensity of B_0= 10 μG as this model is able to retrieve the flux densities of the cluster's radio halo obtained from observations. The $\mu^-\mu^+$ WIMP channel also marginally follows the radio observations when m_χ=10 GeV and 1.06 $\times 10^{-24}$ $\mathrm{cm}^3\mathrm{s}^{-1}$ with B_0= 4.7 μG. We did not find a good fit for the $\tau^-\tau^+$ annihilation channel as it produced the flattest radio signal for all WIMP masses. However, the best fit model with a mass of m_χ=10 GeV is too light to accommodate the electron-plus-positron flux observed by the FERMI-LAT(Abdo et al., 2009) and HESS surveys (Aharonian et al., 2009).
We have also learnt that the WIMP induced radiation is sensitive to the strength of the magnetic field, with the radio signal getting flatter as the B_0 increases. Our upper limit constraints are comparable with studies done for other cool-core clusters such as A2199 (see Figure 4. in Storm et al., 2013), where for a similar model the upper limit cross section for the $b\bar{b}$ channel with the magnetic field intensity B_0= 11.7 μG is $\sim$ 1-3 $\times 10^{-24}$ $\mathrm{cm}^3\mathrm{s}^{-1}$ at m_χ=10 GeV, which is at best 3 times higher than our model. In general the A2199 model in Storm et al., 2013) yielded better upper limit constraints compared to A1689 in this study. Our upper limit constraints also perform poorly by factors of up to $\sim$ 500, even though we did not invoke the use of any boosting factors, when compared to upper limit constraints found for the galactic centre (Abazajian and Keeley, 2016) and dwarf spheroid galaxies (Ackermann et al., 2015) for similar DM annihilation cross section upper limits studies using γ-ray observations.

A number of uncertainties impacted this study, as we obtained both our WIMP cross section upper limits and radio fluxes without invoking the boosting factor from the DM subhalos, which are expected to amplify the synchrotron signal. We have also made brave assumptions on the cluster's magnetic field properties due the lack of polarization studies of the cluster, however this is expected to change with the launch of the SKA's all-sky survey

of Faraday Rotation measures in the near feature. Constraining the magnetic field properties of the clusters is generally expected to improve our ability to determine the amount and the properties of the WIMP induced radiation in clusters and galaxies. The ρ_s and c_{vir} values have been derived from the M_{500} value obtained through the X-ray scaling relation obtained by Chen et al., 2007 and any systematic uncertainties in determining the scaling relations will translate to uncertainties in determining the DM distribution of the cluster. The results could ha ve also been improved if we had a larger set of real observational flux densities of the radio halo to compare with our calculated WIMP signal. This is made difficult due to the lack of high sensitivity and low frequency observations of the cluster.

Data availability

All the data used in this work is available on the archives of the NVSS[2], TGSS[3], VLSS[4] and MWA[5] websites.

Acknowledgements

NF would also like to thank Michael Sarkis for his editorial comments and suggestions.

[2]https://www.cv.nrao.edu/nvss/
[3]http://tgssadr.strw.leidenuniv.nl/doku.php
[4]https://heasarc.gsfc.nasa.gov/W3Browse/all/vlss.html
[5]https://www.mwatelescope.org/gleam

Chapter 5

Concluding remarks

5.1 Concluding remarks

The direct detection of DM would be the definitive evidence of its existence. However, due to its elusive nature we have to turn to other methods of detection in order to understand its nature. In this thesis we have used indirect detection methods to study the possible impact of DM annihilation in galaxy clusters. We selected galaxy clusters which host diffuse radio emission to investigate the possible multi-frequency effects of DM annihilation in clusters and to constrain the cross section upper limits of WIMPs in clusters. These type of studies are important as they help us understand the relationship between DM and baryonic matter. This will enable us to further constrain the properties of DM and eventually narrow down our DM particle searches.
For example, we can use our studies to constrain the window of detectability of DM induced electromagnetic radiation in future surveys such as the SKA and LoFAR and the information found can be complemented with analogous studies in the X-ray and gamma-ray band. The SKA's ability to resolve the intrinsic degeneracy (between magnetic field properties and particle distribution) of synchrotron emission is expected to allow an unbiased detection of emission resulting from secondary particles through DM annihilation and baryonic activities. The limiting factor to this type of detection will be the instrument's sensitivity to the DM particle mass and annihilation cross-section (decay rate) of DM particles.

Our work on the effects of DM annihilation can still be improved by considering more WIMP annihilation channels and a wider range of magnetic fields which were not added into the thesis and by also including boosting effects of sub-halos which are present in dark matter halos. These are some of the factors we will be exploring as we continue to study more galaxy cluster. We will also be looking at the effects of DM annihilation in galaxies in the future,

as they have high levels of gamma ray emissions. Galaxies have also yielded stronger DM annihilation cross section constraints as compared to clusters. A wider spectral band range by different emission processes such as Compton scattering and non-thermal bremsstrahlung emission studies in A1689 and similar clusters can also compliment radio studies. These improvements will allow us to extend the range of spectral bands where this model can predict the spatial and spectral properties of galaxy clusters and to narrow the window of detectability even further. These results could be used to test the different DM annihilation models by comparing it with the observations of future instruments like Astro-H in X-rays, AstroGam in soft gamma rays and CTA in high energy gamma rays as partially done for A520. In our current versions of the DM model we have only considered diffusion of relativistic electrons. In order to provide a full description of the properties of galaxy clusters it can also be beneficial to consider the diffusion of relativistic protons. This would enable us to model the production of secondary electrons and gamma rays resulting from DM annihilation. The analytical solution for the case of diffusing protons is similar as that of electrons but it is necessary to replace the energy loss terms with the appropriate losses for protons.

We also presented multi-frequency analyses of the A1689 cluster using archival radio observations. This study shows how public archival observations, whether old or new, can still be used for new analyses of clusters and galaxies which host interesting radio emissions. Although, there were limitations to our analyses due to us not being in control of the calibration and cleaning process. The resolution of our images also limited the analysis of the diffuse emission in the cluster, however we were still able to find valuable information on the properties of the radio halo and the cluster galaxies. This study could've also been improved, by obtaining higher resolution, low frequency radio maps to get a better understanding of the radio halo. However, this would have been more difficult to obtain due to time constrains and the limit of high sensitive surveys observing the southern hemisphere. In the future we will be applying for observation time with the MeerKAT and LoFAR telescopes to study the relationship between the radio halo and the cluster galaxies for this cluster and more. Observations from these telescopes can also be used to determine better model parameters for indirect DM annihilation studies such as the radial and spectral distribution of the radio halos, as well as the rate of injection of electrons into the cluster's ICM.

Bibliography

Abazajian, Kevork and Savvas M Koushiappas (2006). "Constraints on sterile neutrino dark matter". In: *Physical Review D* 74.2, p. 023527.

Abazajian, Kevork N and Ryan E Keeley (2016). "Bright gamma-ray Galactic Center excess and dark dwarfs: Strong tension for dark matter annihilation despite Milky Way halo profile and diffuse emission uncertainties". In: *Physical Review D* 93.8, p. 083514.

Abazajian, Kevork N et al. (2020). "Strong constraints on thermal relic dark matter from Fermi-LAT observations of the Galactic Center". In: *Physical Review D* 102.4, p. 043012.

Abdo, AA et al. (2010). "Constraints on cosmological dark matter annihilation from the Fermi-LAT isotropic diffuse gamma-ray measurement". In: *Journal of Cosmology and Astroparticle Physics* 2010.04, p. 014.

Abdo, Aous A et al. (2009). "Measurement of the cosmic ray e++ e- spectrum from 20 GeV to 1 TeV with the Fermi Large Area Telescope". In: *Physical Review Letters* 102.18, p. 181101.

Acciari, VA et al. (2018). "Constraining dark matter lifetime with a deep gamma-ray survey of the Perseus galaxy cluster with MAGIC". In: *Physics of the Dark Universe* 22, pp. 38–47.

Ackermann, M et al. (2015). "Searching for dark matter annihilation from Milky Way dwarf spheroidal galaxies with six years of Fermi Large Area Telescope data". In: *Physical Review Letters* 115.23, p. 231301.

Ackermann, Markus et al. (2010). "Constraints on dark matter annihilation in clusters of galaxies with the Fermi large area telescope". In: *Journal of Cosmology and Astroparticle Physics* 2010.05, p. 025.

Ackermann, Markus et al. (2012). "Fermi LAT search for dark matter in gamma-ray lines and the inclusive photon spectrum". In: *Physical Review D* 86.2, p. 022002.

Adam, R et al. (2021). "Gamma-ray detection toward the Coma cluster with Fermi-LAT: Implications for the cosmic ray content in the hadronic scenario". In: *arXiv preprint arXiv:2102.02251*.

Ade, Peter AR et al. (2016). "Planck 2015 results-xiii. cosmological parameters". In: *Astronomy & Astrophysics* 594, A13.

Aharonian, F et al. (2009). "Probing the ATIC peak in the cosmic-ray electron spectrum with HESS". In: *Astronomy & Astrophysics* 508.2, pp. 561–564.

Akerib, DS et al. (2017). "Results from a search for dark matter in the complete LUX exposure". In: *Physical review letters* 118.2, p. 021303.

Andersson, Karl E and GM Madejski (2004). "Complex structure of galaxy cluster A1689: Evidence for a merger from X-ray data?" In: *The Astrophysical Journal* 607.1, p. 190.

Arcadi, Giorgio et al. (2018). "The waning of the WIMP? A review of models, searches, and constraints". In: *The European Physical Journal C* 78.3, pp. 1–57.

Archidiacono, Maria et al. (2019). "Constraining Dark Matter-Dark Radiation interactions with CMB, BAO, and Lyman-α". In: *Journal of Cosmology and Astroparticle Physics* 2019.10, p. 055.

Babcock, Horace W (1939). "The rotation of the Andromeda Nebula". In: *Lick Observatory Bulletin* 19, pp. 41–51.

Barger, V et al. (2009). "PAMELA and dark matter". In: *Physics Letters B* 672.2, pp. 141–146.

Beck, Geoff (2020). "Hunting dark matter in galaxy clusters with non-thermal electrons". In: *Monthly Notices of the Royal Astronomical Society* 494.1, pp. 1128–1132.

Beck, Rainer, Bryan Gaensler, and Luigina Feretti (2007). "SKA and the Magnetic Universe". In: *Exploring the Cosmic Frontier*. Springer, pp. 103–108.

Becker, Robert H, Richard L White, and David J Helfand (1995). "The FIRST survey: faint images of the radio sky at twenty centimeters". In: *The Astrophysical Journal* 450, p. 559.

Bergström, Lars (2009). "Dark matter candidates". In: *New Journal of Physics* 11.10, p. 105006.

Bertone, Gianfranco, Dan Hooper, and Joseph Silk (2005). "Particle dark matter: Evidence, candidates and constraints". In: *Physics Reports* 405.5, pp. 279–390.

Blasi, Pasquale and Sergio Colafrancesco (1999). "Cosmic rays, radio halos and nonthermal X-ray emission in clusters of galaxies". In: *Astroparticle Physics* 12.3, pp. 169–183.

Bœhm, Céline et al. (2014). "Extended gamma-ray emission from Coy Dark Matter". In: *Journal of Cosmology and Astroparticle Physics* 2014.05, p. 009.

Bonafede, A et al. (2010). "The Coma cluster magnetic field from Faraday rotation measures". In: *Astronomy & Astrophysics* 513, A30.

Bonafede, Annalisa et al. (2015). "Unravelling the origin of large-scale magnetic fields in galaxy clusters and beyond through Faraday Rotation Measures with the SKA". In: *arXiv preprint arXiv:1501.00321*.

Boveia, Antonio and Caterina Doglioni (2018). "Dark matter searches at colliders". In: *Annual Review of Nuclear and Particle Science* 68, pp. 429–459.

Boyarsky, Alexey et al. (2019). "Sterile neutrino dark matter". In: *Progress in Particle and Nuclear Physics* 104, pp. 1–45.

Bradač, Maruša et al. (2008). "Revealing the properties of dark matter in the merging cluster macs j0025. 4–1222". In: *The Astrophysical Journal* 687.2, p. 959.

Bringmann, Torsten and Christoph Weniger (2012). "Gamma ray signals from dark matter: Concepts, status and prospects". In: *Physics of the Dark Universe* 1.1-2, pp. 194–217.

Broadhurst, Tom et al. (2005a). "Strong-lensing analysis of A1689 from deep advanced camera images". In: *The Astrophysical Journal* 621.1, p. 53.

Brown, Shea and Lawrence Rudnick (2011). "Diffuse radio emission in/around the Coma cluster: beyond simple accretion". In: *Monthly Notices of the Royal Astronomical Society* 412.1, pp. 2–12.

Brunetti, G et al. (2013). "Is the Sunyaev-Zeldovich effect responsible for the observed steepening in the spectrum of the Coma radio halo?" In: *Astronomy & Astrophysics* 558, A52.

Brunetti, Gianfranco et al. (2004). "Alfvénic reacceleration of relativistic particles in galaxy clusters: MHD waves, leptons and hadrons". In: *Monthly Notices of the Royal Astronomical Society* 350.4, pp. 1174–1194.

Buckley, Matthew R and Annika HG Peter (2018). "Gravitational probes of dark matter physics". In: *Physics Reports* 761, pp. 1–60.

Bullock, James S et al. (2001). "Profiles of dark haloes: evolution, scatter and environment". In: *Monthly Notices of the Royal Astronomical Society* 321.3, pp. 559–575.

Carilli, CL and GB Taylor (2002). "Cluster magnetic fields". In: *Annual Review of Astronomy and Astrophysics* 40.1, pp. 319–348.

Carr, John et al. (2015). "Prospects for indirect dark matter searches with the Cherenkov Telescope Array (CTA)". In: *arXiv preprint arXiv:1508.06128*.

Cavaliere, A and R Fusco-Femiano (1976). "X-rays from hot plasma in clusters of galaxies". In: *Astronomy and Astrophysics* 49, pp. 137–144.

Chen, Yong et al. (2007). "Statistics of X-ray observables for the cooling-core and non-cooling core galaxy clusters". In: *Astronomy & Astrophysics* 466.3, pp. 805–812.

Cholis, Ilias, Tim Linden, and Dan Hooper (2019). "A robust excess in the cosmic-ray antiproton spectrum: implications for annihilating dark matter". In: *Physical Review D* 99.10, p. 103026.

Clowe, Douglas et al. (2006). "A direct empirical proof of the existence of dark matter". In: *The Astrophysical Journal Letters* 648.2, p. L109.

Clowe, Douglas et al. (2012). "On dark peaks and missing mass: a weak-lensing mass reconstruction of the merging cluster system A520". In: *The Astrophysical Journal* 758.2, p. 128.

Cohen, AS et al. (2007). "The VLA low-frequency sky survey". In: *The Astronomical Journal* 134.3, p. 1245.

Colafrancesco, S, P Marchegiani, and G Beck (2015). "Evolution of dark matter halos and their radio emissions". In: *Journal of Cosmology and Astroparticle Physics* 2015.02, p. 032.

Colafrancesco, Sergio and Barbara Mele (2001). "Neutralinos and the origin of radio halos in clusters of galaxies". In: *The Astrophysical Journal* 562.1, p. 24.

Colafrancesco, Sergio, Stefano Profumo, and Piero Ullio (2006). "Multi-frequency analysis of neutralino dark matter annihilations in the Coma cluster". In: *Astronomy & Astrophysics* 455.1, pp. 21–43.

— (2007). "Detecting dark matter WIMPs in the Draco dwarf: A multiwavelength perspective". In: *Physical Review D* 75.2, p. 023513.

Collaboration-XENON et al. (2018). "Dark matter search results from a one ton-year exposure of XENON1T". In: *Physical Review Letters* 121.11, p. 111302.

Colless, Matthew and Andrew M Dunn (1995). "Structure and dynamics of the Coma cluster". In: *arXiv preprint astro-ph/9508070*.

Condon, James J et al. (1998a). "The NRAO VLA sky survey". In: *The Astronomical Journal* 115.5, p. 1693.

Condon, JJ et al. (1998b). "The NRAO VLA sky survey". In: *The Astronomical Journal* 115.5, p. 1693.

Conrad, Jan and Olaf Reimer (2017). "Indirect dark matter searches in gamma and cosmic rays". In: *Nature Physics* 13.3, pp. 224–231.

Depta, Paul Frederik et al. (2019). "BBN constraints on the annihilation of MeV-scale dark matter". In: *Journal of Cosmology and Astroparticle Physics* 2019.04, p. 029.

Drury, L O'C (1983). "An introduction to the theory of diffusive shock acceleration of energetic particles in tenuous plasmas". In: *Reports on Progress in Physics* 46.8, p. 973.

Feretti, L et al. (2001). "The giant radio halo in Abell 2163". In: *Astronomy & Astrophysics* 373.1, pp. 106–112.

Feretti, L et al. (2004). "Spectral index maps of the radio halos in Abell 665 and Abell 2163". In: *Astronomy & Astrophysics* 423.1, pp. 111–119.

Feretti, Luigina et al. (2012). "Clusters of galaxies: observational properties of the diffuse radio emission". In: *The Astronomy and Astrophysics Review* 20.1, p. 54.

Ferrari, C et al. (2008). "Observations of extended radio emission in clusters". In: *Clusters of Galaxies*, pp. 93–118.

Funk, Stefan, JA Hinton, CTA Consortium, et al. (2013). "Comparison of Fermi-LAT and CTA in the region between 10–100 GeV". In: *Astroparticle Physics* 43, pp. 348–355.

Giovannini, G, M Tordi, and L Feretti (1999). "Radio halo and relic candidates from the NRAO VLA Sky Survey". In: *New Astronomy* 4.2, pp. 141–155.

Giovannini, G et al. (1993). "The halo radio source Coma C and the origin of halo sources". In: *The Astrophysical Journal* 406, pp. 399–406.

Giovannini, G et al. (2009). "Radio halos in nearby (z $<$0.4) clusters of galaxies". In: *Astronomy & Astrophysics* 507.3, pp. 1257–1270.

Gitti, Myriam et al. (2007). "Discovery of diffuse radio emission at the center of the most X-ray-luminous cluster RX J1347. 5-1145". In: *Astronomy & Astrophysics* 470.3, pp. L25–L28.

Gondolo, Paolo et al. (2001). "DARKSUSY–A NUMERICAL PACKAGE FOR DARK MATTER CALCULATIONS IN THE MSSM". In: *The Identification Of Dark Matter*. World Scientific, pp. 318–323.

Gondolo, Paolo et al. (2004). "DarkSUSY: Computing supersymmetric dark matter properties numerically". In: *Journal of Cosmology and Astroparticle Physics* 2004.07, p. 008.

Govoni, F et al. (2001b). "Radio and X-ray diffuse emission in six clusters of galaxies". In: *Astronomy & Astrophysics* 376.3, pp. 803–819.

Govoni, F et al. (2004). "Chandra temperature maps for galaxy clusters with radio halos". In: *The Astrophysical Journal* 605.2, p. 695.

Govoni, F et al. (2009). "A search for diffuse radio emission in the relaxed, cool-core galaxy clusters A1068, A1413, A1650, A1835, A2029, and Ophiuchus". In: *Astronomy & Astrophysics* 499.2, pp. 371–383.

Govoni, Federica and Luigina Feretti (2004). "Magnetic fields in clusters of galaxies". In: *International Journal of Modern Physics D* 13.08, pp. 1549–1594.

Halkola, A, S Seitz, and M Pannella (2007). "The sizes of galaxy halos in galaxy cluster Abell 1689". In: *The Astrophysical Journal* 656.2, p. 739.

Hooper, Dan and Stefano Profumo (2007). "Dark matter and collider phenomenology of universal extra dimensions". In: *Physics Reports* 453.2, pp. 29–115.

Huang, Xiaoyuan, Gilles Vertongen, and Christoph Weniger (2012). "Probing dark matter decay and annihilation with Fermi LAT observations of nearby galaxy clusters". In: *Journal of Cosmology and Astroparticle Physics* 2012.01, p. 042.

Huber, B et al. (2013). "Probing the cosmic-ray content of galaxy clusters by stacking Fermi-LAT count maps". In: *Astronomy & Astrophysics* 560, A64.

Hurley-Walker, Natasha et al. (2017). "GaLactic and Extragalactic All-sky Murchison Widefield Array (GLEAM) survey–I. A low-frequency extragalactic catalogue". In: *Monthly Notices of the Royal Astronomical Society* 464.1, pp. 1146–1167.

Ignesti, Alessandro et al. (2020). "Radio and X-ray connection in radio minihalos: Implications for hadronic models". In: *Astronomy & Astrophysics* 640, A37.

Intema, HT et al. (2009). "Ionospheric calibration of low frequency radio interferometric observations using the peeling scheme-I. Method description and first results". In: *Astronomy & Astrophysics* 501.3, pp. 1185–1205.

Intema, HT et al. (2017). "The GMRT 150 MHz all-sky radio survey-First alternative data release TGSS ADR1". In: *Astronomy & Astrophysics* 598, A78.

Jaeger, S (2008). "The common astronomy software application (casa)". In: *Astronomical Data Analysis Software and Systems XVII*. Vol. 394, p. 623.

Jaffe, WJ (1977). "Origin and transport of electrons in the halo radio source in the Coma cluster". In: *The Astrophysical Journal* 212, pp. 1–7.

Jeltema, Tesla E and Stefano Profumo (2008). "Searching for dark matter with X-ray observations of local dwarf galaxies". In: *The Astrophysical Journal* 686.2, p. 1045.

Jungman, Gerard, Marc Kamionkowski, and Kim Griest (1996). "Supersymmetric dark matter". In: *Physics Reports* 267.5-6, pp. 195–373.

Kang, Hyesung, Dongsu Ryu, and TW Jones (2017). "Shock Acceleration Model for the Toothbrush Radio Relic". In: *The Astrophysical Journal* 840.1, p. 42.

Kaplinghat, Manoj, Sean Tulin, and Hai-Bo Yu (2016). "Dark matter halos as particle colliders: unified solution to small-scale structure puzzles from dwarfs to clusters". In: *Physical Review Letters* 116.4, p. 041302.

Kar, Arpan et al. (2019). "Constraints on dark matter annihilation in dwarf spheroidal galaxies from low frequency radio observations". In: *Physical Review D* 100.4, p. 043002.

Khanye, N.F, S.A Thwala, and P. Marchegiani (2021). "Multi-frequency observations of the radio halo in A1689". In: *In prep.*

Kiew, Ching-Yee, Chorng-Yuan Hwang, and Zamri Zainal Abibin (2017). "Constraints on the dark matter neutralinos from the radio emissions of galaxy clusters". In: *Monthly Notices of the Royal Astronomical Society* 467.3, pp. 2924–2933.

Kuchar, Petr and Torsten A Ensslin (2011). "Magnetic power spectra from Faraday rotation maps-REALMAF and its use on Hydra A". In: *Astronomy & Astrophysics* 529, A13.

Lacy, M et al. (2020). "The Karl G. Jansky very large array sky survey (VLASS). Science case and survey design". In: *Publications of the Astronomical Society of the Pacific* 132.1009, p. 035001.

Lane, WM et al. (2014). "The very large array low-frequency sky survey redux (VLSSr)". In: *Monthly Notices of the Royal Astronomical Society* 440.1, pp. 327–338.

Leonard, Adrienne, Lindsay J King, and David M Goldberg (2011). "New constraints on the complex mass substructure in Abell 1689 from gravitational flexion". In: *Monthly Notices of the Royal Astronomical Society* 413.2, pp. 789–804.

Limousin, Marceau et al. (2007). "Combining strong and weak gravitational lensing in Abell 1689". In: *The Astrophysical Journal* 668.2, p. 643.

Longair, Malcolm S (2011). *High energy astrophysics*. Cambridge university press.

Macías-Ramírez, Oscar et al. (2012). "Evaluating the gamma-ray evidence for self-annihilating dark matter from the Virgo cluster". In: *Physical Review D* 86.7, p. 076004.

Mahdavi, Andisheh et al. (2007). "A dark core in Abell 520". In: *The Astrophysical Journal* 668.2, p. 806.

Marchegiani, P, GC Perola, and S Colafrancesco (2007). "Testing the cosmic ray content in galaxy clusters". In: *Astronomy & Astrophysics* 465.1, pp. 41–49.

Marchegiani, Paolo and Sergio Colafrancesco (2015). "Is the radio emission in the Bullet cluster due to dark matter annihilation?" In: *Monthly Notices of the Royal Astronomical Society* 452.2, pp. 1328–1340.

Marchegiani, Paolo and Sergio Colafrancesco (2016). "The role of Dark Matter sub-halos in the non-thermal emission of galaxy clusters". In: *Journal of Cosmology and Astroparticle Physics* 2016.11, p. 033.

Markevitch, M et al. (2005a). "Bow shock and radio halo in the merging cluster A520". In: *The Astrophysical Journal* 627.2, p. 733.

Markevitch, Maxim (2005b). "Chandra observation of the most interesting cluster in the universe". In: *arXiv preprint astro-ph/0511345*.

McDaniel, Alex, Tesla Jeltema, and Stefano Profumo (2018). "Multiwavelength analysis of annihilating dark matter as the origin of the gamma-ray emission from M31". In: *Physical Review D* 97.10, p. 103021.

Miralda-Escude, Jordi and Arif Babul (1994). "Gravitational lensing in clusters of galaxies: New clues regarding the dynamics of intracluster gas". In: *arXiv preprint astro-ph/9405063*.

Mohan, Niruj and David Rafferty (2015). "PyBDSF: Python Blob Detection and Source Finder". In: *Astrophysics Source Code Library*, ascl–1502.

Moskalenko, Igor V and AW Strong (1998). "Production and propagation of cosmic-ray positrons and electrons". In: *The Astrophysical Journal* 493.2, p. 694.

Navarro, Julio F, Carlos S Frenk, and Simon DM White (1997). "A universal density profile from hierarchical clustering". In: *The Astrophysical Journal* 490.2, p. 493.

Nieuwenhuizen, Th M (2009). "Do non-relativistic neutrinos constitute the dark matter?" In: *EPL (Europhysics Letters)* 86.5, p. 59001.

Ogrean, GA et al. (2013). "Challenges to our understanding of radio relics: X-ray observations of the Toothbrush cluster". In: *Monthly Notices of the Royal Astronomical Society* 433.1, pp. 812–824.

Oguri, Masamune and Roger D Blandford (2009). "What is the largest Einstein radius in the universe?" In: *Monthly Notices of the Royal Astronomical Society* 392.2, pp. 930–944.

Oort, Jan Hendrik (1940). "Some Problems Concerning the Structure and Dynamics of the Galactic System and the Elliptical Nebulae NGC 3115 and 4494." In: *The Astrophysical Journal* 91, p. 273.

Padmanabhan, Nikhil and Douglas P Finkbeiner (2005). "Detecting dark matter annihilation with CMB polarization: Signatures and experimental prospects". In: *Physical Review D* 72.2, p. 023508.

Pfrommer, Christoph and Tom W Jones (2011). "Radio galaxy NGC 1265 unveils the Accretion Shock onto the Perseus galaxy cluster". In: *The Astrophysical Journal* 730.1, p. 22.

Pieri, Lidia et al. (2011). "Implications of high-resolution simulations on indirect dark matter searches". In: *Physical Review D* 83.2, p. 023518.

Price-Whelan, Adrian M et al. (2018). "The Astropy project: Building an open-science project and status of the v2. 0 core package". In: *The Astronomical Journal* 156.3, p. 123.

Profumo, Stefano (2017). *An introduction to particle dark matter*. World Scientific Publishing Company.

Prokhorov, DA and EM Churazov (2014). "Counting gamma rays in the directions of galaxy clusters". In: *Astronomy & Astrophysics* 567, A93.

Proust, D et al. (2000). "Dynamics of the X-ray clusters Abell 222, Abell 223 and Abell 520". In: *arXiv preprint astro-ph/0001265*.

Regis, Marco and Piero Ullio (2008). "Multiwavelength signals of dark matter annihilations at the Galactic center". In: *Physical Review D* 78.4, p. 043505.

Regis, Marco et al. (2014). "Local Group dSph radio survey with ATCA (III): constraints on particle dark matter". In: *Journal of Cosmology and Astroparticle Physics* 2014.10, p. 016.

Rephaeli, Y (1979). "Relativistic electrons in the intracluster space of clusters of galaxies-The hard X-ray spectra and heating of the gas". In: *The Astrophysical Journal* 227, pp. 364–369.

Roettiger, Kurt, Chris Loken, and Jack O Burns (1997). "Numerical simulations of merging clusters of galaxies". In: *The Astrophysical Journal Supplement Series* 109.2, p. 307.

Rubin, Vera C and W Kent Ford Jr (1970). "Rotation of the andromeda nebula from a spectroscopic survey of emission regions". In: *The Astrophysical Journal* 159, p. 379.

Rubin, Vera C, W Kent Ford Jr, and Sandro D'Odorico (1970). "Emission-Line Intensities and Radial Velocities in the Interacting Galaxies NGC 4038-4039". In: *The Astrophysical Journal* 160, p. 801.

Sarazin, Craig L (1999). "The energy spectrum of primary cosmic-ray electrons in clusters of galaxies and inverse Compton emission". In: *The Astrophysical Journal* 520.2, p. 529.

Sault, Robert J, Peter J Teuben, and MCH Wright (2006). "A retrospective view of miriad". In: *arXiv preprint astro-ph/0612759*.

Sereno, Mauro and Keiichi Umetsu (2011). "Weak-and strong-lensing analyses of the triaxial matter distribution of Abell 1689". In: *Monthly Notices of the Royal Astronomical Society* 416.4, pp. 3187–3200.

Sereno, Mauro et al. (2013). "Mass, shape and thermal properties of Abell 1689 using a multiwavelength X-ray, lensing and Sunyaev–Zel'dovich analysis". In: *Monthly Notices of the Royal Astronomical Society* 428.3, pp. 2241–2254.

Serpico, Pasquale D and Georg G Raffelt (2004). "MeV-mass dark matter and primordial nucleosynthesis". In: *Physical Review D* 70.4, p. 043526.

Shan, HuanYuan et al. (2010). "Offset between dark matter and ordinary matter: evidence from a sample of 38 lensing clusters of galaxies". In: *Monthly Notices of the Royal Astronomical Society* 406.2, pp. 1134–1139.

Smith, Sinclair (1936). "The mass of the Virgo cluster". In: *The Astrophysical Journal* 83, p. 23.

Stepanov, Rodion et al. (2008). "Magnetic field structures of galaxies derived from analysis of Faraday rotation measures, and perspectives for the SKA". In: *Astronomy & Astrophysics* 480.1, pp. 45–59.

Storm, Emma et al. (2013). "Constraints on dark matter annihilation in clusters of galaxies from diffuse radio emission". In: *The Astrophysical Journal* 768.2, p. 106.

Stref, Martin, Thomas Lacroix, and Julien Lavalle (2019). "Remnants of galactic subhalos and their impact on indirect dark-matter searches". In: *Galaxies* 7.2, p. 65.

Struble, Mitchell F and Herbert J Rood (1999). "A compilation of redshifts and velocity dispersions for ACO clusters". In: *The Astrophysical Journal Supplement Series* 125.1, p. 35.

Taylor, AN et al. (1998). "Gravitational lens magnification and the mass of abell 1689". In: *The Astrophysical Journal* 501.2, p. 539.

Taylor, GB, AC Fabian, and SW Allen (2002). "Magnetic fields in the Centaurus cluster". In: *Monthly Notices of the Royal Astronomical Society* 334.4, pp. 769–776.

Thwala, SA et al. (2019). "The study of extended emission in a radio galaxy detected in the LOFAR Two-Metre Sky Survey". In: *Monthly Notices of the Royal Astronomical Society* 485.2, pp. 1938–1946.

Tyson, J Anthony and Philippe Fischer (1995). "Measurement of the mass profile of Abell 1689". In: *arXiv preprint astro-ph/9503119*.

Tyson, J Anthony, F Valdes, and RA Wenk (1990). "Detection of systematic gravitational lens galaxy image alignments-Mapping dark matter in galaxy clusters". In: *The Astrophysical Journal* 349, pp. L1–L4.

Vacca, V et al. (2011). "Discovery of diffuse radio emission in the galaxy cluster A1689". In: *Astronomy & Astrophysics* 535, A82.

Vacca, V et al. (2012). "The intracluster magnetic field power spectrum in A2199". In: *Astronomy & Astrophysics* 540, A38.

Vacca, VALENTINA et al. (2014). "Spectral index image of the radio halo in the cluster Abell 520, which hosts the famous bow shock". In: *Astronomy & Astrophysics* 561, A52.

Van Dokkum, PG and M Franx (1995). "Dust in the cores of early-type galaxies". In: *arXiv preprint astro-ph/9507101*.

Van Weeren, Reinout J et al. (2010). "Particle acceleration on megaparsec scales in a merging galaxy cluster". In: *Science* 330.6002, pp. 347–349.

Van Weeren, RJ et al. (2011). "Using double radio relics to constrain galaxy cluster mergers: a model of double radio relics in CIZA J2242. 8+ 5301". In: *Monthly Notices of the Royal Astronomical Society* 418.1, pp. 230–243.

Vollmann, Martin et al. (2020). "Radio constraints on dark matter annihilation in Canes Venatici I with LOFAR". In: *Monthly Notices of the Royal Astronomical Society* 496.3, pp. 2663–2672.

Wang, Qian HS, Simona Giacintucci, and Maxim Markevitch (2018). "Bow Shock in Merging Cluster A520: The Edge of the Radio Halo and the Electron–Proton Equilibration Timescale". In: *The Astrophysical Journal* 856.2, p. 162.

Wang, Qian HS, Maxim Markevitch, and Simona Giacintucci (2016). "The merging galaxy cluster A520—a broken-up cool core, a dark subcluster, and an X-ray channel". In: *The Astrophysical Journal* 833.1, p. 99.

Wayth, RB et al. (2015). "GLEAM: The GaLactic and Extragalactic All-Sky MWA Survey". In: *Publications of the Astronomical Society of Australia* 32.

Wright, Edward L et al. (2010). "The Wide-field Infrared Survey Explorer (WISE): mission description and initial on-orbit performance". In: *The Astronomical Journal* 140.6, p. 1868.

Zandanel, Fabio, Christoph Weniger, and Shin'ichiro Ando (2015). "The role of the eROSITA all-sky survey in searches for sterile neutrino dark matter". In: *Journal of Cosmology and Astroparticle Physics* 2015.09, p. 060.

Zhang, Hao et al. (2011). "Effective dark matter model: relic density, CDMS II, Fermi LAT and LHC". In: *Journal of High Energy Physics* 2011.8, p. 18.

Zwicky, Fritz (1933). "The redshift of extragalactic nebulae". In: *Helvetica Physica Acta* 6, pp. 110–127.